Dipl. Ing. Marlene Turner

First Observation of the Seeded Proton Bunch Self-Modulation in Plasma

DOCTORAL THESIS

to achieve the university degree of

Doktorin der technischen Wissenschaften

submitted to

Graz University of Technology

Supervisor

Priv.-Doz. Dipl.-Ing. Dr.techn. Helmut Vincke

Institute of Theoretical and Computational Physics

in cooperation with CERN

Graz, December 2017

AFFIDAVIT

I declare that I have authored this thesis independently, that I have not used other than the declared sources/resources, and that I have explicitly indicated all material which has been quoted either literally or by content from the sources used. The text document uploaded to TUGRAZonline is identical to the present doctoral thesis.

Date

Signature

Thanks & Acknowledgements

I sincerely thank everybody who contributed to this thesis and made this work possible!

First of all I must express my very profound gratitude to my CERN supervisor Edda Gschwendtner. I would like to thank her for her time and extreme patience as well as her contributions to my development as a scientist. She brought me into the world of 'plasma wakefield acceleration' and offered me outstanding opportunities.
I thank my thesis advisor, Helmut Vincke, physics advisor Alexey Petrenko as well as our physics and experimental board leader Patric Muggli for their guidance and support over the years. You have set an example of excellence as researchers, mentors, instructors, and role models.
I would also like to thank my external reviewer Prof. Arnd Specka for his constructive comments and inputs, that clearly improved the quality of this manuscript.

To the AWAKE collaborators and technicians, who contributed to this research: I am very grateful to all of you.

Last but not least, I would especially like to thank my amazing family for the love, support, and constant encouragement I have gotten over the years.

Even though I am the sole author of this thesis I often use the term 'we' when talking about work that was performed. I choose 'we' over 'I' to acknowledge the people working for and contributing to the AWAKE experiment.
The work for this thesis was performed under the Austrian Doctoral Student Program at CERN and financially supported by the österreichische Bundesministerium für Wissenschaft, Forschung und Wirtschaft (BMWFW).

Abstract

In this thesis I observe experimentally and study in simulations the seeded self-modulation of a relativistic proton bunch in AWAKE, the Advanced Proton Driven Plasma Wakefield Acceleration Experiment. The 400 GeV/c proton bunch from the CERN SPS with a rms length of ∼12 cm propagates in a 10 m long plasma with a density adjustable between $2 - 10 \times 10^{14}$ electrons/cm^3. The seeded self-modulation process results in focusing and defocusing of the protons, thereby forming a bunch train that resonantly drives wakefields to large amplitudes.

I use the two-screen measurement setup, to observe the result of the proton bunch self-modulation and to learn about its physics (i.e. growth of the process). The idea is to obtain images of protons that were defocused by the transverse wakefields, 2 and 10 m downstream the end of the plasma. From these images I determine the maximum transverse momentum of the defocused protons as well as infer their point of origin along the plasma. I use simulations to guide the understanding of the experimental results.

At a plasma density of 7.7×10^{14} electrons/cm^3, the maximum defocused protons exit the wakefields with a transverse momentum of (390 ± 25) MeV/c, ∼4 m after the plasma entrance. This measured transverse momentum is larger than that from the bunch emittance (σ_{pr} =∼20 MeV/c) plus that from the initial seed wakefield (∼15 MV/m) integrated over the plasma interaction length. This therefore proves for the first time that the wakefields grow along the plasma and that the proton bunch strongly evolves in its transverse dimension, as a result of the seeded self-modulation process.

Contents

1 Glossary

- e : electron charge ($e = 1.6 \times 10^{-19}\,\mathrm{C}$)
- m_e : electron mass ($9.1 \times 10^{-31}\,\mathrm{kg}$)
- c : speed of light ($c = 2.99\,\mathrm{m/s}$)
- ω_{pe} : plasma electron angular frequency
- E_{max} or E_{WB} : cold plasma wavebreaking field
- n_{pe} : plasma electron density
- m_p : proton mass ($1.67 \times 10^{-27}\,\mathrm{kg}$)
- LHC: Large Hadron Collider
- U_0 : synchrotron radiation loss per turn
- ρ_b : bending radius of the charged particles in a magnetic field
- ϵ_0 : vacuum permittivity ($\epsilon_0 = 8.85 \times 10^{-12}\,\mathrm{Fm}^{-1}$)
- v_b : velocity of the drive bunch
- $\beta = \frac{v_b}{c}$
- γ : Lorentz factor
- E_p : particle energy
- m_0 : particle mass at rest
- λ_{pe} : plasma electron wavelength
- v_{ph} : wakefield phase velocity
- $k_{pe} = \omega_{pe}/c$: plasma wavenumber
- σ_z : rms of the bunch length
- σ_r : rms of the radial bunch size
- σ_{pr} : rms of the radial proton momentum spread
- $v_{\parallel}$: longitudinal velocity
- $v_{\perp}$: transverse velocity
- E : energy or electric field strength
- p : particle momentum
- N_D : plasma parameter
- λ_D : Debye length

1 Glossary

- r : radial coordinate, radius
- c/ω_{pe} : plasma skin depth
- k : wave-vector
- n_d : displaced charge density
- z : longitudinal coordinate
- n_b : proton bunch profile
- ξ : position along the bunch ($\xi = 0$ is the front of the bunch)
- t : time coordinate
- n_{b0} : charge density of the drive bunch
- $n_{b\parallel}$: normalized longitudinal bunch distribution
- $n_{b\perp}$: normalized transverse bunch distribution
- W_z : longitudinal wakefields
- W_r : radial wakefields
- K_0, K_1, I_0, I_1 : Bessel functions
- $E_{0,r}$: transverse seed wakefield amplitude
- Γ : growth rate of the seeded self-modulation
- p_z : longitudinal momentum
- p_r : radial momentum
- ϵ_N : normalized emittance, ϵ_g : geometric emittance
- $\vec{F_r}$: transverse force
- $\vec{E_r}$: radial electric field
- $\vec{B_\theta}$: azimuthal magnetic field
- m_i : ion mass
- Z_c : number of ionizations
- τ_e : electron oscillation period
- τ_i : ion oscillation period
- p_θ : azimuthal proton momentum
- x, y : horizontal and vertical coordinate
- ϕ : azimuthal coordinate
- q : charge
- OD: Optical Density
- R: Reflectance
- α : fine structure constant
- $\lambda_a - \lambda_b$: wavelength range
- N_{CV} : number of Cerenkov photons

- N_{OTR} : number of photons from Optical Transition Radiation
- N_{SCINT} : number of scintillation photons
- ΔE : energy range
- ΔT : temperature change
- ρ_{xx} : density of material xx
- c_{xx} : specific heat capacity of material xx
- r_1 : maximum proton radius at IS 1
- r_2 : maximum proton radius at IS 2
- θ : maximum proton defocusing angle
- O : point (along the plasma) where the maximum defocused protons experience their radial momentum and radially exit the wakefields or plasma
- d_{eIS1} : distance between the entrance of the plasma and IS 1
- d_{IS12} : distance between the two imaging stations
- d_{OIS1} : distance between origin of defocused proton and IS 1
- p_{max} : maximum transverse momentum
- $W_{0,z}$: longitudinal seed wakefield amplitude
- $W_{0,r}$: transverse seed wakefield amplitude
- $W_{r,max}$: maximum transverse wakefield amplitude
- $W_{z,max}$: maximum longitudinal wakefield amplitude
- p_0 : initial transverse proton momentum
- IS: imaging station
- f_{mod} : modulation frequency
- a.u.: arbitrary units

2 Introduction

2.1 Why is Plasma Wakefield Acceleration Interesting ?

2.1.1 High Accelerating Gradient

Scientists explore the smallest building blocks of nature and the forces between them by using accelerators, to collide high-energy particles. Higher collision energies allow the creation of higher mass particles and correspond to resolving smaller structures.

Conventional accelerators accelerate charged particles with longitudinal electric fields created by radio-frequency (RF) cavities. Modern RF-cavities can reach accelerating electric fields up to 100 MV/m. This means that for example an electron can gain 1 GeV in 10 m. The maximum achievable field is limited by electric breakdown of the structures.

Plasmas can sustain higher electric fields strengths, because they consist of ionized particles. The strength of the electric fields created by plasma oscillations depends on the amount of electron charge that is displaced and on the charge separation distance. The maximum fields that can be created at a given plasma density n_{pe} can be estimated by the cold plasma wavebreaking field E_{max}:

$$E_{max} \approx \frac{m_e \cdot c \cdot \omega_{pe}}{e} \sim 100 \frac{\mathrm{V}}{\mathrm{m}} \sqrt{n_{pe}[\mathrm{cm}^{-3}]}, \tag{2.1}$$

where m_e is the electron mass at rest, c is the speed of light, ω_{pe} is the plasma electron angular frequency and e the electron charge.

For example, the maximum field E_{max} reaches 1 GV/m for a plasma electron density of $10^{14}\,\mathrm{cm}^{-3}$ or 100 GV/m for a plasma electron density of $10^{18}\,\mathrm{cm}^{-3}$. Plasma wakefield experiments typically use plasma densities in that range.

2.1.2 Why is a High Accelerating Gradient Important?

Protons versus Electrons or Positrons Accelerators

Protons are composite particles consisting of quarks and gluons and the proton mass m_p is 1.6×10^{-27} kg or 936 MeV. Electrons (and positrons) are elementary, point-like particles with a mass of $m_e = 9.1 \times 10^{-31}$ kg or 0.511 MeV. We note that the proton mass is 1836 times heavier than the electron mass.

On the one hand, proton colliders are often called "discovery machines" because in proton-proton collisions quarks and gluons collide with undefined individual energies. On the other hand electron-positron or electron-electron colliders are "precision machines" because two point like particles with well-defined energy collide.

Circular versus Linear Accelerators

Currently, there are two main geometries to accelerate particles to very high energies: linear and circular accelerators.

Circular particle accelerators (for example CERN's Large Hadron Collider (LHC)) bend charged particles on a circular trajectory using the field of magnetic dipoles. Particles gain energy every turn as they pass through an accelerating section, but they loose energy due to synchrotron radiation. The amount of energy loss of a particle by synchrotron radiation over one turn U_0 is [1]:

$$U_0 = \frac{e^2}{3\epsilon_0}\frac{\beta^3\gamma^4}{\rho_b} \propto \frac{1}{\rho_b}\frac{E_p^4}{m_0^4} \tag{2.2}$$

where ϵ_0 is the vacuum permittivity, $\beta = v_b/c$ with v_b the particle velocity, γ is the Lorentz factor, $\rho_b = \gamma m_0 c/qB_0$ is the bending radius of the charged particles in the magnetic field B_0, E_p is the particle energy and m_0 is the particle mass at rest. Note that Equation 2.2 is only valid for highly relativistic energies ($\beta \approx 1$).

Equation 2.2 shows that the energy loss per turn depends on the particle energy and mass at rest to the power four. The energy loss per turn U_0 decreases only linearly with the bending radius ρ_b, but increases with the fourth power of the particle mass at rest. This makes circular accelerators unfavourable for the acceleration of light particles such as electrons and positrons, but the choice for heavier particles like protons and ions.

Due to the limited acceleration per turn (equivalent for protons and electrons) and the synchrotron radiation loss ($\propto 1/m_0^4$), the energy that electrons and positrons reach in circular colliders is significantly lower than the energy that protons reach. For example, in the LHC, protons are accelerated to 7 TeV in a ring with a circumference of 26.659 km and the corresponding average bending radius is 4.24 km. To compare, in the same nowadays LHC tunnel the Large Electron Positron collider upgrade (LEP2) was accelerating electrons and positrons to a maximum energy of 104.5 GeV, limited by synchrotron radiation loss (at this maximum energy, the loss per turn equals the gain per turn).

Linear particle accelerators (i.e. the Stanford Linear Collider) consist of many and long accelerating sections. Since no dipole bending is needed, the synchrotron radiation loss is negligible. The energy the particles acquire is the product of the accelerator length and accelerating gradient, since the particles pass only once. There are two ways to reach higher particle energies in a linear particle accelerator: a longer accelerator or a larger accelerating gradient. Stronger accelerating gradients decrease the size of the accelerating sections in such a linear machine. A high gradient acceleration technique is therefore desired. Plasma wakefield acceleration holds the potential of high accelerating gradients.

2.1.3 Future Linear Collider Proposals

One current proposal for a conventional (using RF technology) linear electron-positron collider is the Compact Linear Collider project, also called CLIC [2]. CLIC aims to accelerate electrons and positrons to 1.5 TeV per beam using accelerating structures with an electric field of 100 MV/m. The length of the machine would be about 42 km, and the estimated cost about (27 ± 8) Billion US Dollar [3].

Adli et al. proposed a linear plasma-wakefield collider driven by electron bunches. In this design, the collider is 4.5 km long, and accelerates electrons and positrons up to 0.5 TeV each. The wakefields are driven in stages, by 25 eV electron bunches, and the average acceleration gradient is 7.6 GV/m [4].

Leeman et al. proposed a linear 2 TeV electron–positron collider based on laser-driven plasma acceleration with a length of $\sim$1 km and about 100, 1 m-

long stages. For each stage, a 30 J laser pulse drives plasma wakefields and creates accelerating gradients of 10 GeV/m [5].

The possibility of accelerating electrons up to 600 GeV in 600 m of plasma, where the wakefields are driven by a LHC type 7 TeV proton drive bunch, was suggested in 2009 by Allen Caldwell et al. [6]. In this design high energy electrons would collide with high energy protons.

Note that, at this moment, the RF acceleration technique is much more advanced than plasma wakefield acceleration. But a future linear collider based on plasma wakefield acceleration could be considerably more compact than one using conventional RF technology.

2.2 Overview of Plasma Wakefield Acceleration

2.2.1 Laser Driven Plasma Wakefield Acceleration

In 1979, T. Tajima and J.M. Dawson proposed that laser driven plasma oscillations can trap and accelerate electrons [7]. The experimental realization followed in 1992 by C. Clayton using a laser plasma beatwave accelerator [8].

Laser plasma wakefield experiments became possible with the invention of chirped pulse amplification (CPA)[9].

In 2006, three groups have been able to produce electron beams with a finite energy spread (few %), using a short intense laser pulse [10, 11, 12]. These groups used a regime known as the forced wakefield regime. In this regime a laser pulse with dimensions on the order of the plasma wavelength drives the wakefields.

In 2014 a research group at Berkeley used a 300 TW laser system to accelerate 6 pC of electrons to 4.2 GeV in 9 cm of plasma (average accelerating gradient $\sim$ 46 GV/m) with a rms energy spread of 6 % and 0.3 mrad rms divergence [13].

2.2.2 Beam Driven Plasma Wakefield Acceleration

In 1985 P. Chen et al. suggested that the plasma waves can also be driven by a relativistic electron beam [14]. The demonstration followed by J. Rosenzweig [15]. Experiments at SLAC in 2007 demonstrated that some electrons were

accelerated from 42 to 84 GeV in 85 cm of plasma (average accelerating gradient $\sim 50\,\mathrm{GV/m}$) [16]. High gradient two-bunch acceleration was demonstrated in 2008 [17].

2.3 The Seeded Self-Modulation

Section 2.2 shows the experimental demonstration that short laser pulses, electron and positron (not mentioned in 2.2) bunches can be used to drive large amplitude plasma wakefields. As mention in Section 2.1 and described by Equation 2.1, the achievable accelerating gradient E_{max} increases with the plasma electron density n_{pe} ($E_{max} \propto n_{pe}^{1/2}$). The higher the plasma electron density, the higher the plasma electron angular frequency $\omega_{pe} = \sqrt{n_{pe}e^2/m_e\epsilon_0}$ and the shorter the plasma electron wavelength $\lambda_{pe} = 2\pi c/\omega_{pe}$. Note that the expression for λ_{pe} assumes that the phase velocity v_{ph} of the wakefields is tied to the velocity of the driver $v_{ph} = v_b \approx c$. Thus to create high accelerating gradients in the order of 100 GV/m, the plasma electron density n_{pe} needs to be on the order of $\sim 10^{18}\,\mathrm{cm}^{-3}$, which makes the plasma electron wavelength λ_{pe} short ($\lambda_{pe} \approx 30\,\mathrm{mm}$).

Linear theory indicates that to effectively drive wakefields in a plasma with a plasma density n_{pe}, the bunch rms length σ_z must satisfy $k_{pe}\sigma_z \cong 1$ ($k_{pe} = 2\pi/\lambda_{pe}$). In order to be stable against transverse current filamentation instability, the transverse rms size σ_r must satisfy $k_{pe}\sigma_r \cong 1$. Similar scalings also apply to laser driven accelerators (more details in Section 3.2).

As experiments use high plasma electron densities, the drive bunches need to be very short $\sigma_z \sim \lambda_{pe}$ and focused tightly. Short laser or particle bunches carry a limited amount of energy and can drive wakefields only over short distances. For example, laser bunches with $\sim 40\,\mathrm{J}$ in 40 fs drive strong wakefields over $\sim 9\,\mathrm{cm}$ [13], or a 42 GeV electron bunch with $\sigma_z \cong \sigma_r \cong 20\,\mu\mathrm{m}$ over 85 cm [16]. To reach TeV energies for a future collider (as mentioned in Section 2.1.3), one needs much longer accelerating sections than can be driven by one of these pulses or bunches. Therefore staging of many accelerating sections is necessary to reach very high energies.

High energy proton bunches carry much more energy (see Section 2.4.1) and can be focused tightly (i.e. $\sigma_r \approx 0.2\,\mathrm{mm}$, thus $k_{pe}\sigma_r = 1$ for $n_{pe} = 7 \times$

$10^{14}\,\mathrm{cm}^{-3}$), but have a very long bunch length ($\sigma_z \sim 10\,\mathrm{cm}$). Satisfying $k_{pe}\sigma_z \sim 1$, they can only drive several MV/m wakefields in a very low density plasma ($n_{pe} \sim 10^9\,\mathrm{electrons/cm}^3$). Satisfying $k_{pe}\sigma_r = 1$ such a proton bunch could drive wakefields of several GV/m, with $\lambda_{pe} = \sim 1\,\mathrm{mm}$.

Thus, to reach significant gradients ($> 0.1GV/m$) when using a high energy proton drive bunch, one has to choose the plasma electron density based on $k_{pe}\sigma_r = 1$, which makes the longitudinal bunch length much too long for effective wakefield excitation ($k_{pe}\sigma_z \sim 600$). However, since the proton bunch is much longer than the plasma wavelength it is subjected to a transverse instability, called the Self-Modulation Instability (SMI) or if seeded the seeded self-modulation (SSM) [18](also see Chapter 3).

To carry a lot of energy, the longitudinal velocity $v_\parallel$ of the protons is highly relativistic ($v_b = v_\parallel \approx c$), but the transverse velocity $v_\perp$ is not ($v_\perp \ll c$). The proton bunch drives initial transverse and longitudinal plasma wakefield at the plasma frequency. The initial transverse focusing and defocusing plasma wakefields act on the long proton bunch and periodically change the radial proton bunch size. The proton distribution with a modulated density then drives its own stronger wakefields ($\propto \sigma_r$), creating the feedback loop for the instability and resulting in the formation of micro-bunches (proton density modulation). As the instability grows, the bunch radius and density modulation become large, the wakefield amplitude becomes comparable to E_{max} and the instability saturates. At this point, a large fraction of the protons ($> 50\,\%$) may be defocused and outside the wakefield. In this thesis I estimate what fraction of the protons are defocused (see Chapter 6).

Each micro-bunch then drives its own wakefield. Since the micro-bunches are spaced at the plasma electron wavelength (λ_{pe}) their fields add, leading to resonant wakefield excitation and thus strong plasma wakefields (much larger than their initial value some distance behind the bunch front). Later on in this thesis I will prove that a proton bunch can drive wakefields larger than the initial seed value (see Chapter 6).

The proton bunch self-modulation is in general a random process that starts from noise. If it starts from noise, the wakefields phase and amplitude are not fixed. The undefined wakefield phase is a problem for externally injecting particles, because one does not know where in the wakefield to inject. The proper phase for injection, acceleration and focusing for the witness particles

appears randomly along the proton bunch. Thus, wakefields created by a self-modulated proton bunch, where the process starts from noise, cannot be used to build an accelerator.

The solution is to seed the instability for example with a signal above noise level. Seeding the instability fixes the phase and amplitude of the wakefields so that they can be used to accelerate externally injected particles. Seeding will be discussed in Section 3.3.1.

2.3.1 Previous Results on the Seeded Self-Modulation

Experiments from 2014, performed with a 60 MeV electron bunch show that long ($\sigma_z = 1 - 7\,\lambda_{pe}$) charged particle bunches indeed drive wakefields with a period of the plasma wavelength (λ_{pe}) [19]. These results also show that the amplitude of wakefields inferred from the energy gain or loss of the bunch particles corresponds to that expected from linear theory and numerical simulations. These wakefields were the seed for the SSM since the bunch rising edge was shorter than the wakefield period. However no evidence for growth was present.

Also in 2014, experiments with 20 GeV electron and positron bunches showed same characteristics of the self-modulation process, however, again, no evidence of growth was presented [20].

Experiments with 20 MeV electron bunches are currently performed at DESY PITZ. However to this day, no evidence of growth of the self-modulation process has been presented.

2.4 The AWAKE Experiment at CERN

AWAKE [21], the Advanced Proton-Driven Plasma Wakefield Acceleration Experiment is a proof-of-principle R&D experiment at CERN. The first goal of AWAKE is to demonstrate and study seeded proton bunch self-modulation and resonant excitation of strong plasma wakefields. The second goal is to use the wakefields to accelerate an externally injected electron witness bunch. In the longer term the goal is to accelerate electrons to 10-100 GeV, or possibly TeV for electron fixed-target and electron/positron experiments.

The AWAKE experimental program is organized in different Runs -and the

Runs are split into different Phases- as illustrated in the overview planning in Figure 2.1.

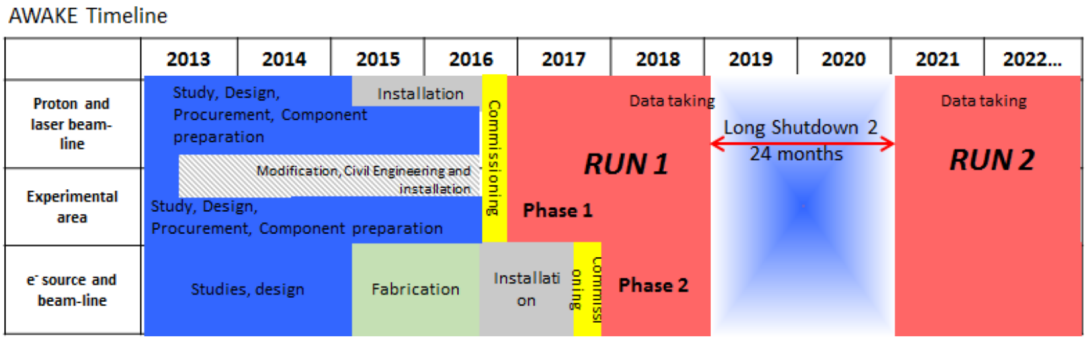

Figure 2.1: Overview of the AWAKE planning.

Figure 2.1 shows that AWAKE was approved in 2013. Design studies, civil engineering, fabrication and installation of the experiments followed the approval. The commissioning of the experimental area, the proton and the laser beam-line was performed in autumn of 2016. After the commissioning period, the experiment was ready for AWAKE Run 1-Phase 1 (2016-2017). Run 1 Phase 1 is dedicated to the measurement and understanding of the seeded self-modulation (SSM) of a long proton bunch in plasma. Simultaneously ongoing is the installation and later commissioning of the electron beam-line (2017). After the completion of the electron beam-line AWAKE will be ready for Run 1 Phase 2 in which the experiment plans to accelerate externally injected electrons in the created plasma wakefield (2018).

In 2018 AWAKE plans to submit a proposal for AWAKE Run 2, which would take place after the two-year long shut-down of the CERN accelerator complex. The goal of Run 2 is to apply the technique developed in the first Run and to create a 10s of GeV electron bunch with low emittance ($\sim 1\,\mathrm{mm{\cdot}mrad}$) and low relative energy spread ($\sim 1\,\%$).

2.4.1 Motivation for Using a Proton Drive Bunch

As briefly mentioned before, the distance over which plasma wakefields can be driven depends on the energy stored in the particle drive bunch. In AWAKE protons drive the plasma waves. The total energy E stored in one particle is:

$$E = \gamma m_0 c^2, \tag{2.3}$$

where γ is the Lorentz factor given by:

$$\gamma = \sqrt{1 + \left(\frac{p}{m_0 c}\right)^2}, \tag{2.4}$$

p is the particle momentum.

We know from Equation 2.3 that the SPS 400 GeV/c proton drive bunch with 3×10^{11} particles sent to AWAKE contains $\approx$ 20 kJ. To compare, the 42 GeV electron bunch with 1.8×10^{10} particles at SLAC only carries 0.12 kJ of energy.

As mentioned in Section 2.3, there is one problem though: plasma wakefields can only be created effectively, when the drive bunch length is on the order of the plasma wavelength. Proton bunches available, for example from the CERN Super Proton Synchrotron (SPS) at 400 GeV/c, have a longitudinal rms bunch length $\sigma_z \approx 12$ cm. Using linear plasma wakefield theory and the condition of most effective wakefield excitation ($\sigma_z = \sqrt{2} \cdot c/\omega_{pe}$, see Section 3.2) we can estimate that the optimum plasma density for a σ_z =12 cm bunch is $n_{pe} = 4 \times 10^9$ cm^{-3}. If we estimate the maximum achievable field in plasma by using the cold plasma wave-breaking limit E_{max} (see Equation 2.1) the maximum achievable electric field for a plasma electron density of $n_{pe} = 4 \times 10^9$ cm^{-3} is only $\approx$ 6 MV/m.

To reach GV/m plasma wakefield amplitudes, AWAKE uses a plasma density of $n_{pe} = 7 \times 10^{14}$ cm^{-3} (E_{max} =2.5 GV/m), which corresponds to an optimum drive bunch length (calculated from linear plasma wakefield theory with $k_{pe}\sigma_z = \sqrt{2}$, see Chapter 3) of $\sigma_z = 0.3$ mm. We note that the experiment has to rely on the seeded self-modulation (SSM) to modulate the $\sigma_z = 12$ cm long proton bunch into micro-bunches spaced at the plasma wavelength λ_{pe}. These micro-bunches each satisfy $k_{pe}\sigma_z \leq 1$ and resonantly drive plasma wakefields.

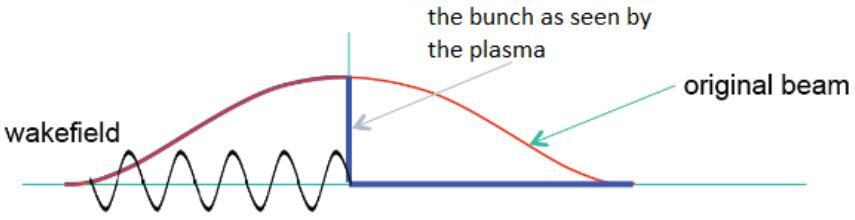

Figure 2.2: Schematic drawing of the sharp proton bunch edge to seed the SSM. The proton bunch moves to the right.

In AWAKE the SSM is seeded by the ionization front created by a short

laser pulse overlapping with the proton bunch [22]. This overlapping creates a sudden turn on of the plasma (see Figure 2.2), creating an ionizing front that moves together with the bunch. The development of the SSM in the case of AWAKE will be explained in details in Chapter 3 and 4.

From AWAKE simulations with baseline parameters (see Chapter 4) we expect that the proton bunch SSM saturates after $\sim$ 3 - 4 m of plasma ($n_{pe} = 7 \times 10^{14}$ electrons/cm^3). The development and seeding of the SSM is further discussed in Chapter 4.

2.4.2 General Layout of the Experiment

A schematic layout for Run 1 of the AWAKE experiment can be seen in Figure 2.3.

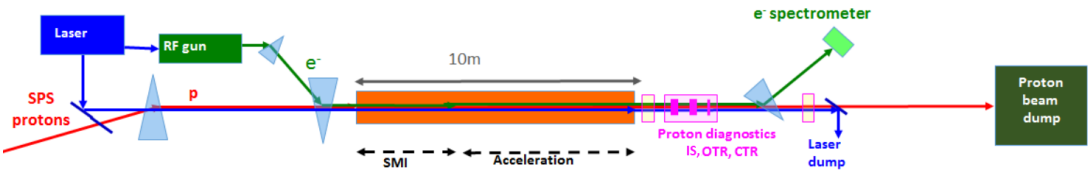

Figure 2.3: Schematic layout of the AWAKE facility. The orange box indicates the position of the 10 m long rubidium vapour source.

The core of the experiment is a 10 m long rubidium vapour cell (see Figure 2.4). A 10 m long fluid-heated heat-exchanger evaporates rubidium at 180 - 230 ^{o}C to reach the required rubidium vapour density of $0.5 - 10 \times 10^{14}$ atoms/cm^3. The rubidium vapour is then ionized by a 100 fs, 450 mJ laser pulse ($\lambda = 780$ nm) creating a plasma channel with a radius of approximately 1 mm.

We measure the rubidium vapour density 20 cm into the plasma at both ends by interferometry [23] and we assume that the laser pulse ionizes the outermost electron of each rubidium atom within the 1 mm laser radius.

Upstream the plasma three beamlines merge (see Figure 2.3) bringing together:

- the proton drive bunch from the CERN SPS (red), to create the plasma oscillations,
- the laser pulse (blue) to ionize the rubidium vapour and seed the SSM,
- the witness electron bunch (green), to be accelerated.

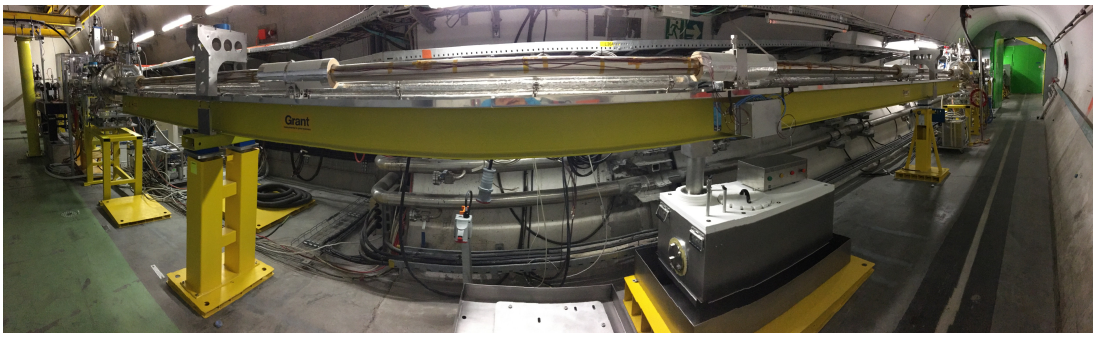

Figure 2.4: Photograph of the rubidium vapour cell installed in AWAKE.

The baseline spatial and temporal overlap of the three bunches is shown in Figure 2.5, where the laser pulse (red) is in the middle of the proton bunch (orange) to seed the SSM and the electron bunch (blue) is located at $\approx 1\sigma$ of the proton bunch behind the laser pulse. The protons in front of the laser pulse only see rubidium vapour. The 100 fs, 450 mJ laser pulse ionizes the outermost electron of the rubidium atoms creating the plasma. Protons and electrons after the laser pulse interact with the plasma and the created plasma wakefields. Note that in the experiment we are able to change the relative position of the laser, electron and proton bunch.

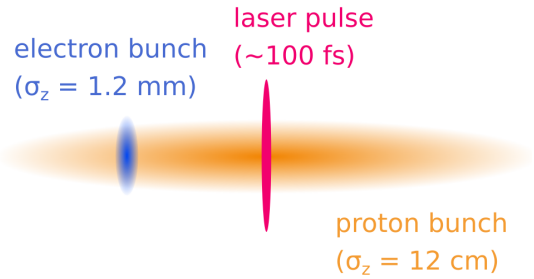

Figure 2.5: Schematic drawing of the spatial and temporal overlap of the proton, electron and laser bunch.

Diagnostics for Run 1 Phase 1

We measure the proton bunch position along the beam-line with beam-position monitors, the transverse bunch profile with cameras imaging screens that emit visible light [24] and the time resolved bunch profile with a streak camera imaging visible light emitted by a metallic foil up and downstream of the plasma. To reconstruct the position and transverse profile of the high power

laser at the plasma entrance and exit, approximately 1-2 % of the laser light is propagated on a virtual laser line over the same distances as to the entrance and exit of the plasma. This light is then measured with digital cameras. The high-power laser is dumped after the exit of the plasma by a 0.2 mm thick aluminium foil.

Specifically, to observe the self-modulation of the proton drive bunch, AWAKE has installed three different diagnostics downstream the plasma exit:

1. Two-screen measurement:
   The two-screen measurement is the topic of this thesis and will be extensively discussed later.
2. Optical Transition Radiation (OTR) streak camera measurement [25]:
   The idea of the streak camera measurement is to resolve with ps resolution the longitudinal density modulation of the proton bunch. As the protons traverse a metallic foil, they emit forward and backward OTR. The OTR light emission is prompt and proportional to the number of protons. The backward OTR is imaged on the entrance slit of the streak camera. The streak-camera produces an image of the transverse dimension of the proton bunch as a function of time. On a long time-scale ($\sim$ 1 ns) the image shows the seeding effect and on a short timescale ($\sim$ 70 ps) the micro-bunches themselves (up to plasma densities of $\sim 4 \times 10^{14}$ electrons/cm^3). At higher plasma densities the frequency can be obtained from a Fourier transform of the image.
3. Coherent transition radiation (CTR) measurement [26]:
   The CTR diagnostic measures the coherent part of the transition radiation i.e. with a wavelength larger than the typical structure of the proton bunch. The radiation is emitted when the proton bunch traverses a metallic foil. Since the modulated proton bunch consists of many micro-bunches, the CTR emission spectrum includes the modulation frequency. When the charge density modulation is non-linear, peaks at its harmonics are also present.

Parameter	Value
Plasma parameters:	
Plasma type	Laser-ionized rubidium vapour
Plasma length	10 m
Plasma density	$n_{pe} = 7 \times 10^{14}$ electrons/cm^3
Plasma radius	$r \geq 1$ mm
Wavebreaking field $E_{max} = m_e c \omega_{pe}/e$	2.54 GV/m
Proton bunch:	
Bunch momentum	400 GeV/c
Protons per bunch	3×10^{11}
Bunch length	$\sigma_z = 12$ cm
Bunch transverse size at plasma entrance	$\sigma_r = 0.2$ mm
Normalized emittance	3.6 mm-mrad
Beta-function	4.5 m
Laser pulse:	
Laser type	Fibre, Titanium:Sapphire
Wavelength	780 nm
Pulse length	100 fs
Laser energy	450 mJ
Focused size at plasma entrance	$\sigma_r = 1$ mm

Table 2.1: Summary of the AWAKE proton bunch, laser pulse and plasma baseline parameters.

2.4.3 Experimental Parameters

The baseline AWAKE proton bunch, laser pulse and plasma parameters for the SSM studies are summarized in Table 2.1.

2.5 Topics of this Thesis

During Run 1 Phase 1 (2016,2017), the experiment aims to demonstrate proton bunch self-modulation within 10 m of plasma as well as to improve the understanding of the physics of the SSM. The two-screen measurement is the topic of this thesis.

This topics discussed include:

- The design and realization of the two-screen measurement setup.
- PIC-code simulation studies of the SSM.
- Observation of the SSM, by measurements performed with the two-screen setup.
- Discussion of the measurement results and the physics of the SSM including:
  - A proof that the SSM developed and grew within the plasma, by measuring the maximum defocusing angle.
  - The amount of charge defocused by the transverse plasma wakefields.
  - An estimate of the transverse wakefield strength from measured parameters.

2.5.1 The Two-Screen Measurement System

The two-screen measurement setup detects protons that got defocused by the transverse plasma wakefields to indirectly prove that the proton bunch self-modulates in the plasma. The concept is illustrated in Figure 2.6.

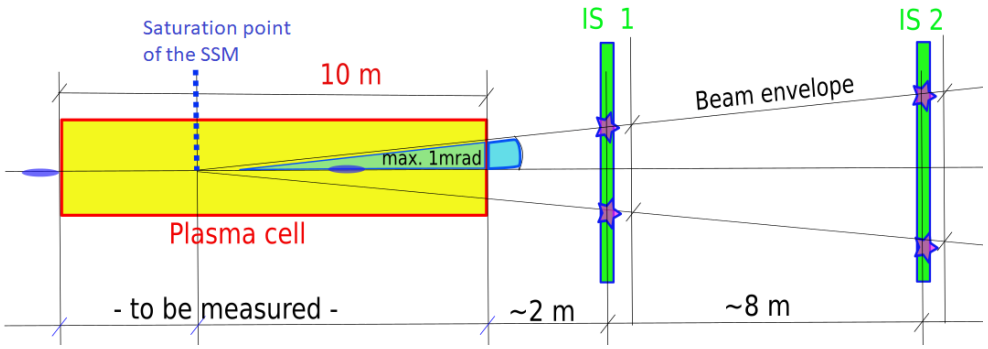

Figure 2.6: Schematic drawing of the two-screen measurement setup.

Using the setup, I measure the radial, time-integrated proton bunch profile ≈ 2 and 10 m downstream the end of the plasma with two imaging stations (IS 1 and IS 2). The idea is to detect the protons with the largest radial momentum because these protons experienced the largest product of transverse wakefield strength times interaction distance. After determining the outermost proton radius at both screens, I can estimate the maximum proton defocusing angle,

from which I can calculate the maximum transverse proton momentum. By showing that the maximum transverse proton momentum is much larger than the initial transverse momentum ($\sim 20\,\mathrm{MeV/c}$) from the bunch emittance plus the momentum gained from the seed wakefields, I can show that wakefields grew due to the development of the SSM and the resonant wakefield excitation of the micro-bunches. Simulations show that when the maximum proton defocusing angle is on the order of 1 mrad, GV/m wakefields were created. Note that strongly defocused protons radially exit the plasma wakefields and do not experience wakefields over the entire 10 m of the plasma.

After defocused protons radially exit the transverse wakefield, their trajectory is ballistic (straight). By tracking back from the two-screen images to the axis, I can estimate where the maximum defocused protons exit the plasma wakefields (plasma channel radius $\approx 1\,\mathrm{mm}$) and experience their transverse momentum. This calculation is an approximation because the proton trajectory in the plasma is not straight, but: first, I observe in simulations that the maximum defocused protons gain most of their momentum just before they radially exit the wakefields (see Section 4.4); and second we know from linear theory the the transverse wakefields have their maximum amplitude around $r = \sigma_r \sim 0.2\,\mathrm{mm}$ (see Section 3.2), which is close to the axis.

The two-screen measurement works continuously during the experiment, which means that by looking at the radial proton bunch profiles, one can immediately see the defocused protons if present, to get a first idea on whether self-modulation developed event to event. The two-screen measurement is complementary to the other diagnostics and in order to get more details about for example the modulation frequency or the modulation depth, one has to use the streak camera image or CTR signal of a given event.

2.6 Conclusions

Plasma wakefield acceleration is interesting because the technique can offer high accelerating gradients. In the AWAKE experiment, we use protons to drive the plasma wakefields, because of the high amount of energy stored in relativistic proton bunches. Unfortunately, short highly relativistic proton bunches are not available, but are needed to drive GV/m wakefields. Thus the AWAKE experiment, that aims to use protons to drive the wakefields, relies on

the seeded self-modulation (SSM) to modulate the long proton bunch from the CERN SPS ($\sigma_z = 12\,\text{cm}$) into micro-bunches spaced at the plasma wavelength ($\lambda_{pe} \sim 1\,\text{mm}$). These micro-bunches then resonantly drive plasma wakefields. The measurements of the two-screen setup, which is the topic of this thesis, aim to show that the SSM developed and to learn about the physics of the SSM by detecting defocused protons (protons defocused by the transverse plasma wakefields).

3 Theoretical Background

3.1 Definition of Plasma

To fullfill the definition of a plasma, the following properties must be satisfied:

- Quasi-neutrality: The number of positive and negative charges must be the same, so that the plasma appears neutral from outside.
- Collective behaviour: The plasma-parameter N_D (N_D is the number of particles within a Debye sphere) is much larger than one.

$$N_D = \frac{4}{3}\pi\lambda_D^3 n_{pe} \gg 1 \tag{3.1}$$

  where $\lambda_D = \sqrt{\frac{\epsilon_0 T_e}{n_{pe}e^2}}$ is the electron Debye length of a plasma with electron density n_{pe}. If a plasma has much more than one particle in a Debye sphere, charges do not only interact with their nearest neighbours but many nearby charges. Consequently plasma waves can exist due to the collective response of the plasma. If the plasma-parameter N_D is much larger than one, the potential of a test charge is radially screened as $e^{-\lambda_D r}$, which is much faster than the $\frac{1}{r}$ scale outside a plasma.
- Electrostatic interactions dominate over ordinary gas kinetics as well as over collisions.

3.1.1 The AWAKE plasma

The plasma is created by ionizing rubidium vapour with a 100 fs and 450 mJ laser pulse focused to $r \approx 1$ mm at the plasma entrance. With these parameters the focused intensity exceeds the ionization appearance intensity for the outermost rubidium electron ($2 \times 10^{12}\,\mathrm{W/cm^2}$). The ionization potential of the outermost electron of the rubidium atoms is 4.12 eV. Both electrons and ions are present in the plasma and the plasma is quasi-neutral. The AWAKE electron plasma density is adjustable from $n_{pe} = 0.5$ to $10 \times 10^{14}\,\mathrm{electrons/cm^3}$.

In the AWAKE plasma the electron temperature is a few eV. For a temperature of 4 eV and $n_{pe} = 7 \times 10^{14}$ electrons/cm^3, the Debye length is approximately 0.6 μm. The AWAKE baseline plasma has on the order of 500 particles in a Debye sphere which is not much larger than 1 (typical plasmas have $\sim 10^5$ particles / Debye sphere). The definition of the electron Debye-length is only meaningful if the plasma electrons have undergone many collisions and reached an equilibrium temperature. In the time-scale (few ns) relevant for AWAKE, the plasma does not reach this thermal equilibrium. The more relevant scale is given by the plasma skin-depth (c/ω_{pe}), because the plasma skin-depth is a measure of the amplitude of the electron oscillations.

3.1.2 Creation of Plasma Wakefields

Highly relativistic proton bunches carry almost purely transverse electric fields. When the proton bunch drives plasma wakefields [1], part of the stored energy can be converted into a longitudinal electric field that can then be used for charged particle acceleration.

AWAKE uses the fields of a relativistic (400 GeV/c) proton bunch to drive the wakefields. As the positively charged drive bunch (in this case the bunch length is short compared to the plasma wavelength) enters the plasma, the surrounding free plasma electrons respond by moving towards the proton bunch (see Figure 3.1). Once the electrons reach the drive bunch axis, they overshoot because of the kinetic energy they gained from the electric field of the proton bunch. After moving away from the proton axis, the electrons are pulled back by the field of the central ion column, because the plasma ions do not move within the discussed time-scales, due to their high mass compared to the electrons.

As a consequence, electric fields are present in the wave because of the separation of charges as indicated in Figure 3.1. The fields in one electron oscillation switch from transversely negative to positive and longitudinally positive to negative for a negatively charged witness bunch. The arrows for the fields in Figure 3.1 correspond to focusing (blue), defocusing (red), accelerating (green) and decelerating (yellow) for negatively charged particles.

[1] fields sustained by a electron plasma density perturbation generated by a charged particle bunch travelling in plasma

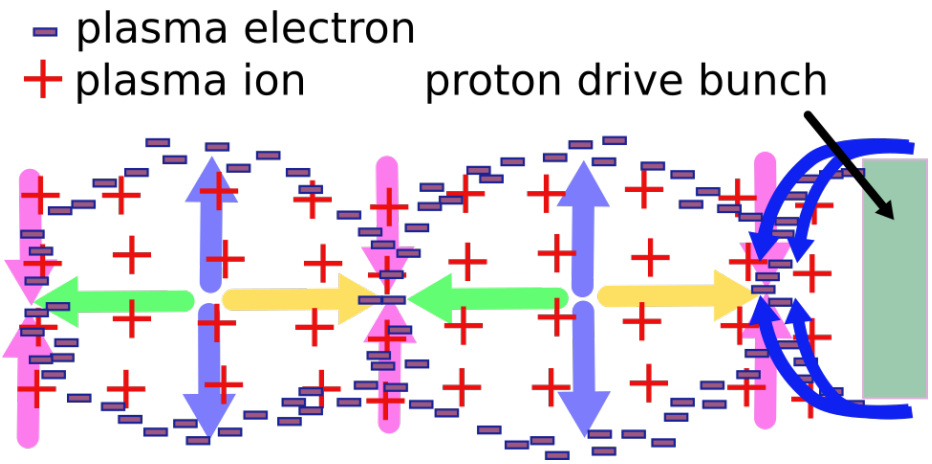

Figure 3.1: Schematic drawing of the charge separation created by a proton bunch. Here, the proton bunch length is shorter than the plasma wavelength. The drawing also shows the plasma wakefield sustained by the charge separation and deduced from simple electrostatic considerations.

The concept of charged particle acceleration by plasma waves works because the drive bunch creates electrostatic waves with an electric field component E in the direction of the wave-vector k ($E \parallel k$) in the plasma [2]. The electrostatic wave phase velocity v_{ph} is equal to that of the relativistic drive bunch ($v_{ph} = v_b \sim c$). Therefore, trailing particles or a witness bunch can gain energy.

3.2 Mathematical Description of Plasma Wakefields

3.2.1 Linear Plasma Wakefield Theory

Linear theory allows us to calculate the wakefields created by a charge distribution as long as the density of the displaced charges n_d is small compared to the total density n_{pe} ($n_d <\sim 0.1 \cdot n_{pe}$). Here I consider the 2D cylindrical case (r,z). I define the longitudinal and radial bunch profile as n_b:

$$n_b(\xi = ct - z, r) = n_{b0} \cdot n_{b\parallel}(\xi) \cdot n_{b\perp}(r) \tag{3.2}$$

[2] It is not possible to use electromagnetic waves in vacuum for particle acceleration in the forward direction because in electromagnetic waves the electric field E is perpendicular to the wave-vector k ($E \perp k$).

where ξ is the position along the relativistic proton bunch moving at ($v_b \simeq c$), n_{b0} is the charge density of the drive bunch, $n_{b\parallel}$ is the longitudinal bunch distribution and $n_{b\perp}$ is the radial bunch distribution, both normalized to one. The longitudinal plasma wakefields (W_z) created by a bunch distribution defined by equation 3.2 can be calculated with [27]:

$$W_z(\xi, r) = \frac{n_{b0}e}{\epsilon_0} \int_{-\infty}^{\xi} n_{b\parallel}(\xi') \cos(k_{pe}(\xi - \xi'))d\xi' \cdot R(r) \tag{3.3}$$

and the radial wakefields (W_r) with:

$$W_r(\xi, r) = \frac{-n_{b0}e}{\epsilon_0 k_{pe}} \int_{-\infty}^{\xi} n_{b\parallel}(\xi') \sin(k_{pe}(\xi - \xi'))d\xi' \cdot \frac{dR(r)}{dr}, \tag{3.4}$$

where R(r) is defined by:

$$R(r) = k_{pe}^2 K_0(k_{pe}r) \int_0^r r' n_{b\perp}(r') I_0(k_{pe}r')dr' + k_{pe}^2 I_0(k_{pe}r) \int_r^{\infty} r' n_{b\perp}(r') K_0(k_{pe}r')dr' \tag{3.5}$$

and $\frac{dR(r)}{dr}$, the derivative of R(r) can be calculated as:

$$\begin{aligned}\frac{dR(r)}{dr} &= k_{pe}^2 K_0(k_{pe}r) r n_{b\perp}(r) I_0(k_{pe}r) - k_{pe}^3 K_1(k_{pe}r) \int_0^r r' n_{b\perp}(r') I_0(k_{pe}r')dr' \\ &+ k_{pe}^2 I_0(k_{pe}r) r n_{b\perp}(r) K_0(k_{pe}r) - k_{pe}^3 I_1(k_{pe}r) \int_r^{\infty} r' n_{b\perp}(r') K_0(k_{pe}r')dr'.\end{aligned} \tag{3.6}$$

The term $R(r)$ defines the radial dependency of the longitudinal wakefields. $R(0)$ is the on-axis value where the longitudinal wakefields are also maximum. The derivative of $R(r)$ ($\frac{dR(r)}{dr}$) shows the radial dependency of the radial wakefields. The radial wakefields are zero on axis by symmetry and have their maximum amplitude around $r = \sigma_r$.

From linear theory, the conditions for the most effective wakefield excitation by a drive bunch with σ_z and σ_r are:

$$k_{pe}\sigma_z = \sqrt{2} \tag{3.7}$$

and

$$k_{pe}\sigma_r = 1, \tag{3.8}$$

with $k_{pe} = \omega_{pe}/c$.

If the drive bunch and the plasma fullfill these conditions, plasma wakefield theory indicates that the accelerating field can reach a significant fraction of the wavebreaking field E_{wb} defined as [28] (called E_{max} in Chapter 2 Equation 2.1):

$$E_{wb} = \frac{m_e c \omega_{pe}}{e}. \tag{3.9}$$

We note that the E_{WB} is the electric field which accelerates an electron to the energy of $m_e c^2$ over a distance of the plasma skin-depth c/ω_{pe}.

3.2.2 Linear Theory Applied to AWAKE - Initial Seed Wakefields

The AWAKE baseline plasma density is chosen to be 7×10^{14} electrons/cm^3 based on the radial proton bunch size at the plasma entrance (σ_r =0.2 mm), which fullfills Equation 3.8. As already discussed in Chapter 2, the optimum bunch length (based on Equation 3.7) for the same plasma density would be 0.3 mm. Since the proton bunch from the SPS has a bunch length of σ_z =12 cm (this is much longer than the plasma wavelength $\lambda_{pe} = 1.2$ mm, and makes $k_{pe}\sigma_z \sim 600$), the initial wakefields reach only MV/m.

To illustrate Equation 3.2 to 3.6 I calculated the longitudinal (W_z) and radial (W_r) plasma wakefields created by a Gaussian proton bunch with a longitudinal size $\sigma_z = 12$ mm, a radial size $\sigma_r = 0.2$ mm and a proton density of $n_{b0} = 4 \times 10^{11}$ protons/cm^3 in a plasma with a density of $n_{pe} = 7 \times 10^{14}$ electrons/cm^3. To speed up the computing time (for the integration) I decided to make the proton bunch a factor ten shorter than the bunch sent to AWAKE by the SPS. However, since I also decreased the charge by a factor of ten (and this calculation is linear), the initial seed wakefields are the same as for the AWAKE baseline parameters. We note that the bunch density n_{b0} is much smaller that the plasma electron density n_{pe} and linear theory does indeed apply at least near the plasma entrance and before the SSM grows.

Figure 3.2 shows that for the AWAKE baseline parameters, the initial seed wakefields are on the order of 5 MV/m for both, the longitudinal (W_z) and transverse (W_r) wakefields. The lower charts in Figure 3.2 show $R(r)$ and $\frac{dR(r)}{dr}$ from Equation 3.5 and 3.6, respectively. Figure 3.2 confirms that the longitudinal wakefields (W_z) are maximum on-axis and that transverse wakefields (W_r) are maximum around σ_r. We also note that the transverse wakefields are glob-

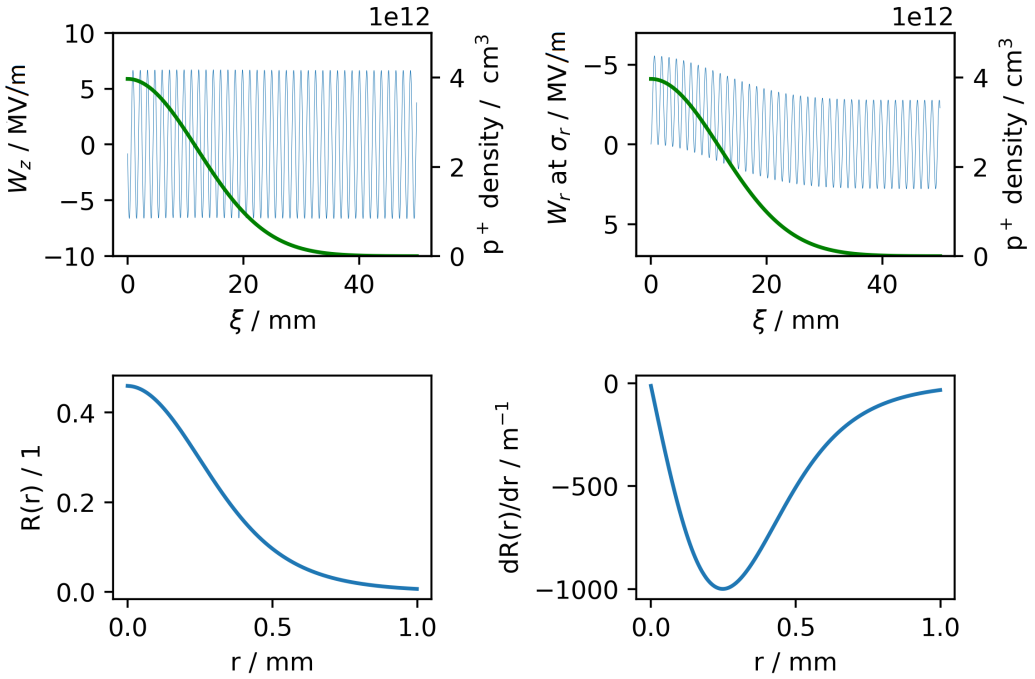

Figure 3.2: Initial radial (at σ_r) and longitudinal plasma wakefields created by a half-cut (in z) proton bunch with $\sigma_z = 12\,\text{mm}$ and $\sigma_r = 0.2\,\text{mm}$ and a plasma density of 7×10^{14} electrons/cm^3. The green line in the top plots indicates the charge density profile and the blue line the created wakefields. Blue lines in the bottom plots show R(r) and $\frac{dR(r)}{dr}$ from Equation 3.5 and 3.6. The head of the half-cut proton bunch is located at $\xi = 0$; the bunch moves to the left.

ally focusing for the proton drive bunch, becoming periodically defocusing only in the back of the bunch (top right chart in Figure 3.2).

Figure 3.3 shows the maximum initial wakefields (longitudinal and transverse) as a function of the plasma density. I observe that the initial transverse wakefields decrease with increasing density, because the plasma skin-depth (c/ω_{pe}) is smaller for larger densities and less drive bunch protons can contribute to the wakefield growth.

The initial longitudinal wakefields increase with higher plasma densities also because of geometric considerations: the field created by the charge separation of the plasma electrons from the plasma ions increases as the distance between the different charges decreases. As the plasma density increases, the plasma wavelength (λ_{pe}) and distance between the charges decreases.

These calculations show that the initial seed wakefields of the 12 cm long

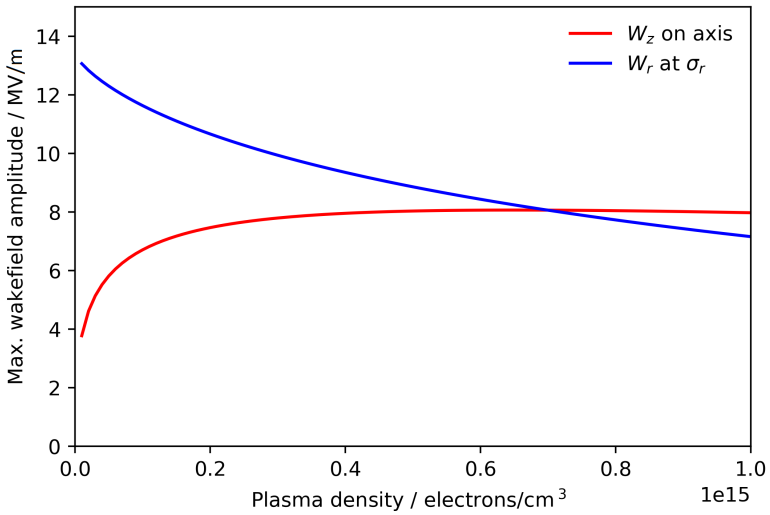

Figure 3.3: Maximum amplitude of the initial wakefields (longitudinal in red and transverse in blue) created by a proton bunch with AWAKE baseline parameters as a function of the plasma density.

proton bunch are only around 5 MV/m. These wakefields strengths are not interesting, since accelerating fields in the mega-volt range are easily achievable with current technology.

3.3 Effective Wakefield Excitation

For baseline parameters, the AWAKE proton drive bunch is much longer than the plasma wavelength ($\sigma_z \sim 12\,\text{cm} \gg \lambda_{pe} \simeq 1.2\,\text{mm}$). To create wakefields with a field strength of GV/m in AWAKE, the experiment relies on the development of the seeded self-modulation (SSM): The transverse wakefields created by the front of the bunch modulate the trailing proton bunch into micro-bunches spaced at the plasma wavelength and satisfy Equation 3.7 and 3.8 to effectively drive wakefields. These micro-bunches then resonantly drive wakefields.

3.3.1 Seeded Self-Modulation

The initial seed wakefields created by the front of the half-cut Gaussian proton bunch (calculated in Section 3.2) co-propagate with the proton bunch and

periodically focus (and defocus) protons. From linear theory we know that the wakefields are proportional to the proton bunch density or inversely proportional to the bunch radius squared. Where the bunch is focused, the proton density increases and so do the wakefields. Stronger wakefields focus the bunch more, which increases the wakefields and provides the feedback loop for the growth. Where the bunch is defocused the contribution to the wakefield decreases. Overall the wakefield amplitude increases and the bunch self-modulates.

This self-modulation can in principle start from noise, i.e. from the random low amplitude wakefields driven by the long proton bunch. To ensure that the long proton bunch self-modulates in the plasma and other competing instabilities like for example the hosing instability [29] [3] do not develop, the self-modulation is seeded. Seeding means generating initial wakefields of larger amplitude than the noise. Calculations [30] show that the wakefield noise amplitude is on the order of 10 kV/m.

The SSM is seeded by overlapping the ionizing laser pulse with the proton bunch. The protons ahead of the laser pulse do only see rubidium vapour and do not interact with it. Due to the sudden turn on of the plasma, the protons after the laser pulse create an initial wakefields amplitude (estimated in Section 3.2.2), from which the SSM grows. Figure 3.3 shows that the seed wakefield amplitude ($E_{0,r} \approx 5\,\mathrm{MV/m}$) is indeed much larger than the noise level.

3.3.2 Growth Rate of the Seeded Self-Modulation

In the linear regime, the growth rate Γ of the SSM along the plasma can be calculated by linear theory [31]. The reference shows that the growth of the wakefields W_r along the plasma (while the seeded instability develops) can be described with:

$$W_r(z) = E_{0,r} \cdot \exp\left(\Gamma z/c\right) \tag{3.10}$$

assuming that the drive bunch velocity is c. The growth rate Γ is given by:

$$\Gamma = \frac{3\sqrt{3}}{4}\omega_{pe}\left(\frac{n_{b0}m_e}{2n_{pe}m_p\gamma}\frac{\xi}{ct}\right)^{1/3} \tag{3.11}$$

[3] oscillations of the beam centroid that can lead to beam breakup

Figure 3.4 shows the growth rate Γ for the first two meters of plasma, for different plasma densities and proton bunch populations. We note that the

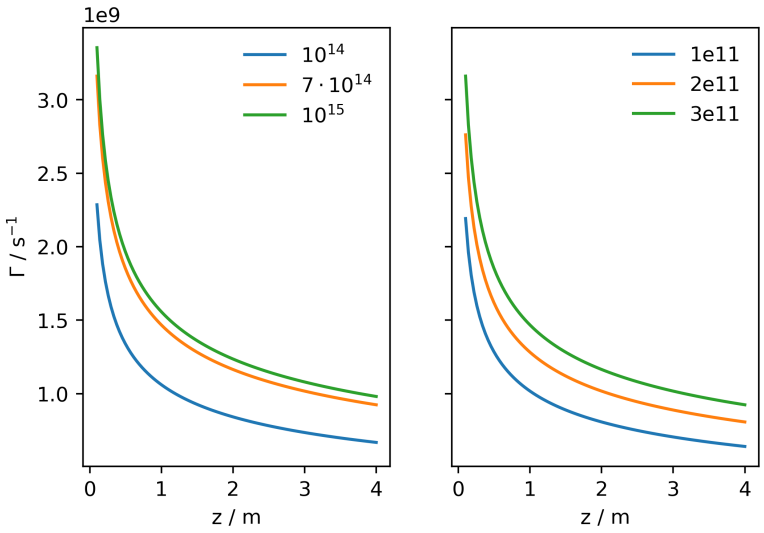

Figure 3.4: Growth rate Γ along the beginning of the plasma for different plasma electron densities n_{pe} in cm^{-3} and 3×10^{11} protons/bunch (left), and for different proton bunch populations (right), for a plasma electron density of 7×10^{14} cm^{-3}.

growth rate of the seeded self-modulation increases for higher plasma electron densities and higher proton bunch bunch populations and decreases along the plasma. The expression for the growth rate Γ (Equation 3.11) is only valid as long as the wakefields are in the linear regime.

3.4 Proton Defocusing due to Seeded Self-Modulation

3.4.1 Longitudinal Motion of the Protons during Seeded Self-Modulation

During the development of the SSM protons experience the accelerating and decelerating longitudinal wakefields, but since the longitudinal momentum (p_z) of the proton bunch is 400 GeV/c the longitudinal momentum change ($\Delta p_z \ll p_z$) is small.

The proton bunch is highly relativistic ($\gamma = 427$) and moves at $\sim 99.99999727\,\%$

of the speed of light. Even if the longitudinal momentum decreases by 10 GeV/c (due to wakefields in the order of GV/m over 10 m), the velocity is still $\sim$ 0.9999999712 c. The velocity change is only 45 m/s. Since the AWAKE plasma is 10 m long, a proton with 400 GeV/c would arrive 1.3 μm ahead or behind one with 390 GeV/c.

Thus, the longitudinal momentum of the proton bunch due to the wakefields does not lead to significant bunching at the scale of the plasma wavelength (λ_{pe}) and over tens of meters.

3.4.2 Transverse Motion of the Protons during Seeded Self-Modulation

The initial transverse momentum of the proton bunch can be calculated from the normalized (ϵ_N) or geometric (ϵ_g) bunch emittance ($\epsilon_N = \gamma\epsilon_g$) and is around σ_{pr} =20 MeV/c, corresponding to a radial velocity of $5 \cdot 10^{-5}$ c or an opening angle of 0.05 mrad. From the simulation shown in Chapter 4, I expect that the maximum defocused protons gain up to 400 MeV/c transverse momentum (opening angle of 1 mrad), which corresponds to a velocity of 10^{-3} c or a displacement of several milli-meter over a longitudinal distance of 10 m. This means that the radial velocity of the proton changes from $\sim$ 15 km/s to $\sim$ 300 km/s.

I estimate the order of magnitude of the defocusing angle as follows: assuming that the initial radial proton bunch momentum is negligible, the maximum defocusing angle θ is defined as :

$$\theta = \frac{\Delta p_r}{p_z} \tag{3.12}$$

where Δp_r is the change of radial momentum acquired during interaction along the plasma and p_z the longitudinal momentum. The total transverse force $\vec{F}_r/c = (\vec{E}_r + \vec{v}_b \times \vec{B}_\theta)$ are due to: $\vec{E}_r$, the radial component of the wakefield's electric field caused by charge separation and $\vec{B}_\theta$, the azimuthal B-field created by the plasma electron motion.

Under the influence of an electric field E_r, protons move according to Newton's equation:

$$\frac{\Delta p_r}{\Delta t} \approx eE_r \Rightarrow \Delta p_r \approx eE_r\Delta t \tag{3.13}$$

with Δt being the time that the particle takes to travel the transverse distance Δr. In this particular case Δp_r is due to transverse wakefields W_r, which can reach a fraction of the wavebreaking field E_{WB} (the maximum electric field that can be generated at a given plasma density) (see Equation 3.9).

Assuming that the transverse electric field reaches a significant fraction of the wavebreaking field, let us say $E_r = E_{WB}/2$ (simulations show that $E_{max} < E_{WB}/2$) and using $\Delta r/\Delta z \sim \Delta p_r/p_z$, Δt, the time that a defocused proton interacts with the wakefield, can be estimated as:

$$\Delta t \sim \sqrt{\frac{p_z}{eE_r}\frac{\Delta r}{c}} \tag{3.14}$$

with Δr being the extend of the transverse wakefields. In this calculation I estimate the plasma channel width to be $\sim 2\,c/\omega_{pe}$. Combining Equation 3.14 with Equation 3.12, Equation 3.13, $p_z = \gamma m_p c$ and assuming that the proton bunch moves with the speed of light, the following defocusing angle θ can be obtained:

$$\theta = \frac{\Delta p_r}{p_z} \sim \sqrt{\frac{m_e}{\gamma m_p}}. \tag{3.15}$$

Using the AWAKE parameters (400 GeV/c, $\gamma = 427$), the maximum defocusing angle θ is estimated to be ~ 1 mrad. Note that according to this estimate the maximum angle of the defocused protons does not depend on the plasma density, provided that the wakefield amplitude reaches the same fraction of E_{WB} (Equation 3.9), also independently of the plasma density.

3.5 Conclusions

Using linear plasma wakefield theory, I can estimate the strength of the initial seed wakefields of the AWAKE proton bunch to be on the order of 5 MV/m. To be able to create wakefield amplitudes on the order of hundreds of MV/m or GV/m, AWAKE has to rely on the development of the seeded self-modulation (SSM) to modulate the proton density on axis, by transverse motion of the protons. After the proton bunch modulated, each micro-bunch contributes resonantly to the wakefield growth, and drives large wakefield amplitudes over long distances.

I estimate the growth rate Γ of the SSM from linear theory and show that it is higher for larger plasma densities and a higher proton bunch population.

If the SSM develops successfully in the 10 m of plasma, I expect to measure maximum defocusing angles on the order of 1 mrad.

4 Seeded Proton Bunch Self-Modulation Simulation Results

4.1 LCODE

To simulate the interaction of the proton and electron bunches with the plasma, we use the quasi-static particle-in-cell code LCODE. The usage and underlying physics of the simulation code is described in detail in [32, 33, 34]. The simulations are performed in a 2D-cylindrical (r,z) coordinate system. However, the momentum of the particles is computed in 3D (p_r,p_θ,z). Thus the term 2d3v is sometimes used. This means that by definition 3D effects cannot occur. Furthermore, in our simulations we sometimes assume that the ions are immobile. This is justified because the rubidium ion mass ($m_i \approx 10^{-25}$ kg) is large compared to the mass of the plasma electrons ($m_e = 9.1 \times 10^{-31}$ kg). Therefore the ions do not respond to the wakefields over the relevant time-scales: the relevant time-scale for plasma wakefields is given by the electron oscillation period $\tau_e = 1/\omega_{pe}$. Since the plasma electron frequency is proportional to the inverse square root of the electron mass ($\omega_{pe} \sim m_e^{-\frac{1}{2}}$), the electron oscillation period is proportional to the electron mass ($\tau_e \sim m_e^{\frac{1}{2}}$). The ions respond on a time-scale of the ion plasma frequency $\omega_{pi} \sim m_i^{-\frac{1}{2}}$. Thus the ion oscillation period $\tau_i = \left(\frac{m_i}{m_e}\right)^{1/2} \tau_e \gg \tau_e$ is much larger than the electron oscillation period. Please note that in a neutral plasma, where the electron density is equal to the ion density ($n_e = n_i$) and the ions are singly ionized ($Z_c = 1$) the ion plasma frequency ω_{pi} is defined as:

$$\omega_{pi} = \sqrt{\frac{n_i Z_c^2 e^2}{\epsilon_0 m_i}} = \sqrt{\frac{n_e e^2}{\epsilon_0 m_i}} = \omega_{pe}\sqrt{\frac{m_e}{m_i}} \ll \omega_{pe}. \tag{4.1}$$

4.1.1 From 2d3v Cylindrical Simulations to 3D coordinates

Even though the simulations are 2D cylindrical, I can calculate the horizontal x and vertical y particle positions as shown in this Section. Thus, sometimes I choose to plot simulation results against the horizontal and vertical coordinates instead of the radius.

The output parameters from the LCODE simulations include the following parameters for each particle:

- r the proton radial coordinate
- z the proton position in the plasma along the bunch axis
- t the propagation time in plasma
- $\xi = z - ct$ the longitudinal protons position along the bunch ($\xi = 0$ is the front of the bunch and the turn on of the plasma)
- p_z the longitudinal momentum
- p_r the transverse momentum
- p_θ the azimuthal momentum

Instead of the radius and the momenta I would like to have the horizontal and vertical coordinate (x, y) as well as the particles momentum along those coordinate axes (p_x, p_y).

It turns out that it is possible to get these parameters out of the simulation output with only one unknown value, the initial azimuthal position of the proton (ϕ_0). I assign ϕ_0 a random value from a uniform distribution from $(0, 2\pi]$. Then we can calculate the horizontal x and vertical y position according to:

$$x = r \cdot \cos(\phi) \text{ and } y = r \cdot \sin(\phi) \tag{4.2}$$

since p_r and p_ϕ are defined as:

$$p_r = (p_x x + p_y y)\frac{1}{r} \text{ and } p_\phi = (-p_x y + p_y x)\frac{1}{r} \tag{4.3}$$

we can calculate p_x and p_y as:

$$p_x = \frac{x p_r - y p_\phi}{r} \text{ and } p_y = \frac{x p_\phi + y p_r}{r}. \tag{4.4}$$

We additionally know that:

$$v_x = \frac{dx}{dt} = \frac{p_x}{\gamma m_p} \text{ and } v_y = \frac{dy}{dt} = \frac{p_y}{\gamma m_p}. \tag{4.5}$$

The next step can then be calculated as:

$$x_i = x_{i-1} + dx \text{ and } y_i = y_{i-1} + dy \tag{4.6}$$

where dx and dy are:

$$dx = v_x \cdot dt \text{ and } dy = v_y \cdot dt. \tag{4.7}$$

The azimuthal position of the next step is calculated with:

$$\phi_i = \tan\left(\frac{y}{x}\right) \tag{4.8}$$

and used to calculate the x and y coordinates of the next time-step.

4.2 Baseline LCODE Simulations of the Self-Seeded Modulation

Using LCODE, we simulate the development of the seeded self-modulation (SSM) for the AWAKE baseline parameters (see Chapter 2, Table 2.1). The half-cut proton bunch propagates the plasma with a uniform density of 7×10^{14} electrons/cm^3.

Figure 4.1 shows the evolution of the proton bunch density after a propagation of 0.2, 2, 4, 6, 8 and 10 m into the plasma.

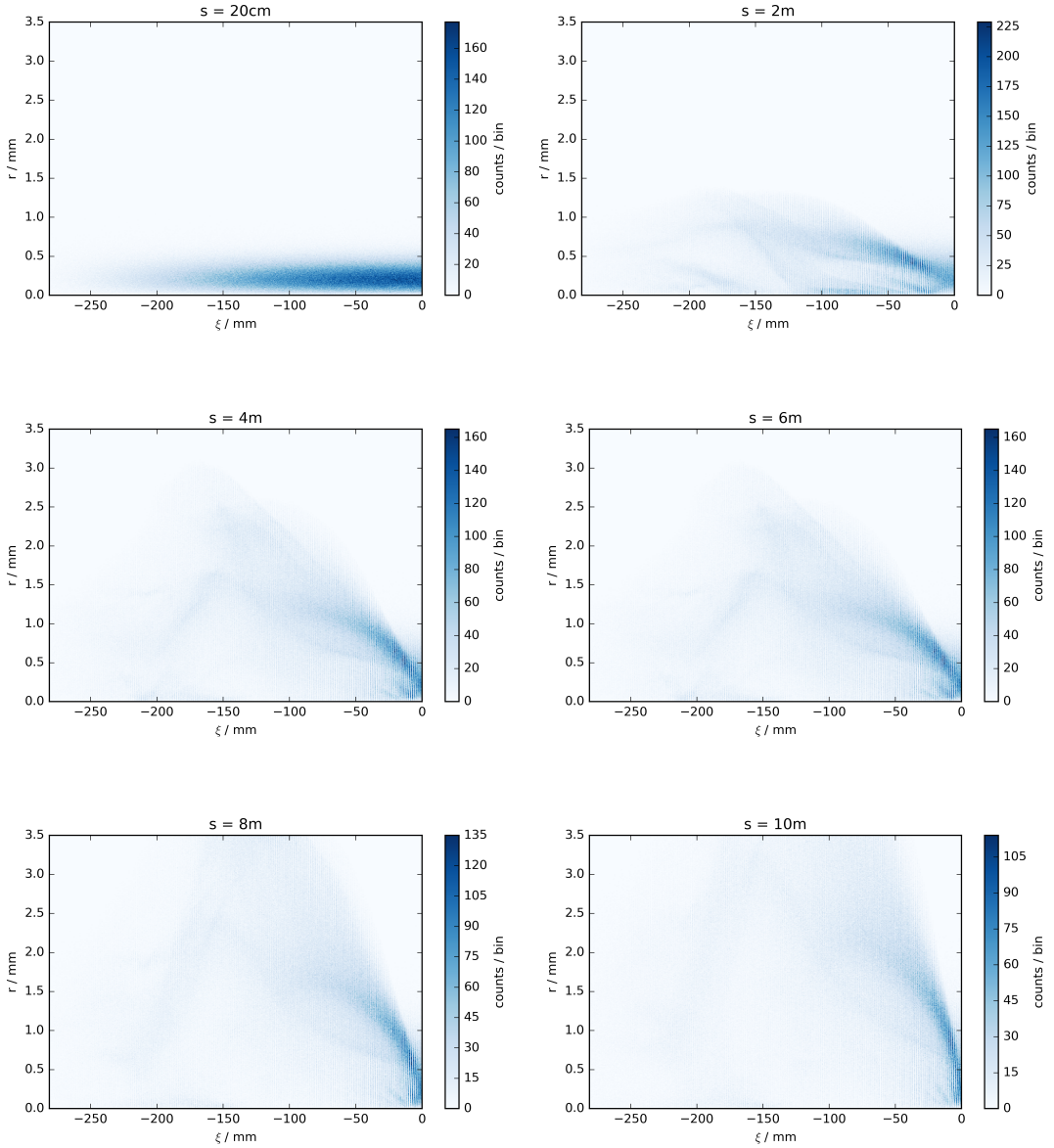

Figure 4.1: Development of the SSM over 10 m of plasma with a plasma density of 7×10^{14} electrons/cm^3. Proton bunch distribution in a window of $\sim 3.5 \times 300\,\mathrm{mm}^2$, where $\xi = 0$ is the head of the cut proton bunch; the bunch moves to the right.

The density plots in Figure 4.1 show the results from a 2d3v cylindrical simulation and each horizontal pixel-line reflects the amount of charge at one set radius, corresponding to a cylinder shell. The displayed proton density decreases close to the axis because the number of protons per ring area ($2\pi rdr$) decreases towards the axis as the radius r becomes small.

Close to the plasma entrance (0.2 m into the plasma) the proton bunch profile is still Gaussian, as delivered by the CERN SPS. This is because the wakefields driven by the bunch have not yet affected its density.

As a reminder, the first half of the proton bunch does not interact with the plasma and is not shown. The plasma is preformed with a radius of 1 mm (not shown) in Figure 4.1.

As the proton bunch propagates further into the plasma, the initial seed wakefields created by the sharp front of the half-cut Gaussian bunch (see Chapter 3) act back on the proton bunch itself. The protons either experience a focusing or a defocusing force and move in the transverse direction creating regions of lower and higher on-axis proton density. This proton density modulation starts the growth. The defocused protons appear as a transverse increase of bunch radius starting from the second panel (2 m into the plasma) in Figure 4.1. The protons that experience focusing fields form the micro-bunches near the axis. We note that with the AWAKE baseline parameters and the selected field of view ($\sim$ 30 cm) of these simulations, the number of wakefield periods along the bunch is large ($\sigma_z = 12$ cm, $\lambda_{pe} = 1.2$ mm) and the periodic structure of the modulation is only visible on the zoomed images of Figure 4.2.

The transverse proton bunch size increases the further the proton bunch propagates in the plasma. As long as the SSM grows, the amplitude of the wakefields increases and protons experience stronger focusing and defocusing fields. During the development of the SSM, the phase of the wakefields along the bunch changes because of the evolution of the proton bunch distribution (the wakefields at a given point ξ are determined by the proton distribution ahead of ξ). I observed in simulations that after the SSM saturates (when there are no more protons in the defocusing phase of the wakefields), the wakefields amplitude decreases because the phase of the wakefield keeps changing and part of the protons that used to be in the focusing phase experience defocusing fields. Thus the amount of charge that drives the wakefields decreases. Also,

the distribution of protons experiencing decelerating fields (contributing to the wakefields) and experience accelerating fields (extracting energy from the wakefields) evolves.

The transverse size of the plasma in simulations ($r \approx 1\,\mathrm{mm}$) as well as the wakefields ($\approx 5\,c/\omega_{pe}$) are finite. After the defocused protons leave the wakefields radially, their trajectories are straight lines. The earlier the protons experience the maximum defocusing fields and the larger the radial momentum change, the larger the radius of the protons downstream the plasma.

The radius of the defocused protons in Figure 4.1 also shows that the transverse proton bunch size (and the strength of the plasma wakefields) increases along the proton bunch, reaching a maximum around $\xi \sim \sigma_z = 12\,\mathrm{cm}$.

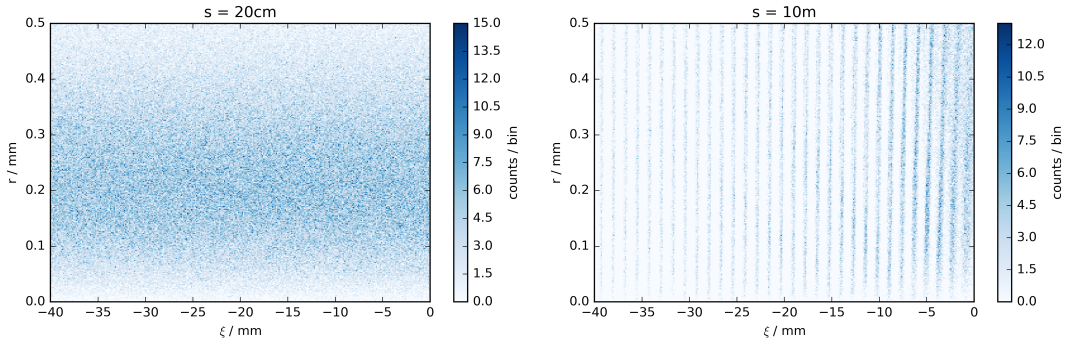

Figure 4.2: Proton distribution at the plasma entrance (left) and after 10 m of plasma. The images are zoomed in near the axis and beginning of the half-cut proton bunch.

Figure 4.2 shows the difference of the proton bunch density near the axis in the beginning of the plasma and at the end, zoomed into the front of the bunch (showing the first 4 cm of the half-cut proton bunch and radially up to 0.5 mm).

The left panel of Figure 4.2 shows the Gaussian proton bunch density 20 cm into the plasma. The density distribution looks uniform along the proton bunch for this field of view (4 cm of the bunch with a rms length of $\sigma_z = 12\,\mathrm{cm}$). The right panel shows the density profile after 10 m of interaction in plasma, where the density modulation at the plasma wavelength (formation of micro-bunches) is clearly visible.

It is important to note that the motion of the protons during the development of the SSM is purely transverse, because the protons are highly relativistic. Even though plasma wakefields change the longitudinal and transverse momentum of the protons, only transverse velocity change is significant over meter distances (see Chapter 3, Section 3.4).

Figure 4.1 and 4.2 show that the formation of micro-bunches spaced at the plasma wavelength ($\lambda_{pe} = 1.2\,\text{mm}$) as well as proton defocusing are consequences of SSM. The formation of micro-bunches occurs because the wakefield amplitude is proportional to the density modulation on-axis and the wakefield amplitude can only grow if the density modulation increases. Proton defocusing occurs because as I established earlier, the motion of the protons during SSM is only transverse and not longitudinally. In between micro-bunches there are regions of lower proton density and the only way for the protons to leave these region is by moving radially outwards. Hence, the experimental observation of micro-bunches as well as defocused protons is evidence for proton self-modulation.

4.3 Defocused Protons

4.3.1 Origin of Defocused Protons

Some protons experience a transverse defocusing force from the plasma wakefields. The angle with which they exit the wakefields depends on their total radial momentum. The total radial momentum after the proton exits the plasma is a sum of the initial transverse momentum from the bunch emittance plus the average wakefield strength multiplied by the interaction distance (or time) of the proton with the wakefield.

The blue line in Figure 4.3a) shows the transverse wakefields that a strongly defocused proton experiences. The total transverse force acting on the proton $\vec{F}_r$ per charge q is:

$$\frac{\vec{F}_r}{q} = \vec{E}_r + \vec{v}_b \times \vec{B}_\theta, \tag{4.9}$$

with $v_b \approx c$:

$$\frac{\vec{F}_r}{q} = \vec{E}_r - c\vec{B}_\theta, \left(\frac{\vec{F}_r}{q} = \vec{E}_r - \vec{B}_\theta \text{ in CGS normalized units}\right). \tag{4.10}$$

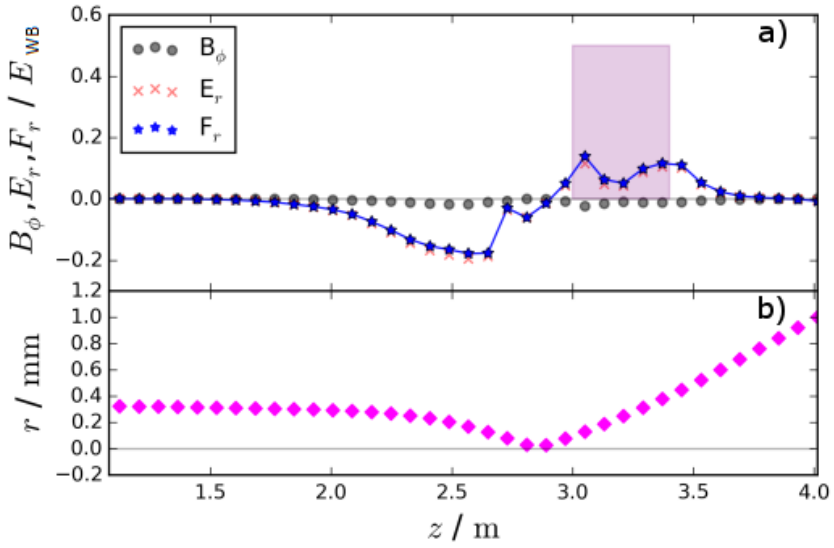

Figure 4.3: (a) Fields and the transverse force acting on the maximum defocused proton as a function of the longitudinal position z along the plasma. The pink are indicates the field ($0.5\,E_{WB}$) and interaction distance that I used for the order of magnitude estimate of the maximum defocusing angle in Chapter 3, Section 3.4.2. (b) The radial proton r position as a function of z.

Simulations show that the proton deflection results mainly from the radial electric field E_r while the azimuthal magnetic field B_ϕ contributes approximately ten-times less (see Figure 4.3).

The proton shown in Figure 4.3 first experiences a focusing force and moves towards the bunch-axis. There are no transverse wakefields on the axis, the proton crosses the axis. Then the proton enters defocusing wakefields (as the SSM develops the wakefield change its phase) and experiences a defocusing force. Our simulation results confirm that this kind of trajectory is typical for strongly defocused protons.

The wakefields that the proton experiences along the plasma are shown in Figure 4.3. They shift from the focusing to the defocusing phase of the wake, while the proton's longitudinal position ξ within the bunch remains the same. The wakefield at this ξ-position is determined by the protons distribution ahead in the bunch. Since the shape of the proton bunch evolves during SSM, the phase of the wakefield changes as well. The phase shift is an accumulated effect that increases along the proton bunch.

Simulations show that in general protons exciting the wakefields with the

largest defocusing angle come from the back of the bunch ($\xi \approx \sigma_z$). They are also in the focusing phase of the wakefields at the beginning of the plasma. Because of the phase shift of the wakefields, later on they find themselves in the large amplitude defocusing phase of the wakefields where they acquire their large momentum. As a consequence, the number of protons in the decelerating focusing phase decreases towards the end of the proton bunch and the wakefield amplitude saturates.

In Chapter 3, Section 3.4.2 I made an estimate showing that the maximum defocused protons experience a transverse field of approximately half the wavebreaking field over a radial distance of $2c/\omega_{pe}$ (corresponding to 40 cm longitudinal distance) resulting in a maximum defocusing angle around 1 mrad (see pink box in Figure 4.3). In simulations I observe that the average transverse wakefield is approximately four times weaker ($0.15\, E_{WB}$), but the interaction distance is about four times longer (1.6 m). So in total, the defocused proton gains the same radial momentum of 400 MeV corresponding to a maximum defocusing angle of 1 mrad.

4.3.2 Simulated Transverse Proton Bunch Profiles for AWAKE

To estimate the transverse proton bunch profiles and the maximum defocusing radius at the two imaging stations in AWAKE, I use the simulated proton positions and velocities of the self-modulated proton bunch after 10 m of plasma (shown in Figure 4.1) and track the protons flying ballistically until the first IS ($\sim$2 m) and second IS ($\sim$10 m) in vacuum.

Figures 4.4 and 4.5 show the predicted transverse proton bunch distributions on a linear and logarithmic scale at the location of the two imaging station (IS 1 and IS 2) for plasma densities 1,3,5 and 7×10^{14} electrons/cm^3, as well for when no plasma is present. All simulations are for a Gaussian 400 GeV/c proton bunch with 3×10^{11} protons/bunch, a proton bunch length of $\sigma_z = 12$ cm and seeding at the center of the bunch. The protons ahead of the laser pulse that are not included in the simulations were added to the Figures. They propagate according to the bunch parameters (σ, ϵ).

Figure 4.4 and 4.5 clearly show the presence of defocused protons (protons with a radius larger than $\sim 3\sigma_r$) in the form of wings next to the proton

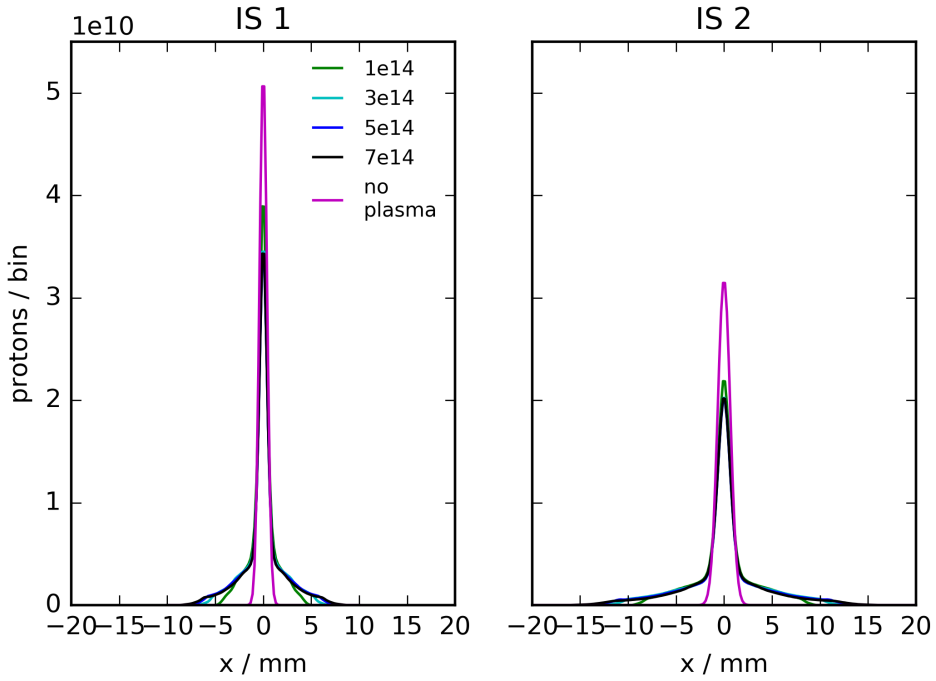

Figure 4.4: Self-modulated transverse proton bunch profiles at the two imaging station for 1,3,5 and 7×10^{14} electrons/cm^3 as well for no plasma. Only projections in the x-directions are shown. The y-projections are identical by cylindrical symmetry. The bin size is $(0.2 \times 20)\,\mathrm{mm}^2$.

bunch core. The maximum radius of the defocused protons varies from ~ 5 to $\sim 8\,\mathrm{mm}$ on IS 1 and ~ 10 to $\sim 16\,\mathrm{mm}$ on IS 2. Even though the transverse proton bunch distributions look similar for different plasma densities, the difference between plasma and self-modulation and without plasma is clearly visible.

The number of protons per bunch must be (and is) conserved. As protons are defocused, the peak value of the intensity of the proton bunch core decreases. In these simulations, the front half of the Gaussian bunch propagates in rubidium vapour, only the second half self-modulates in the plasma. These protons propagating in vapour are again included in the profiles. Figure 4.4 shows that I expect the maximum proton bunch core amplitude to decrease by roughly 20-25 % depending on the plasma density.

Figure 4.6 shows the expected time-integrated transverse proton bunch distribution at the location of the two IS on a logarithmic scale. The charts show the proton bunch density as I expect to measure them on the cameras of

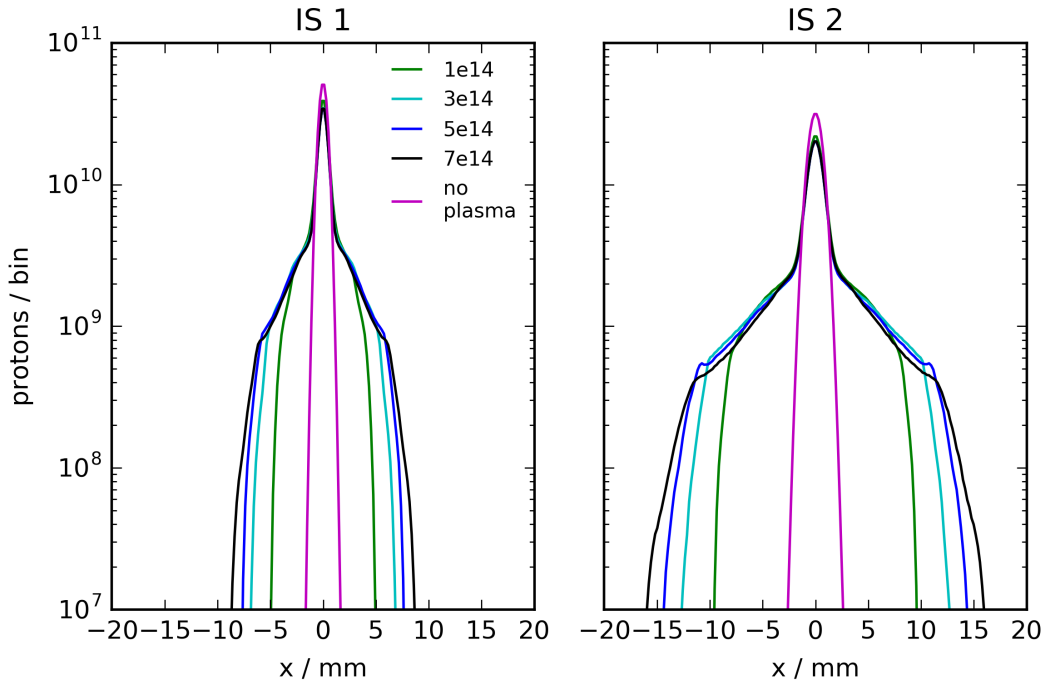

Figure 4.5: Self-Modulated transverse proton bunch profile at the two imaging station in a log scale for 1,3,5 and 7×10^{14} electrons/cm^3 as well for no plasma.The bin size is (0.2×20) mm^2.

the IS.

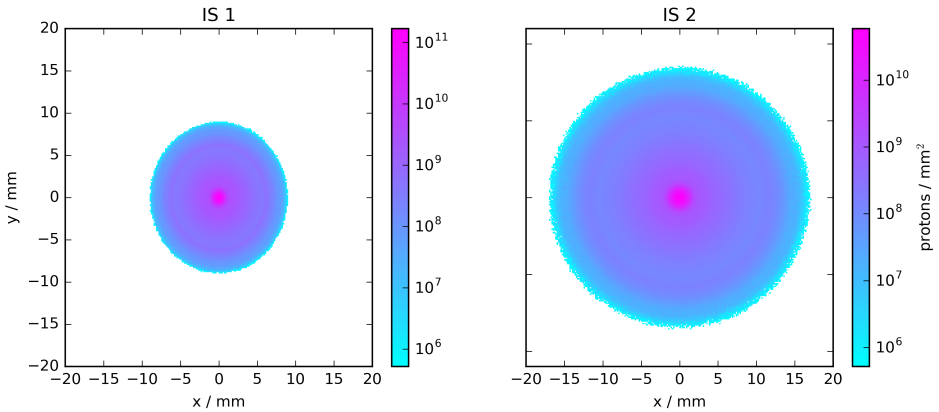

Figure 4.6: Expected transverse proton bunch profile on IS 1 and IS 2 for proton bunch self-modulation with a plasma density of 7×10^{14} electrons/cm^3 on a logarithmic scale.

The results presented in this Section show that in simulations, SSM at various densities leads to a maximum radius of the proton bunch distribution

(at two locations downstream from the plasma (IS 1,2)) that increases with increasing plasma density. Results also suggest that there is a sharp drop in proton density up to the maximum proton defocusing radius.

4.4 Proton Density Evolution along the Plasma

Figure 4.7 shows a density plot of the proton bunch evolution inside ($0 \leq z \leq 10\,\mathrm{m}$) and outside of the plasma ($z > 10\,\mathrm{m}$). The plasma density is $n_{pe} = 7 \times 10^{14}\,\mathrm{electrons/cm^3}$. Protons start leaving the wakefields after about 3 m of plasma and then continuously until the end (10 m). They form a radially continuous distribution at the two IS with an on-axis core surrounded by a halo with a well defined radius (also see Figure 4.6).

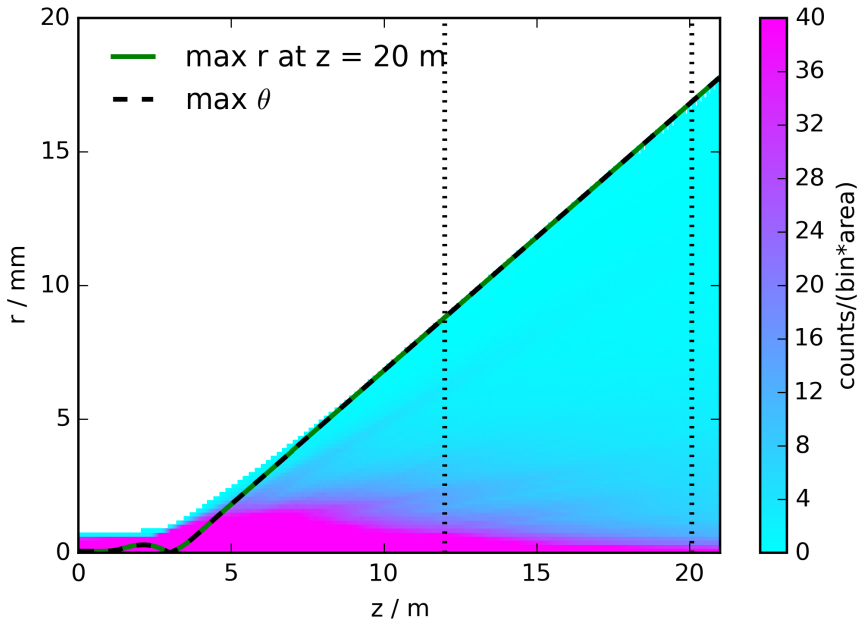

Figure 4.7: Proton bunch density evolution for a plasma density of $n_{pe} = 7 \times 10^{14}\,\mathrm{electrons/cm^3}$. The plasma starts at $z = 0$ and ends at $z = 10\,\mathrm{m}$. The two screens (IS 1 at 12 m and IS 2 at 20 m) are marked by vertical dashed lines.

We see that the outermost particle (I chose the proton with the maximum radial position at $z = 20\,\mathrm{m}$) has the maximum radius at both imaging stations (at $z = 12$ and $20\,\mathrm{m}$), a straight trajectory, and consequently the maximum defocusing angle θ. We previously determined [35] (attached in the Appendix) that we expect to see this behaviour for plasma densities larger than

5×10^{14} electrons/cm^3 (and baseline proton bunch parameters). Simulations show that, below a plasma density of 5×10^{14} electrons/cm^3 the outermost protons on IS 1 are not necessarily the outermost on IS 2 and thus neither the maximum defocusing angle, nor the point of origin can be calculated from the measurement of the maximum radii.

In the experiment -if the outermost protons on IS 1 are the outermost protons on IS 2- I measure the maximum radial proton positions at the two locations downstream the plasma, calculate the maximum proton momentum and estimate where the protons exit the wakefields (see Chapter 6, Section 6.3). To understand whether the calculation of the maximum defocusing angle is justified in the experiment, we will compare the measurement results to simulation results.

The protons transverse momentum change Δp_r is the product of the radial wakefield strength (W_r) times the interaction distance ($\Delta p_r = \int W_r(z) \cdot dz$).

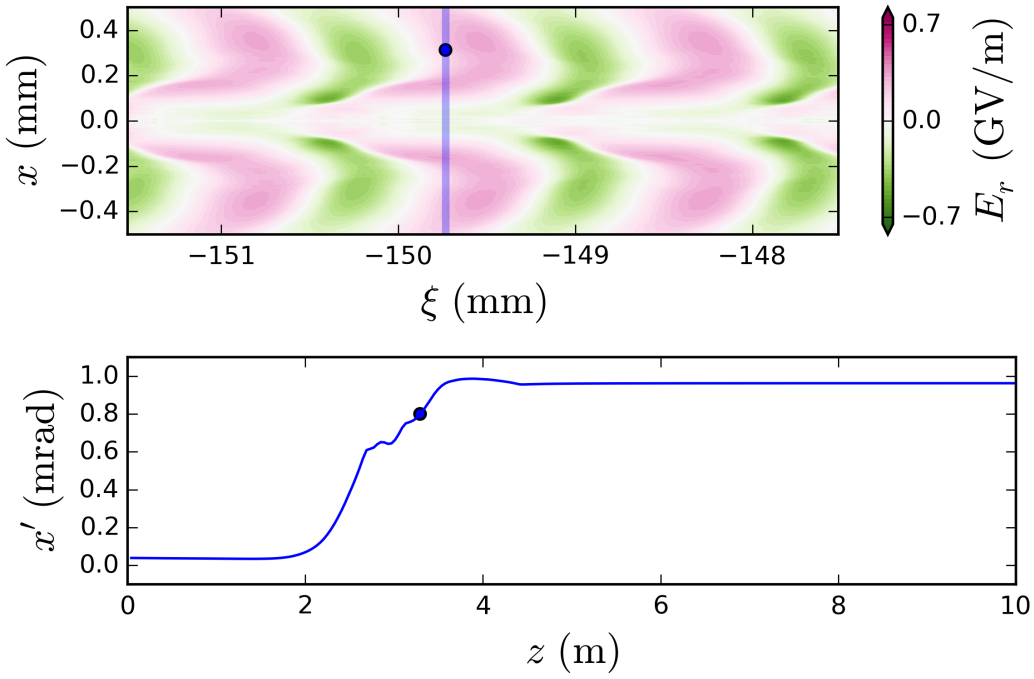

Figure 4.8: Top: a strongly defocused proton gaining transverse momentum from the radial electric fields. The blue line indicates its position along the plasma and is meant to show that the proton does not move along the bunch (ξ). Bottom: angle of the defocused proton along the plasma.

The top chart of Figure 4.8 shows a proton (that will be strongly defocused

after 10 m of plasma) on top of the transverse plasma wakefields amplitude map ≈3.3 m into the plasma. Green areas show focusing and pink areas defocusing wakefield amplitudes. From this point on, the proton moves transversely to larger x-values. The proton does not move longitudinally and stays at the same ξ location (on the blue line).

The lower chart of Figure 4.8 shows the angle of the proton along the 10 m of plasma. We note that the angle is constant and small up to approximately 2 m into the plasma. In this region, the wakefields amplitude is low (near its seeding value) and the proton experiences a weak transverse field. Then the angle increases up to 4 m into the plasma, where it also reached the maximum value and radially exits the wakefields. Once the proton exits the wakefields, the defocusing angle remains constant all the way to the two IS.

4.5 Conclusion

We use the code LCODE to simulate the interaction of the proton bunch with the plasma. Using simulation results, I study the development of the seeded-self-modulation and the resulting proton defocusing. We conclude that the appearance of proton defocusing is a necessary condition for self-modulation, and that the defocused protons gain a large transverse momentum ($\gg \epsilon_g/\sigma_r$) from the transverse plasma wakfields. We expects that when the SSM develops and saturates along the plasma, the protons with the maximum transverse momentum travel after the plasma with an angle of around 1 mrad.

5 Two-Screen Measurement Setup

This Chapter describes the two-screen measurement setup integrated in the AWAKE experiment. I focus on the design choices of the two imaging stations (IS) downstream of the plasma, as well as on the realization of the system.

The first two-screen measurement setup was commissioned in September and October 2016 and was used for the December 2016 measurements. The setup is described in detail in [36]. The paper is attached in the appendix. We identified several limitations of the system [37], also attached in the appendix.

To overcome these limitations, the system was upgraded between January and May 2017 and used for the June/September 2017 measurements. In this Chapter I only discuss the upgraded two-screen measurement setup, since all the results presented in Chapter 6 were performed with this setup.

5.1 Two-Screen Measurement Requirements

We installed two imaging stations IS 1 and IS 2, two and ten meters downstream the AWAKE plasma, respectively, and use the two imaging stations to study the properties of the seeded self-modulation. The setup shall perform the following measurements:

- Image the maximum proton bunch radius: The protons with the largest radial position [1] can be detected at each imaging station. From the proton bunch edge and the distance between the stations I then calculate the maximum defocusing angle.
- Reconstruct the origin of the defocused protons: From the measurement of the radial proton bunch edge at both IS I can determine -by backtracking- where the protons radially exited the plasma wakefields.

[1] the expected minimum proton density for the protons with the largest radius is around 10^5 protons/mm^2, see Chapter 4

- Estimate the amount of defocused charge: Analysing the transverse proton bunch distribution gives information about the amount of charge in the defocused part of the bunch.

5.2 Realization of the Two-Screen Setup

Apart from the cameras and the optical components, the imaging stations IS 1 and IS 2 consist of a scintillating screen mounted onto a motorized rotatable screen-holder and a stainless steel vacuum vessel. The motorized screen-holder allows us to remotely move the scintillating screen in and out of the proton bunch path. The installed screen consists of the scintillating material Chromox (Al_2O_3:CrO_2). Chromox was chosen based on screen tests performed in CERN's HiRadMat facility (see Section 5.4).

As the proton bunch traverses the scintillating screen, the bunch particles deposit energy in the screen material. Part of this energy excites atoms in the screen, which then de-excite by emitting photons in the visible range, uniformly over 4π. The light output is proportional to the deposited energy (i.e. to the number of protons per bunch, further discussed in Section 5.5.3).

The screen is installed in vacuum, part of the light emitted by the screen exits the vacuum vessel through a vacuum window. After the window, I put optical components to image the emitted light onto a camera. Looking at these images enables me to measure the transverse (time-integrated) proton bunch distribution.

Figure 5.1 shows the beam-line downstream the plasma, including the vacuum vessels of the two imaging stations. Figure 5.2a shows a photo of IS 1 and Figure 5.2b a photo of IS 2.

The design of imaging station IS 1 and IS 2 is challenging because simulations results indicate that after self-modulation the transverse proton bunch density ranges over four to five orders of magnitude (see Section 4.3.2). However, the dynamic range of cameras is typically around two to three orders of magnitude.

When I adjust the exposure time of the camera as well as the attenuation filters to measure the core of the proton bunch without saturation of the camera, I expect to be blind to most of the defocused proton bunch, which has much lower density and light yield. To image the defocused protons I

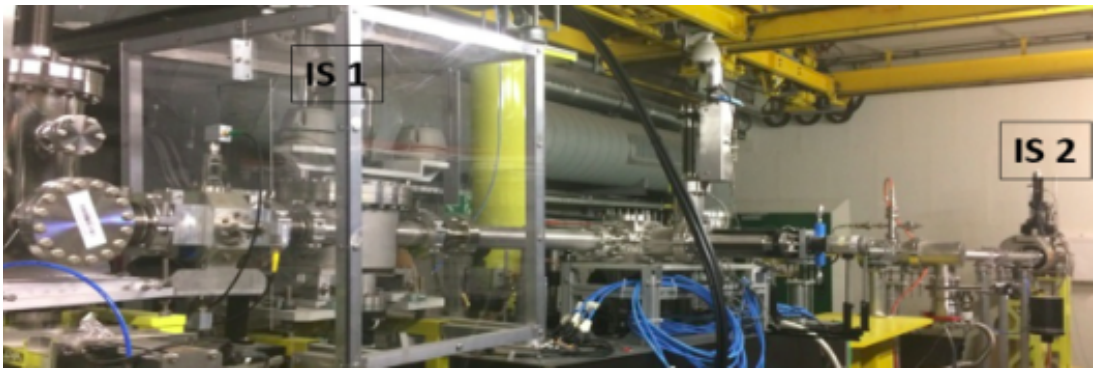

Figure 5.1: Photograph of the AWAKE diagnostics section located downstream of the vapour source (the vapour source is located out of the photo on the left hand side). The protons come from the left hand side. The two imaging stations are marked with IS 1 and 2.

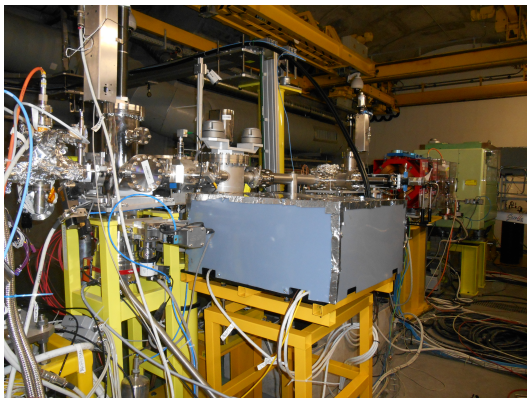

(a) Photograph of IS 1 in the tunnel. The protons come from the left hand side. The optics components are installed under the box.

(b) Photograph of IS 2 in the tunnel. The protons come from the right hand side. The optics components are installed under the box.

therefore need to block the light emitted by the bunch core, e.g. with a mask.

5.3 Optical Setup

A schematic of the optical system for IS 1 is shown in Figure 5.3. The layout for IS 2 is similar.

The light emitted by the scintillating screen exits the vacuum vessel (not shown). The light is then split with a 3 inch pellicle beam splitter that reflects 8% and transmits 92% of the light.

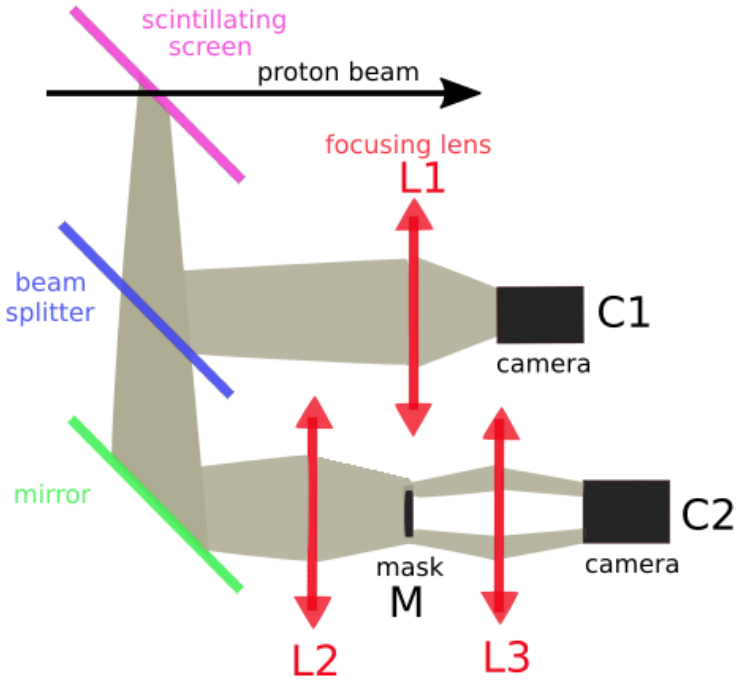

Figure 5.3: Schematic of the optical setup of the imaging system of IS 1. The optical layout for IS 2 is similar.

5.3.1 Core Camera

The light reflected by the beam splitter is directly imaged onto the core camera C1 by the lens L1 (2 inch, f=75 mm). The image of camera C1 provides information about the size and position of the bunch core.

At both imaging stations, the cameras (C1) directed at the proton bunch core (imaging the light reflected by the beam splitter) are analogue cameras with an interlaced video feed. These types of cameras are used due to their good performance in radiation environments. The camera and readout system is described in [38]. Each camera is equipped with a camera lens (C1) and a filter wheel (not shown in Figure 5.3) with four filter positions. The filters were chosen to be transmitting 100 to 0.01 % of the light on both IS.

5.3.2 Defocused Proton Camera

The light transmitted by the beam splitter is imaged by lens L2 (2 inch for IS1 and 3 inch for IS 2, f=200 mm) onto the plane M, where the mask is placed. An opaque disk functioning as the mask blocks the intense light that comes from

the bunch core. A technical drawing of the mask setup is shown in Figure 5.4. The mask is re-imaged by lens L3 (2 inch, f=75 mm) onto camera C2.

The distance between the imaging screen and the first lens (L2) for the defocused proton measurement is 60 cm (for both IS). The lens L2 images the transverse proton bunch in the mask plane that is located 30 cm after the focusing lens. The camera lens L3 is located 32.5 cm after the mask and re-images the transverse proton bunch profile onto the camera chip which is located 9.75 cm behind the camera lens. The cameras (C2) total field of view is $(53.3 \times 40)\,\mathrm{mm}^2$ on the first imaging station and $(63.36 \times 47.52)\,\mathrm{mm}^2$ on the second. Since the camera chip size is $(7.2 \times 5.4)\,\mathrm{mm}^2$ (1/1.8 inch) the magnifications are 0.135 and 0.11 on IS 1 and IS 2, respectively. The magnification in the mask plane was set to 0.5. The calibration of the images is described in Section 5.7.

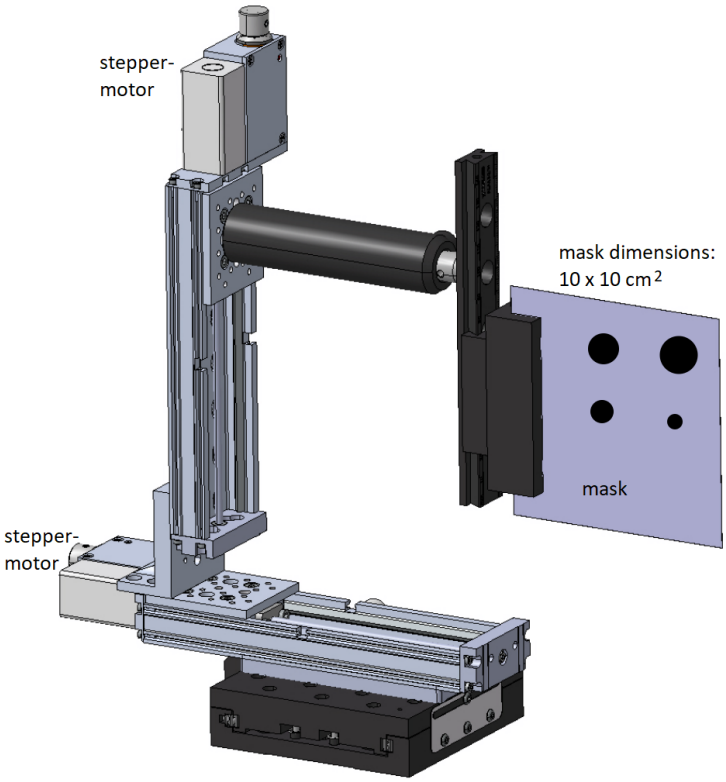

Figure 5.4: Technical drawing of the light-core blocking mask system.

The mask system (see Figure 5.4) consists of a 1 mm thick fused silica window with different size opaque coatings, a glass holder, two stepper motors for horizontal and vertical alignment and a manual translation stage to

facilitate imaging by longitudinal positioning on the table. The light passing around the mask is then re-imaged onto an externally triggered 12 bit camera C2 (Basler ac1600-60gm). The camera exposure time can be set from 0.01 ms to 100 ms and the trigger signal can be delayed (up to 0.1 s) to after the proton bunch passage to minimize background contributions (counts due to prompt secondaries from the proton bunch). The scintillating material Chromox emits light for many milli-seconds after the proton bunch passage. To adjust the light exposure of the camera, we installed a motorized filter wheel with 6 filter positions. The available filters range from optical density OD 0 (100% transmission) to OD 5 (0.001% transmission).

The optical setup for IS 2 is very similar to the one for IS 1 (see Figure 5.3), but due to space restrictions the positions of the beam splitter and the mirror are switched. Figure 5.5 and 5.6 show the technical drawings of the imaging stations. Note that the camera lenses L1 and L3 are not implemented in the drawings.

The available mask sizes (to block the intense light from the proton bunch core) range from $r = 0.5$ to 8 mm and I can remotely adjust and align the mask for various measurements campaigns (i.e. plasma densities, changing proton bunch trajectory, etc.). Since the cameras (C2) are externally triggered and I have different mask sizes available I can directly compare counts for different events and explore the radial proton bunch profile in detail.

5.3.3 Core Camera Upgrade

Between the June and September measurement campaign, we performed the following small upgrade:

- On IS 1: We added a 50:50 beam splitter before the focusing lens L1 and added another synchronized Basler ac1300-30gm core camera.
- On IS 2: We replaced the unsynchronized Watec core camera by a synchronized Basler ac1300-30gm one.

This allows to measure the proton bunch core more precisely and combine the measurement of the defocused protons for each event.

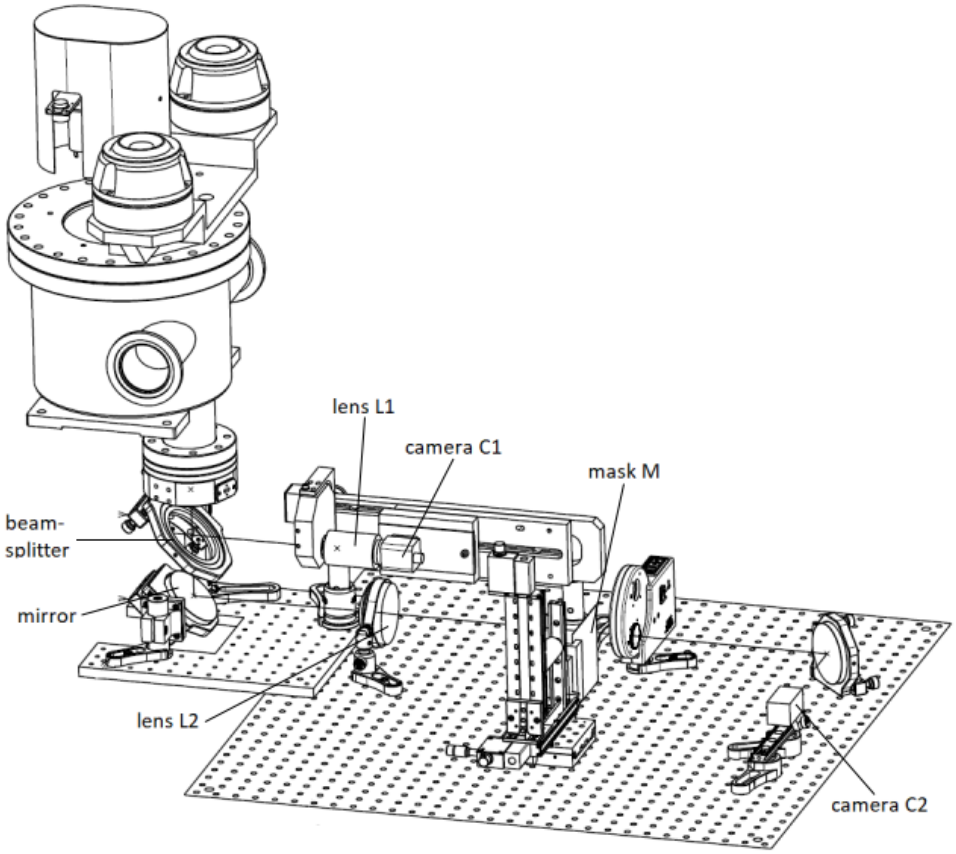

Figure 5.5: Technical drawing of of the upgraded imaging station 1, located 2 m downstream from the plasma end.

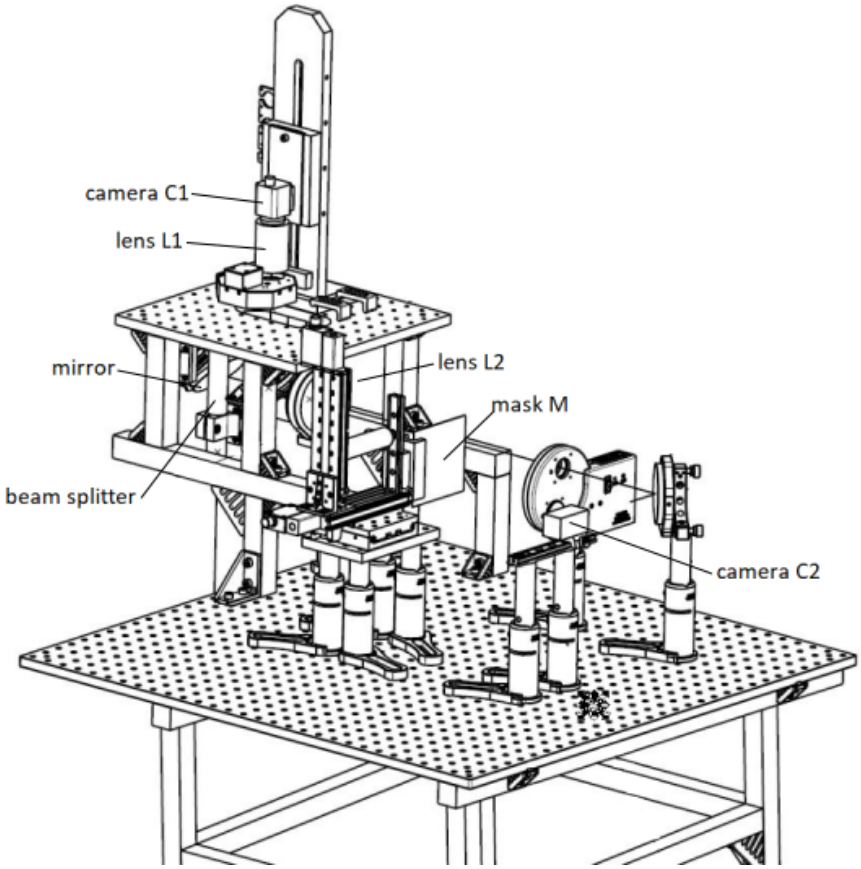

Figure 5.6: Technical drawing of the upgraded imaging station 2, located 10 m downstream from the plasma end.

5.4 Screen Tests at the HiRadMat Facility

In order to find a satisfactory imaging screen material for using in the AWAKE experiment, we tested 16 screen materials [39] at the HiRadMat facility at CERN [40]. We used a 440 GeV/c proton bunch from the CERN SPS with a bunch population of $5 \times 10^{10} - 2 \times 10^{11}$ protons. To simplify the measurement setup, we decided to perform the measurements in an air environment. All materials tested are listed in Table 5.1.

The experimental setup for the HiRadMat screen tests is shown in Figure 5.7. To avoid reflections and ambient light from reaching at the camera, the setup has been surrounded by a blackened aluminium box.

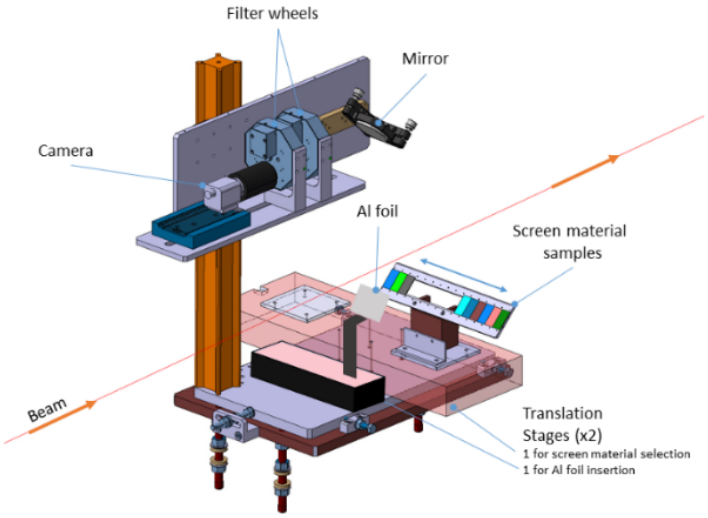

Figure 5.7: Technical drawing of the HiRadMat screen test setup.

As the proton bunch traverses the screen sample, the screen emits either optical transition radiation (OTR)[41], when the screen is metallic, or mainly scintillation light, when the screen is a scintillator. Part of the emitted light is reflected by a mirror, traverses a filter in the filter wheel, and is imaged onto the sensor of the camera by a camera lens.

Since the measurements were performed in an air environment, the proton bunch exits the vacuum through a vacuum window 2 m upstream our measurement setup. When the proton bunch travels through the air it produces

Screen Nr.	Material	Thickness/mm	Supplier
1	Chromox (Al_2O_3:CrO_2)	3	CeraQuest
2	Chromox (Al_2O_3:CrO_2)	1	CeraQuest
3	Chromox (Al_2O_3:CrO_2)	0.5	CERN stock
4	Aluminium	0.2	CERN stock
5	YAG (YAG:Ce)	0.5	Crytur
6	YAG (YAG:Ce)	0.1	Crytur
7	YAG back-coated (YAG:Ce+Al)	0.5	Crytur
8	YAG back-coated (YAG:Ce+Al)	0.1	Crytur
9	Alumina (Al_2O_3)	1	GoodFellow
10	Chromox old type (Al_2O_3:CrO_2)	1	CERN stock
11	ESS screen sample	1	ESS
12	Aluminium	1	CERN stock
13	Titanium	1	GoodFellow
14	Aluminium coated Silicon	0.25	MicroFabSolutions
15	Silver coated Silicon	0.3	Sil'Tronix
16	Stainless steel	0.2	CERN stock

Table 5.1: Materials tested in the HiRadMat experiment. red color font indicate a scintillating material whereas black font marks screens that emit OTR.

Cerenkov light along its way before reaching the screen sample. In order to block most of the Cerenkov light produced by the proton bunch in air, the measurement setup offers the possibility to insert a 0.2 mm thick light blocking aluminium foil 4 cm upstream the screen samples. When this light blocking foil is inserted, forward OTR produced at this foil and Cerenkov light produced over 4 cm (distance between foil and screen sample) of air arrive as background on the screen sample.

5.4.1 Estimation of the Signal

Optical Transition Radiation

The amount of OTR light N_{OTR} emitted by a proton traversing a screen can be estimated by [41]:

$$N_{OTR}[\text{photons/proton}] = 2R\frac{2\alpha}{\pi} ln\left(\frac{\lambda_b}{\lambda_a}\right) \cdot \left(ln(2\gamma(E)) - \frac{1}{2}\right) \approx 0.03 \quad (5.1)$$

where R is the reflectance of the screen material (I assume 0.9), α the fine-structure constant, λ_a - λ_b the wavelength range of interest (for us this is the visible range detectable by the cameras from λ_a =380 - λ_b =780 nm, or 3.26 - 1.59 eV), γ the Lorentz factor of the proton bunch at a given energy (E). OTR is emitted in the forward (along the axis of the protons) and backward (in the specular reflection direction of the beam on the screen) direction. The maximum amount of the light is emitted with an opening angle of $\frac{1}{\gamma}$ with respect to the light emission direction.

Scintillation

From literature, I expect the light yield of scintillators (e.g. Chromox [42]) to be on the order of 10^4 photons/MeV deposited energy. The Bethe-Bloch formula shows that a 440 GeV/c proton deposits roughly 0.6 MeV/mm when traversing aluminium. Scintillation light is emitted over 4π and to estimate the amount of photons reaching a camera, I take the acceptance of the system into account (1 inch diameter camera lens at a distance of 50 cm). Consequently I obtain approximately 1 photons/proton when considering 1 mm of Chromox.

5.4.2 Estimation of the Background

I can estimate the number of Cerenkov photons N_{Cv} produced by the proton bunch in air by using a simplified version of the Frank-Tamm formula [43]:

$$N_{Cv}[\text{photons/proton/cm}] = 369.8 \left(1 - \frac{1}{n^2\beta^2}\right) \cdot \Delta E \approx 0.3 \qquad (5.2)$$

where n is the refractive index of the material that the proton bunch traverses (in our case air) and $\beta = \frac{v_b}{c}$ where v_b is the velocity of the proton bunch, $\Delta E = h(\nu_1 - \nu_2)$ is the energy range, the camera is sensitive, in eV (1.6-3.2 eV or λ = 380 - 780 nm). Cerenkov radiation is emitted in a cone with an angle on the order of $\frac{1}{\gamma} \approx \frac{1}{470} \approx 2.1$ mrad.

I discuss two scenarios:

1. The screen sample is a scintillator: The amount of forward OTR and Cerenkov light (produced between the foil and the screen sample) reaching the camera chip is much smaller than the amount of scintillation light, because of the low reflectivity of the scintillating screen samples. Assuming a reflectivity of 5 % for Chromox an additional 0.06 photons/proton would arrive from Cerenkov and OTR background contributions.
2. The screen sample is made of metal: The light produced by the light blocking aluminium foil reflects off the screen sample and adds to the backward OTR emitted by the screen sample itself; summed up we measure twice the amount of OTR light because the backward OTR also depends linearly on the reflection coefficient of the screen sample. The two foils are not close enough to see coherent effects; unfortunately the amount of Cerenkov plus background OTR light dominates over the OTR signal (see Equation 5.2), because the measurement is performed in air. To be conclusive, these measurements would have to be repeated in a vacuum environment, where there is no contribution from Cerenkov radiation.

5.4.3 Measurement Results

The relevant and conclusive results of these measurements are summed up in Figure 5.8 and Table 5.2. The results confirm that the tested scintillating

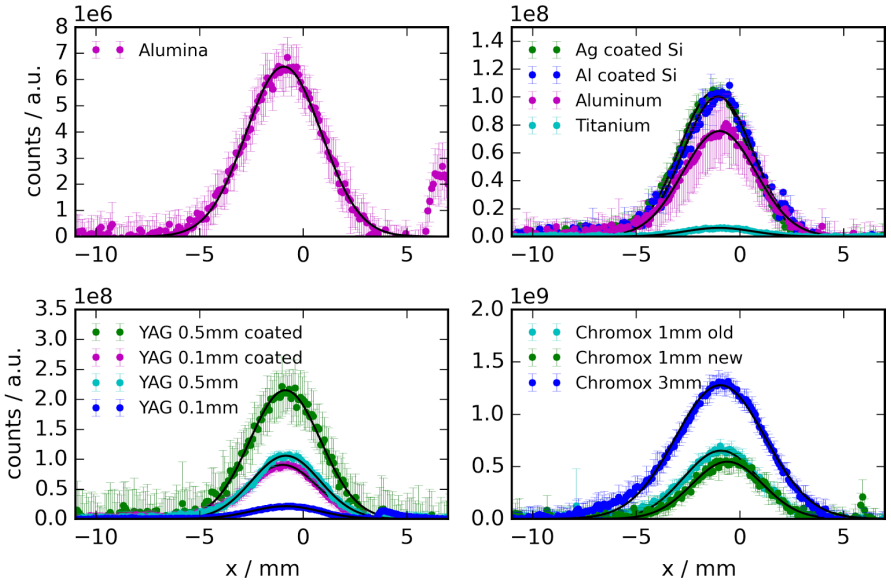

Figure 5.8: Transverse proton bunch profiles (images are integrated in the vertical direction) for various screen materials. The number of counts are normalized to the extracted proton bunch population and light attenuation. Please note the multiplication factor for the vertical axis on the top left corner.

Chromox screens emit the highest number of photons. The light yield for scintillators increases with the thickness of the screen sample while the resolution (the measured transverse bunch size with respect to the real one) of the measurement decreases. Based on these measurements I decided to use a 1 mm thick Chromox screen in the two imaging stations in AWAKE because it emits the second highest amount of photons while having a better resolution than the 3 mm thick screen.

Figure 5.8 shows transverse proton bunch profiles obtained with various screens.

The measurements presented in Figure 5.8 show relatively large errorbars, because we used analogue, unsynchronized, interlaced video cameras for these tests, the same type as the bunch core cameras (C1), used in the AWAKE experiment and described in Section 5.3. The cameras triggered every 20 ms and integrated the light over 20 ms. A frame-grabber then selects and digitizes the image in which the proton bunch arrives. Thus, the amount of collected light changes depending on when the proton bunch arrived within the frame. The frame capture time is 20 ms. The scintillating screens emits light exponentially over tens of milliseconds ($N_{\text{scint}} = \exp -\alpha t$; $\alpha \propto \frac{1}{10\text{'s ms}}$), meaning

Material	Type	relative yield/a.u.	measured σ_r/mm
3 mm Chromox	Scint.	100 ± 5	2.17 ± 0.06
1 mm Chromox (old type)	Scint.	50 ± 4	1.79 ± 0.06
1 mm Chromox	Scint.	43 ± 4	1.7 ± 0.1
0.5 mm YAG coated	Scint.	17 ± 2	1.7 ± 0.1
0.5 mm YAG	Scint.	8 ± 1	1.64 ± 0.06
0.1 mm YAG coated	Scint.	7 ± 5	1.8 ± 0.5
0.1 mm YAG	Scint.	1.6 ± 0.1	1.64 ± 0.05
1 mm Alumina	Scint.	0.5 ± 0.1	1.8 ± 0.1

Table 5.2: Light yield and radial bunch rms (σ_r) obtained with different screen samples. The rms is obtained through a Gaussian fit. All measurements were performed with 2×10^{11} protons/bunch.

that most of the light is emitted and captured right after the proton bunch passage. However sometimes the proton bunch arrives late in the 20 ms frame and the number of counts is significantly lower than for other measurements. I rejected approximately 30 % of the collected measurements because of the low number of counts. OTR on the other hand is emitted instantaneously and always all of the light is collected within one frame.

I showed that we can image a proton bunch with a maximum bunch density of 2×10^9 protons/mm^2 using a scintillation 1 mm thick Chromox screen and a light attenuation filter with 0.01 % transmission. Assuming that the light response of the screen is linear with proton bunch population, I expect the light yield to be enough to image a proton bunch density of 2×10^4 protons/mm^2 in an experimental setup with similar distances. The from simulations expected proton bunch density in the defocused proton bunch edge is around $10^5 - 10^6$ protons/mm^2(see Chapter 4).

5.5 Screen Requirements

The result of the screen tests, performed in CERN's HiRadMat facility and described in the previous Section, is that a 1 mm thick Chromox screen offers the best compromise between light yield and resolution. To be a suitable screen for imaging the maximum edge of the defocused protons in the two imaging

stations in AWAKE, the material must fullfill the following requirements:

5.5.1 Energy Deposition in the Screen

Screen tests (see Section 5.4) show that all screen materials tested withstood the impact of a 440 GeV/c SPS proton bunch with 2×10^{11} protons per bunch.

In AWAKE the self-modulated proton bunch passes through the screen and it deposits energy in the screen material. The energy deposition of a self-modulated (LCODE simulated proton bunch distribution after self-modulation in a 10 m long plasma with a plasma density 7×10^{14}atoms/cm^3) proton bunch in 1 mm thick Chromox was simulated with FLUKA [44]. From the energy deposition (ΔE) I can calculate the temperature rise (ΔT) with:

$$\Delta T = \frac{\Delta E}{\rho_{xx} c_{xx}} \tag{5.3}$$

where ρ_{xx} is the density of the material that the proton bunch traverses and c_{xx} its specific heat capacity. To estimate the temperature rise in the Chromox screen in Figure 5.9, I used the density and specific heat capacity of Aluminium ($\rho_{\text{Alu}} = 2.7\,\text{g/cm}^3$, $c_{\text{Alu}} = 897\,\text{J/(kg K)}$) as an indicator because the data for Chromox is not available. This estimate assumes that all the deposited energy goes to heat as photon emission is neglected.

Figure 5.9 shows that the maximum temperature rise in the screens is expected to be approximately 2 K per self-modulated proton bunch pulse. The AWAKE experiment will get a bunch every ~30 seconds. I conclude that the Chromox screens will handle this small, locally limited temperature increase, as the melting point of the Chromox is 2000 degrees Celsius.

5.5.2 Chromox Light Yield

FLUKA calculations as well as the Bethe-Bloch formula indicate that a 400 GeV/c proton looses about 0.6 MeV when traversing 1 mm of Chromox. From simulations I expect $\sim 10^6$ protons/mm^2 in the self-modulated maximum defocused proton bunch edge. I also expect that 1 MeV of deposited energy emits $\sim 10^4$ photons over 4π [42]. The acceptance of our optical setup is limited by the 3 inch opening of the lens and the distance between the scintillating screen and the lens ($\approx$ 60 cm). I therefore estimate that more than 10^4 photons arrive

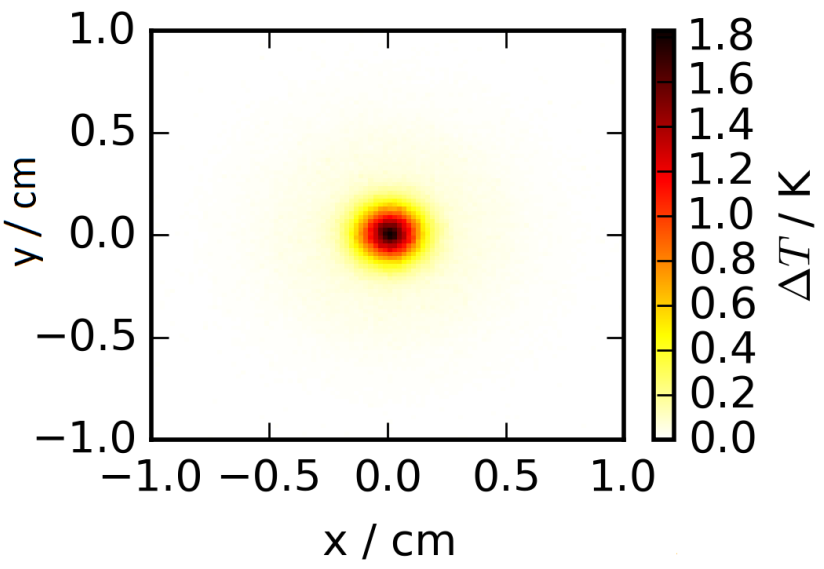

Figure 5.9: Expected temperature rise in a 1 mm thick Chromox screen caused by the energy deposition of the self-modulated ($n_{pe} = 7 \times 10^{14}$atoms/cm^3) proton bunch.

on one pixel imaging $\approx 40 \times 40\,\mu$m^2. From the specifications of the CMOS cameras, I conclude that the measurement setup is sensitive enough to resolve the protons with the maximal radial position.

5.5.3 Linearity of the Screen Response

Using the same filter and camera exposure time, I measured in AWAKE the transverse proton bunch profile of an incoming proton bunch with two different proton populations (1.5 and 3×10^{11} protons/bunch). The measurements (three for 1.5×10^{11} and two for 3×10^{11} protons/bunch) are shown in Figure 5.10.

The measured light yields are (53000 ± 2000) counts for 1.5×10^{11} protons/bunch and (100000 ± 3000) counts for 3×10^{11} protons/bunch. The relative amplitudes agree with the relative proton bunch population within the error of the measurement. These measurements show that the amount of light emitted by the screen is linearly proportional to the proton bunch charge for the proton populations we use in AWAKE.

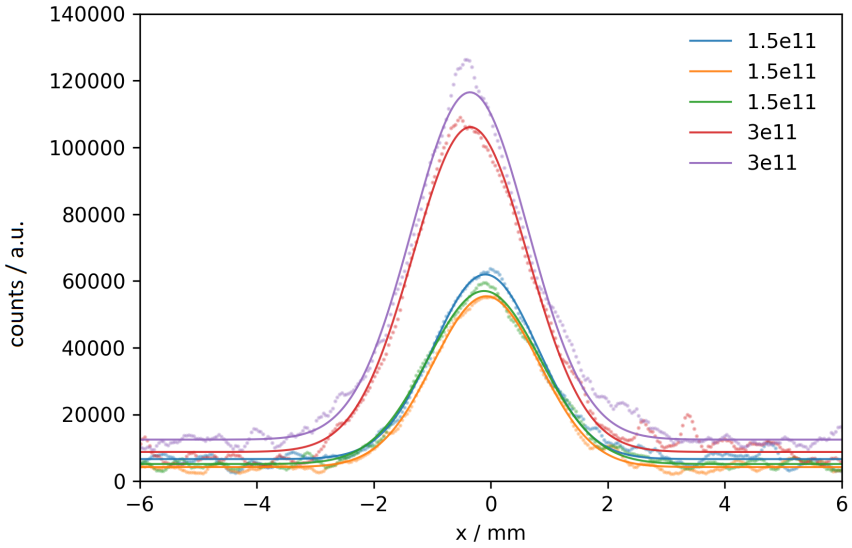

Figure 5.10: Bunch profiles (horizontal projections) measured in AWAKE with two different proton bunch populations using the same filter and exposure time settings of the camera. Measured data points (dots) are fitted with a Gaussian profile (solid line).

5.6 Camera Exposure Time and Delay

The cameras we use to measure the defocused protons (cameras C2 in Section 5.3) receive a trigger synchronous to the arrival of the proton bunch at the screen. The camera then collects light for a given exposure time. The exposure time can be varied from 0.01 to 100 ms.

The scintillator material Chromox emits light over tens of ms. Thus, by changing the exposure time I can change the amount of light captured for a given proton bunch population. Figure 5.11 shows the total number of counts (after background subtraction) as a function of the exposure time of the camera chip for each IS. The total number of counts is calculated by summing all the individual pixels of the image divided by the number of protons per bunch.

The total number of counts is higher with the IS 2 camera because the first focusing lens has a diameter of 3 inch, instead of 2 inch on IS 1. Until an exposure time of approximately 5 ms, the total number of counts increases linearly with exposure time. After approximately 5 ms, the light emission of the Chromox screen decreases and the number of counts increases less than proportionally to the camera exposure time. Further increase of the exposure time increases the number of counts only marginally until saturation.

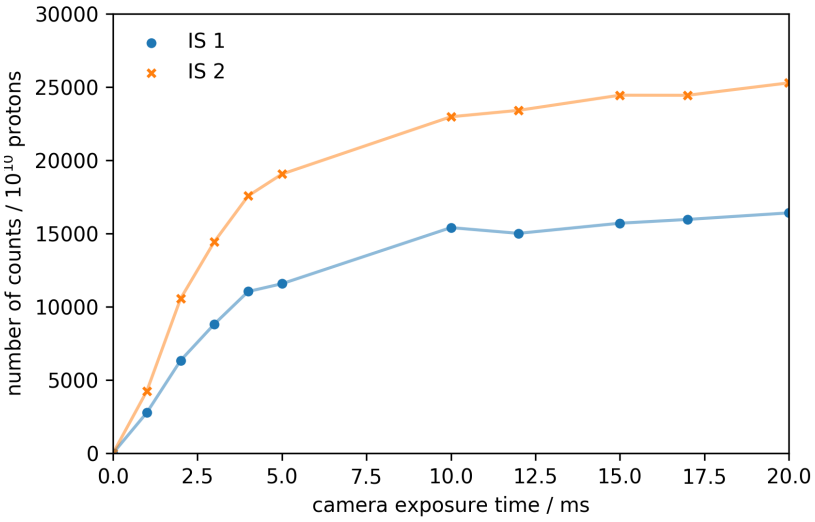

Figure 5.11: Number of counts per image as a function of camera exposure time.

Furthermore I have the option to delay the exposure time with respect to the bunch arrival. Experience showed that a delay of approximately 5 ms greatly improves the signal to noise ratio because the main background contributions (secondary particles directly impacting on the camera chip) are removed.

We note that as I increase the camera exposure time and/or reduce the delay of the image with respect to the bunch arrival, the number of counts increases. This is to be included in the data analysis when images with different settings are compared.

5.7 Spatial Screen Calibration and Measurement Resolution

To calibrate the field of view of the cameras we printed markings onto the Chromox screens. The markings are rectangular with a size of $30 \times 22 \cdot \sqrt{2}\,\mathrm{mm}^2$ on IS 1 and $40 \times 32 \cdot \sqrt{2}\,\mathrm{mm}^2$ on IS 2. Since the screens are inserted into the beam-line at an angle of 45 degrees, the markings appear to be $30 \times 22\,\mathrm{mm}^2$ on IS 1 and $40 \times 32\,\mathrm{mm}^2$ on IS 2. Additionally the rectangle appears as a trapezoid on the camera image. Figure 5.12 shows the markings on the IS 1 camera image. The markings are visible because I turned on the light installed on the view-port. Additionally, Figure 5.12 shows that the mask plane is in

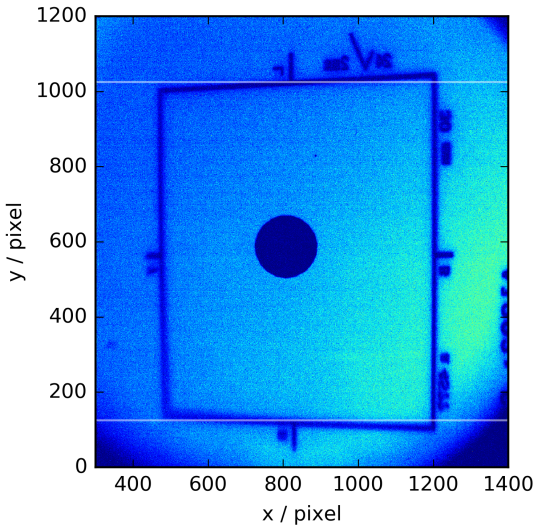

Figure 5.12: Camera image of the calibration markings on the Chromox screen installed in IS 1. The white horizontal lines indicate the vertical distance used for calibration.

focus (see black circle in the center of the image). From the markings on the screen, I know the distance between the white lines. To obtain the calibration per pixel I divided the height of the markings by the number of pixels between the white lines. Since the camera pixels are square, the horizontal calibration is the same as the vertical one. The calibration per pixel for the cameras looking at the defocused protons is 33 μm/pixel and 40 μm/pixel on IS 1 and IS2, respectively. The calibrations of the cameras looking at the proton core (C1) are 95 μm/pixel on IS 1 and 116 μm/pixel on IS 2. At the moment I estimate the screen resolution to be four times the pixel size, but to measure the resolution properly, I will rebuild the optics setup and measure the resolution of the two imaging stations using a 1951 USAF resolution test target [45].

5.7.1 Image Treatment

Before further analysis and as a first step, I apply a median filter [46] (a spatial filter which reduces noise in an image) to the measurement images from the IS to remove background signal or dead camera pixels. Figure 5.13 shows a comparison between an image where no median filter was applied (top row) and where the filter was applied (middle row). The lower row in Figure 5.13 shows the comparison of horizontal profiles (integrated in y) between

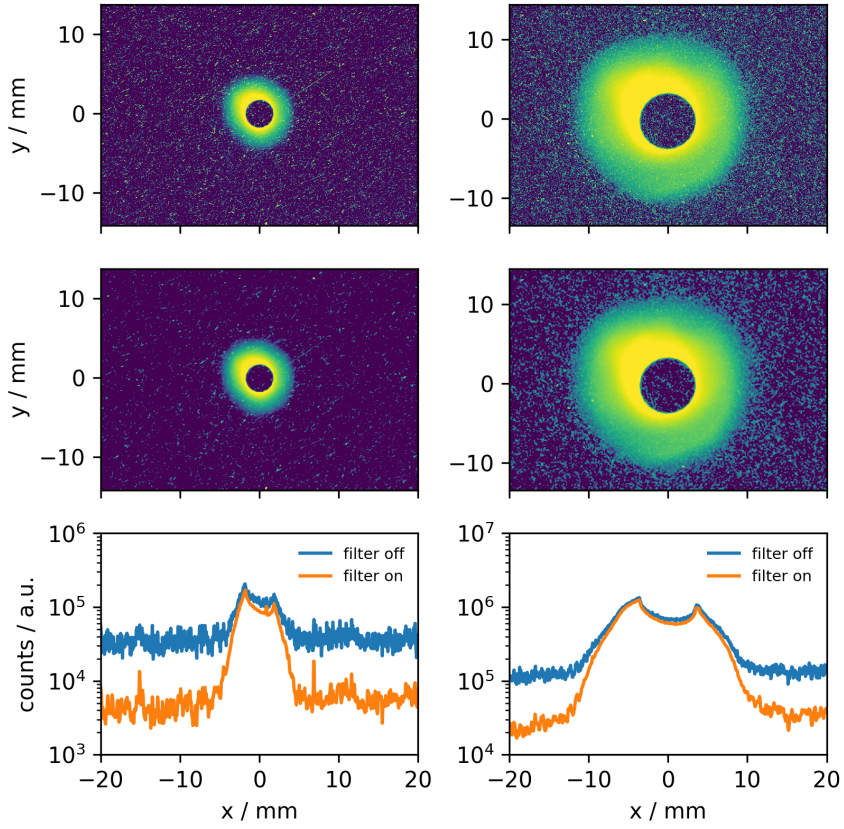

Figure 5.13: Comparison of a bunch image that was treated with a median filter (middle row), to an untreated image (top row). The lower images show the comparisons of the horizontal (integrated in the vertical direction) bunch profiles.

the image treated with the median filter (filter on) and the untreated image (filter off). The profile of the signal does not change with the application of the median filter, but the signal to noise ratio increases by almost one order of magnitude.

5.8 Conclusions

The two-screen measurement setup consists of two imaging stations separated by a distance of $\sim 8\,\mathrm{m}$, located downstream the end of the plasma. Each imaging station uses a scintillating, 1 mm thick Chromox screen and two cameras to image the self-modulated proton bunch core as well as the defocused protons surrounding the core. To be able to measure the less intense light emitted by the defocused proton region of the screen I block the light emitted

by the intense core by a mask. Both imaging stations are capable to image the defocused proton edge of a self-modulated proton bunch at the AWAKE plasma densities, because the Chromox screens emit a sufficient amount of light.

6 Experimental Results

I use the two-screen measurement setup described in Chapter 5 to measure the transverse, time-integrated distribution of the proton bunch after traversing 10 m of plasma. When the proton bunch self-modulates, defocused protons appear at large radial positions ($r \gg \sigma_r$) downstream the plasma exit. The aim of this measurement is to infer characteristics of the self-modulation process by detecting protons that are defocused by the transverse plasma wakefields. Through the analysis of these profiles I attempt to:

- calculate the maximum deflection angle and the maximum transverse proton momentum.
- calculate the fraction of protons that experience defocusing wakefields.
- refer to the point of origin of the defocused protons along the plasma; if these protons originate from within the 10 m of plasma, I can learn about the growth of the SSM.
- estimate the growth rate of the seeded instability.
- estimate the transverse and longitudinal maximum wakefield amplitudes from the growth rate.

From all those measurements combined I infer that the SSM has grown along the plasma. This also means that the transverse proton bunch structure has strongly evolved before exiting the plasma.

Previous experiments mentioned in Section 2.3.1 did not prove growth of the SSM. They showed that the bunch particles gained transverse and longitudinal momentum from the wakefields. The results presented here are the first ones that show evidence for the growth of the self-modulation process. This is an essential characteristic needed to drive large amplitude wakefields from the low amplitude seed fields.

The occurrence of self-modulation results in the formation of three proton bunch populations: those that do not interact with the plasma or wakefields,

because they are located before laser pulse with the AWAKE seeding method, those that are defocused ($r \gg \sigma_r$) and those that are focused by the transverse wakefields. Therefore in AWAKE, at IS 1 and 2, I expect to observe these three populations: In particular defocused protons appear as a halo surrounding the bunch core. The core consists of the other two populations.

The measurements discussed were performed during the AWAKE measurement campaigns beginning of June and September 2017. Note that proton bunch parameters delivered by the CERN SPS differed from the ones in the simulations in Chapter 4. In particular the proton bunch radius at the plasma entrance was σ_r =0.15 mm, smaller than the baseline value of σ_r =0.2 mm. The bunch length was varied between $\sigma_z = 6$ and 15 cm (baseline value $\sigma_z = 12$ cm) and the radial normalized proton bunch emittance in the experiment was $\epsilon = 2.2$ mm mrad instead of the baseline value of $\epsilon = 3.6$ mm mrad. To directly compare the simulations with the measurements, we redid part of the simulations (shown in this Chapter) with the experimental parameters.

However, this only changes the quantitative value of the results presented in Chapter 4, not their qualitative value. I can therefore use all the simulation results to guide the understanding of the experimental results.

6.1 Detection of Defocused Protons

6.1.1 Observation of Proton Bunch Propagation in Vapour

When the proton bunch does not interact with the plasma, i.e. because there is no ionizing laser pulse or there is no rubidium vapour present, its transverse distribution downstream the plasma source remains Gaussian while propagating. This statement is verified by Figure 6.1 which shows a typical measurement of the transverse proton bunch distribution on the two imaging stations (IS 1 left and IS 2 right). In this case the proton bunch traverses 10 m of rubidium vapour (without plasma, no laser pulse, also depicted in Figure 6.3). For the measurements shown in this Section, the laser pulse is placed in the middle of the proton bunch.

We note that we do not expect large effects from the rubidium vapour on the proton bunch. Plasma is created by proton triggered impact ionization of the vapour, however its density is estimated to be very low ($< 10^{-3}$ of the vapor

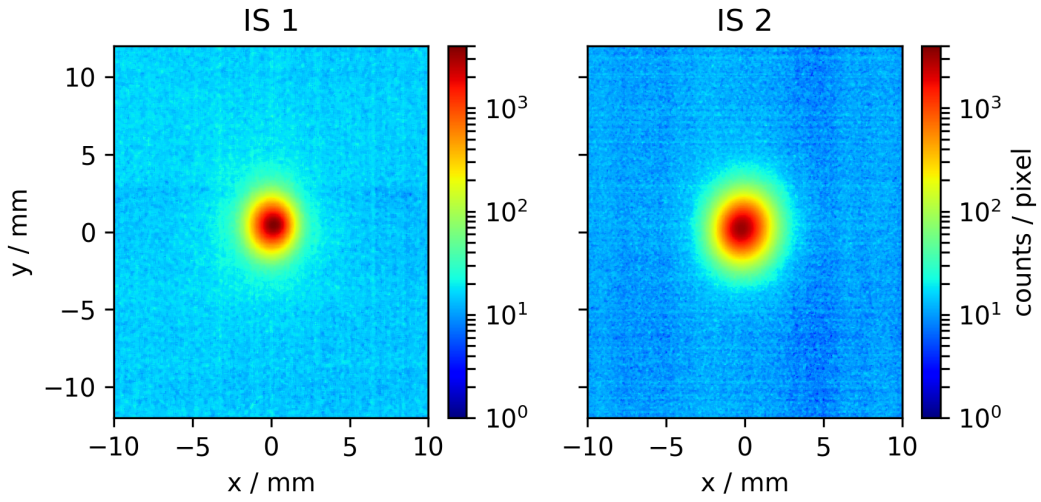

Figure 6.1: Transverse proton bunch distribution at the imaging stations after the bunch (3×10^{11} protons) traversed 10 m of rubidium vapour with a density of $1.95 \times 10^{14}\,\mathrm{cm}^{-3}$ (no laser pulse, no plasma). Note the logarithmic color scale.

density [47]). The scattering of the protons on the rubidium atoms increases the size of the proton bunch only by a negligible amount (based on my FLUKA simulations). I verified this statement experimentally by measuring the proton bunch sizes after propagation in 10 m of rubidium vapour (density $7 \times 10^{14}\,\mathrm{cm}^{-3}$) and 10 m of vacuum. No change in bunch size was detected.

6.1.2 Observation of Proton Bunch Propagation in Plasma

When the proton bunch self-modulates within the 10 m of plasma, I expect to observe protons with large radial positions (defocused proton radius $\gg \sigma_r$) at the two IS. This is due to the transverse wakefields that the bunch drives and the defocusing wakefields that act on it. The protons that are focused by the transverse wakefields form a tight core. Compared to the no plasma case, the proton population in the core decreases because the defocused protons radially exit the bunch core.

Figure 6.2 shows a measurement for the case of the proton bunch that is self-modulated after traversing plasma with a density of 1.95×10^{14} electrons/cm^3. As expected, the transverse bunch profile is no longer Gaussian and the intensity of the proton bunch core is lower than the one in the no plasma case. When compared to Figure 6.1, Figure 6.2 clearly shows that defocused protons

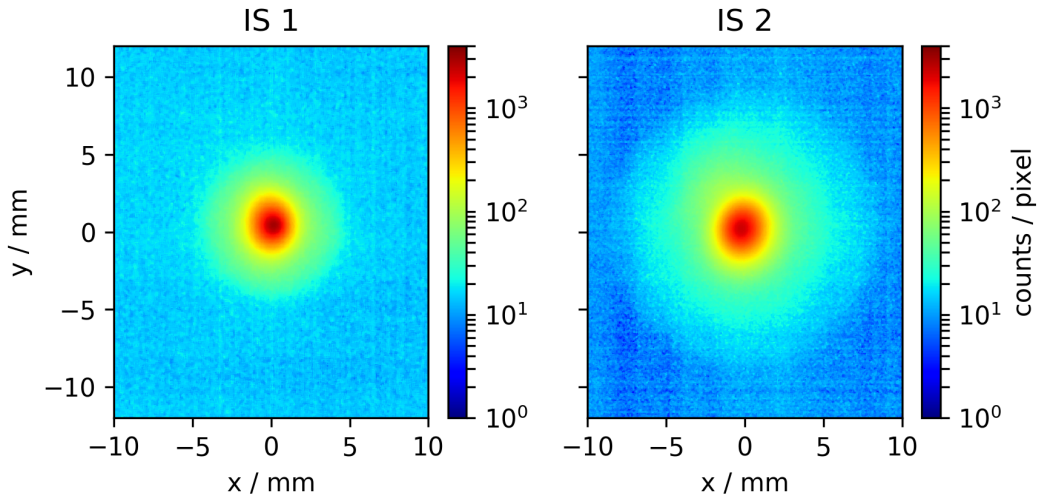

Figure 6.2: Transverse proton bunch distribution (3×10^{11} protons) on the imaging stations after 10 m of rubidium plasma with a plasma density of 1.95×10^{14} electrons/cm^3. Note the logarithmic color scale.

reach large radial positions ($r \gg \sigma_r$) and form a symmetric halo around the bunch core.

Figure 6.1 and 6.2 are two consecutive measured images with the same proton bunch parameters within experimental variation (bunch length $\sim \pm 0.5$ cm, bunch population $\sim \pm 20$ %, etc.) and the same camera settings (filter, camera exposure time, etc.). While there was no ionizing laser pulse present in Figure 6.1, for Figure 6.2 the high power laser pulse was co-propagating with the proton bunch, creating a plasma for all the protons after the laser and seeding the SSM.

On Figure 6.3 I compare on a linear scale the vertical projections of the measurements shown in Figures 6.1 and 6.2, normalized to the respective bunch charge and to the maximum of the unmodulated proton bunch profile. The blue line shows the unmodulated bunch measurement (laser off). We note that when the laser is on (plasma is present), protons form wings around the bunch core (blue line). In addition to this effect, the proton population in the bunch core decreases. Since Figure 6.3 shows profiles obtained with the core cameras, the attenuation filters and exposure time settings were adjusted to the bunch core. Thus the strongly defocused protons are below the detection threshold.

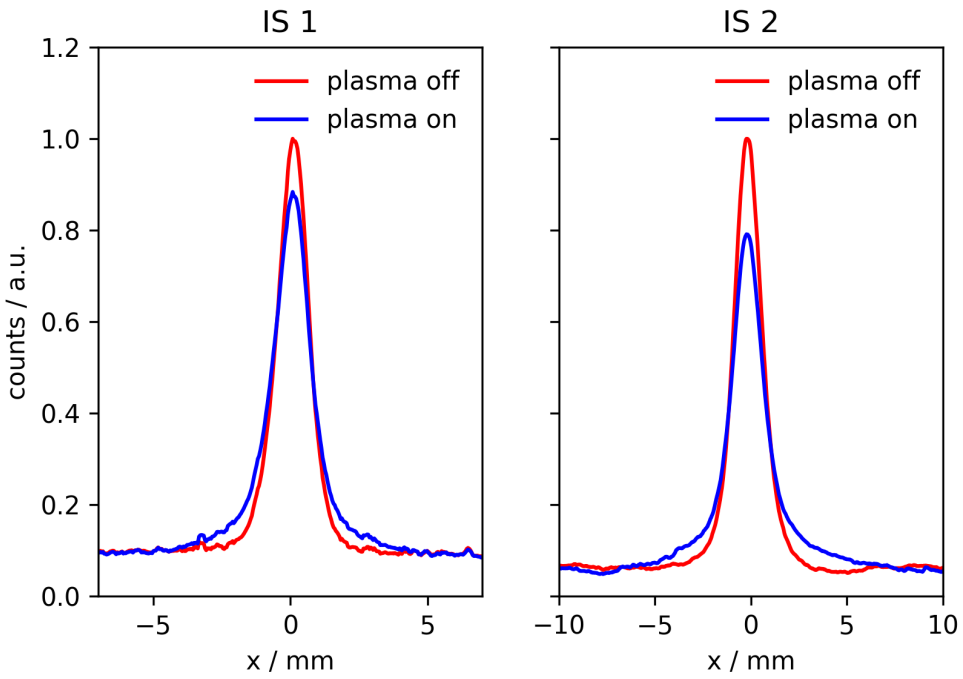

Figure 6.3: Comparison of the unmodulated (no plasma, no laser, red line) and self-modulated (plasma, laser, blue line) proton bunch density profiles on the two imaging stations. The lines show the horizontal profiles summed in the vertical direction. Projections on the orthogonal y axis show similar features. The profiles are normalized to the no plasma peak values.

6.1.3 Observation of Proton Bunch Self-Modulation on the Streak Camera

The results above show proof that transverse fields were present in the plasma. At the same time we observed micro-bunches, spaced at the plasma period, on the streak camera images [25]. The streak camera images show a time-resolved image of the proton bunch (see Figure 6.4) on either a nano-second or 70 pico-second time-scale. Note that the streak camera measurement was briefly introduced in Section 2.4.2.

Figure 6.4 shows the time-resolved streak camera measurements of the proton bunch. While the IS measure the time-integrated images of the proton bunch distribution with a transverse structure related to SSM, the streak-camera diagnostics shows the time-resolved, longitudinal structure of the proton bunch. This is the structure of the populations forming the core of the bunch.

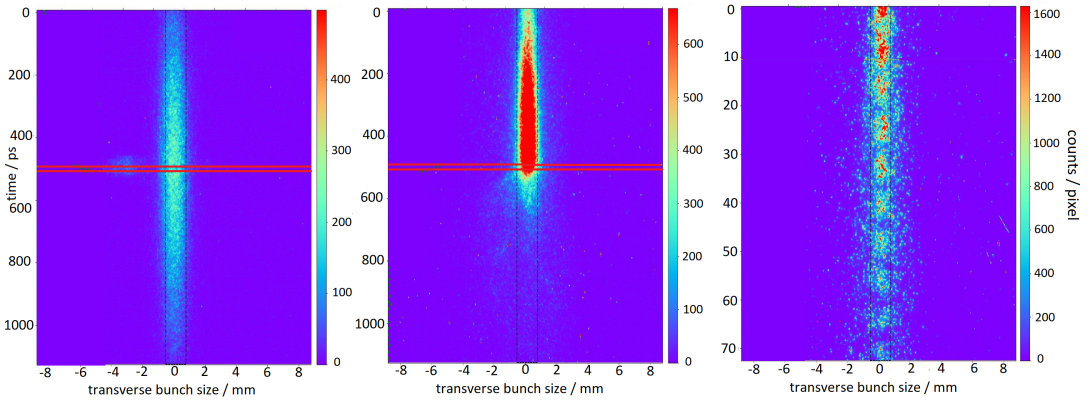

Figure 6.4: Left: time resolved streak camera image of the proton bunch propagating from bottom to top without plasma, the red horizontal lines mark the position of the laser pulse (the laser energy in this image is less than a nano-Joules), center: time-resolved image of the proton bunch with the high power laser at the position of the red horizontal line, right: proton bunch on the 70 ps scale zoomed into the region after the laser pulse, the micro-bunches are clearly visible; Image by K. Rieger.

The left panel of Figure 6.4 shows the proton bunch on a nano-second scale after propagation in rubidium vapour (no plasma). The laser pulse is located within the two red lines near the middle of the bunch. For this image, the laser pulse is in low power mode (energy less than a nano-Joule) and therefore does not ionize the rubidium vapour significantly.

The middle panel shows again the proton bunch on a nano-second time-scale. The high-power laser pulse is at the center of the proton bunch (again between the red horizontal lines). We note that the proton bunch is defocused after the laser pulse and that the defocusing effect starts at the position (or time) of the laser pulse. This is evidence of the seeding of the self-modulation process.

The right panel shows the time resolved proton bunch on a 70 ps scale after the high-power laser pulse and propagation in a plasma with a density of 2.1×10^{14} electrons/cm^3. At that short time scale the micro-bunches resulting from self-modulation are clearly visible.

During the experiment, the observation of SSM on the streak camera image and that of a halo of defocused protons on IS 1 and IS 2 were always present together. Hence I claim that the proton defocusing I observe with the two-screen method is directly related to SSM development. Observation

of micro-bunches and proton defocusing is proof for self-modulation of the proton bunch and the presence of transverse and longitudinal wakefields since transverse and longitudinal wakefields always come together.

Among the main experimental results, we measured the frequency of the proton modulation with percent accuracy using both: Optical Transition Radiation and Coherent Transition Radiation (see Section 2.4.2). The measurements show that, as expected, the modulation frequency f_{mod} scales with the square root of the rubidium vapour density and with the expected value:

$$f_{mod} = \frac{1}{2\pi}\sqrt{\frac{n_{pe}e^2}{\epsilon_0 m_e}}. \tag{6.1}$$

This confirms that the laser ionization process fully ($> 99\,\%$) strips the rubidium atoms from their outermost electron.

6.2 Maximum Defocused Proton Bunch Edge

Due to the limited dynamic range of the cameras, I do not expect to be able to detect on a single image the unsaturated focused proton core and the edge of the defocused proton bunch distribution. Measurements show that the dynamic range of the cameras is approximately three orders of magnitude, because I use 12 bit cameras, while the signal intensity ranges over four to five orders of magnitude, according to simulations. Thus I split the light and insert a mask to block the light emitted by the intense bunch core on one of the cameras at each IS (see Section 5.3). Blocking the light from the core allows us to reduce the light attenuation in the optical line and to increase or adjust the exposure time of the camera to optimally image the defocused protons (as explained in Section 5.3). The top panels of Figure 6.5 show a measurement of the defocused protons with the bunch core blocked by a mask for a plasma density of 1.95×10^{14} electrons/cm^3.

After inserting the mask, I can reduce the optical density of the attenuation filters and better resolve the transverse intensity profile of the defocused protons, in particular the edge of its distribution. The two panels on the bottom of Figure 6.5 show on a logarithmic scale the horizontal profiles of the images on top (red line) compared to a measurement for which the laser was off (blue line). The comparisons of the plasma on and off measurements clearly

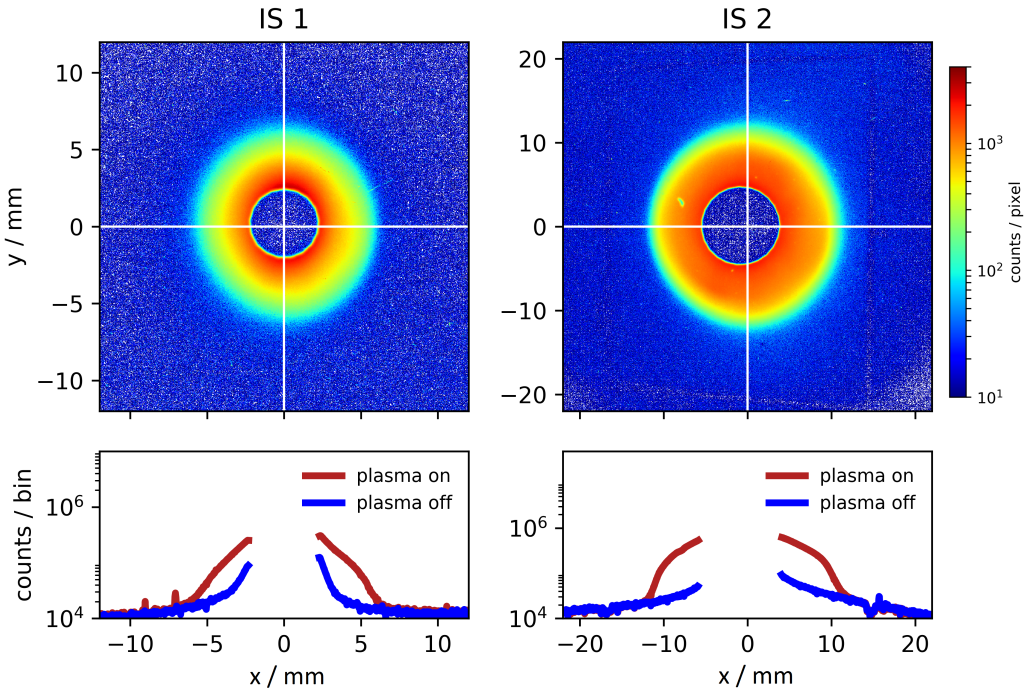

Figure 6.5: Top: Images of the transverse proton bunch distribution obtained on the two imaging stations with a plasma density of 1.95×10^{14} electrons/cm^3, showing the defocused protons. The light from the proton bunch core is blocked by a mask. Note the logarithmic scale for the image counts. The white cross indicates the center of the core of the bunch. Bottom: Horizontal projections of the images on the top panels (plasma on) compared to an event without laser pulse (plasma off). The points on which the mask blocks part of the light were removed from the profiles.

show that the transverse proton bunch distribution after self-modulation has an outermost edge.

Simulations show that there is a well defined maximum radius of the distribution (see Figure 4.5). Measurements with various attenuation filter values and camera exposure times confirm that: when increasing the exposure time of the camera or decreasing the level of light attenuation, the size (radius) of the defocused proton distribution does not change.

Even though I do not see the center of the proton bunch on Figure 6.5, I can determine that position on each imaging station because I record the image of the bunch core with another camera (see Figure 5.3). By fitting a Gaussian profile to the upper half of the integrated profiles in the horizontal and vertical directions and knowing the offsets and scaling between the camera images

through previous measurements without mask and plasma, I can determine the position of the proton bunch center on the images of Figure 6.5. The uncertainty on the determined proton bunch center is smaller than 10 μm in both planes and is thus neglected in further calculations.

6.2.1 Maximum Defocused Proton Bunch Radius

The method that I use to obtain the maximum radius from the images obtained by the imaging stations is described in detail in [48]. The paper named "A Method to Determine the Maximum Defocused Proton Radius of a Self-Modulated Proton Bunch in AWAKE" is attached in the appendix and was submitted to NIM A as part of the EAAC 2017 [1] proceedings.

In [48], we explain that we use a Python-contour routine to calculate the longest contour above background level that is closed around the bunch core. From each contour point, we calculate the distance to the bunch core center. The maximum radius (r_1 or r_2) is then obtained from the mean of the radii and the uncertainty (Δr_1 or Δr_2) by the standard deviation of the measured values. Figure 6.7 shows the determined contour (in red) on top of the measured images.

The maximum proton radii are the basis to calculate the maximum defocusing angle. From the radii and the maximum defocusing angle, I estimate where along the plasma the protons radially left the wakefields (see Section 6.3). A precise measurement of the maximum defocusing radii is important because this error determines the error on the maximum defocusing angle and the origin of the defocused protons. Due to the shallow angles ($\approx$1 mrad) and long distances ($\approx$10 m) a relatively small error on the radii measurement translates to a large error on the origin location of the protons (see Section 6.3).

6.3 Point of Origin of Defocused Protons

I explained how I determine the maximum radius of the transverse proton bunch distribution observed at the two screens downstream from the plasma. Assuming that the outermost protons on IS 1 are the same as the outermost

[1] European Advanced Accelerator Conference, La Biodola, Elba 24-30 September 2017

at IS 2, I calculated the maximum defocusing angle. Knowing the maximum radial position at one of the imaging station (i.e. r_1), the maximum defocusing angle (θ), the distance between the imaging stations (d_{IS12}= 8.09 m) and the distance between the plasma entrance and IS 1 (d_{eIS1}= 11.96 m), I can determine the point of origin of the protons along the plasma ($O = 0$ m is the plasma entrance) where the defocused protons leave the wakefields by:

$$O[\text{in m}] = d_{eIS1} - \frac{r_1}{\theta}. \tag{6.2}$$

The maximum angle θ is defined by:

$$\theta = \frac{r_2 - r_1}{d_{IS12}}. \tag{6.3}$$

The error of the maximum defocusing angle $\Delta\theta$ is calculated by quadratic addition of the absolute errors of the maximum defocusing radius Δr_1, Δr_2.

$$\Delta\theta = \frac{\sqrt{\Delta r_1^2 + \Delta r_2^2}}{d_{IS12}}, \tag{6.4}$$

where d_{IS12} is the distance between the imaging stations and have a negligible and constant error. The error on the origin of the defocused protons (ΔO) is also calculated by quadratic addition of the relative errors:

$$\Delta O = O \cdot \sqrt{\left(\frac{\Delta r_1}{r1}\right)^2 + \left(\frac{\Delta\theta}{\theta}\right)^2}, \tag{6.5}$$

where the uncertainty on d_{eIS1} is again assumed negligible.

6.3.1 Maximum Defocusing Radius and Point of Origin of Defocused Protons as a Function of Proton Bunch Charge

The top plot of Figure 6.6 shows the maximum defocused proton radius measured at the two IS as a function of the proton bunch charge. The vapour density for this measurement was set to 1.95×10^{14} atoms/cm^3, the proton bunch length was around $\sigma_z = 7$ cm and the laser pulse was one-quarter σ_z ahead of the center of the proton bunch.

The measured maximum radii of IS 1 and IS 2 are shown with blue crosses and orange circles, respectively. The maximum defocusing radius at both IS

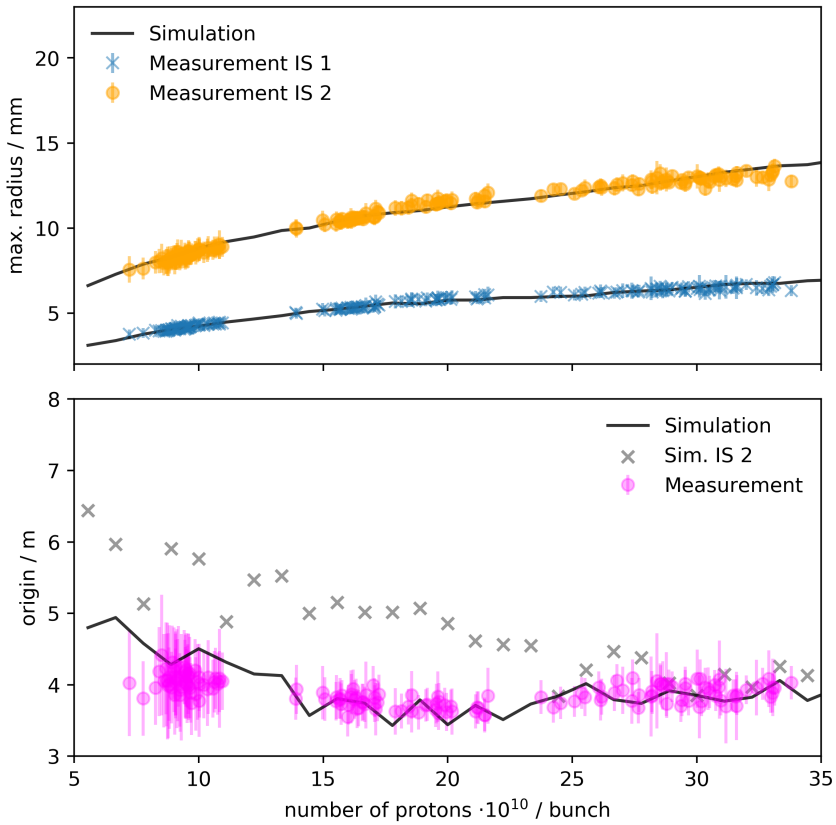

Figure 6.6: Top: measured maximum radial proton position on IS 1 (blue crosses) and IS 2 (orange circles) as a function of the proton bunch charge. Note that most errorbars are too small to be visible. Simulation results are shown as black lines; Bottom: the point of origin as calculated from the maximum radii of the measurements and Equation 6.2 and 6.3 (pink) and from simulations (black line, grey crosses). The black line shows the origin calculated from the simulated maximum radii (Equation 6.2 and 6.3); the grey crosses show the origin calculated from the protons transverse momentum at IS 2. The origin gives the position inside the plasma, measured from the vapour cells entrance.

increases with increasing number of protons in the bunch. The trends are very clear.

To fully understand and interpret the measurement results, we compare them to LCODE simulation results. The simulations were performed by the group of K. Lotov [2]. They used the proton bunch and plasma parameters from the experiment as an input and performed 30 simulations with bunch charges varying from $5 - 35 \cdot 10^{10}$ protons/bunch. The simulated maximum

[2] from the Budker Institute of Nuclear Physics, Novosibirsk

radii are shown by black lines on the top plot of Figure 6.6. We note that the simulations confirm the measurement results.

From the measured and simulated maximum proton bunch radii, I calculate the maximum defocusing angle (see Equation 6.3). From those two numbers I estimate where along the plasma the protons radially left the wakefields (see Equation 6.2), that is their point of origin. This point is plotted with pink circles (measurement) and black line (simulation) on the bottom plot of Figure 6.6. The plasma entrance in this Figure is located at 0 m and the exit at 10 m.

As mentioned previously, by calculating the maximum defocusing angle, we assume that the outermost protons on IS 1 are the same as the outermost on IS 2. In simulations we can validate this assumption because we identify the maximum defocused protons at each IS, measure their transverse momentum and calculate their point of origin.

Simulations indicate that for the experimental parameters used for this measurement, the calculation of the maximum defocusing radius and point of origin is justified for proton bunch populations larger than 2.9×10^{11} protons/bunch. Apart from calculating the point of origin from the maximum radii of the simulation results (black line on the bottom plot of Figure 6.6), we can track the origin of the maximum defocused protons, which are the outermost protons on IS 2, from the protons transverse momentum (see grey crosses on the bottom plot of Figure 6.6).

Even though we cannot observe the effect directly, simulations suggest that the protons with the maximum transverse momentum exit earlier along the plasma for higher proton bunch charges. This trend is as expected, because the initial transverse seed field ($W_{0,r}$) as well as the growth rate (Γ) of the SSM increase with increasing proton bunch population (see Section 3.3.1).

6.4 Seeded Self-Modulation Growth

Figure 6.7 shows a measurement performed at a plasma density of 7.7×10^{14}electrons/cm^3 (close to the AWAKE baseline parameters). Simulation results confirm that the outermost protons on IS1 are the outermost on IS2 and that the calculation of the maximum defocusing angle is justified (see Figure 4.7).

The maximum proton bunch radii (r_1,r_2) are $r_1 = (7.7 \pm 0.2)$ mm on IS 1

and $r_2 = (15.6 \pm 0.3)$ mm on IS 2. The distance between the imaging stations is 8.089 m, the resulting maximum defocusing angle is $\theta = (0.98 \pm 0.06)$ mrad. This angle is also given by the ratio of the transverse to longitudinal momentum of the proton bunch, defined by:

$$\theta = \frac{p_r}{p_z} \simeq \frac{p_r}{p} \text{ for } p_r \ll p_z \approx p \tag{6.6}$$

Thus the measured maximum defocusing angle of 0.98 mrad corresponds to a radial momentum of $p_r \approx (390 \pm 25)$ MeV/c. Furthermore I observe that protons radially exit the wakefield approximately 4-5 m downstream the beginning of the plasma.

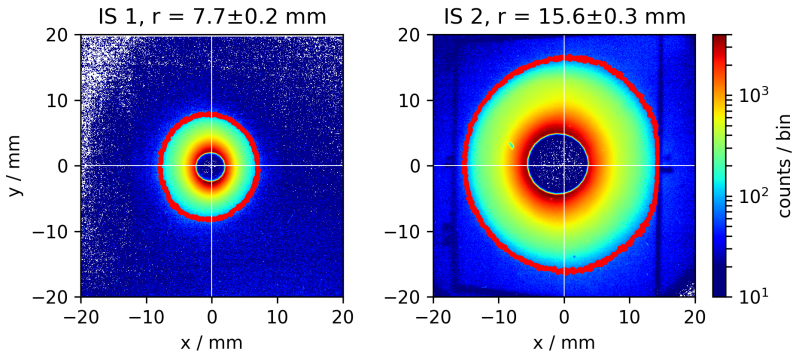

Figure 6.7: Typical defocused proton measurement for a plasma density of 7.7×10^{14} electrons/cm^3, 3×10^{11} protons/bunch, seeding at the center of the proton bunch and a bunch length of ~ 8 cm. The contour calculated as described in Section 6.2.1 is shown in red. The center of the proton bunch is shown with a white cross.

The initial radial rms transverse momentum spread of the protons σ_{pr} when propagating without plasma can be calculated from the bunch emittance (ϵ)[3] and the radial bunch size at the entrance of the plasma (σ_r) (at a waist) to be $\sigma_{pr} = \frac{\epsilon_g}{\sigma_r} = \frac{\epsilon_N}{\gamma\sigma_z} \approx 0.04$ mrad or $\sigma_{pr} = 17$ MeV/c, much less than that of the maximum defocused protons. This is of course seen on the IS 1 and IS 2 images, where the edge of the defocused protons is at radii much larger than σ_r of the incoming bunch. The initial radial wakefields created by the proton bunch ($\sigma_r = 0.15$ mm, $\sigma_z = 8$ cm, 3×10^{11} protons/bunch) reach a maximum value of $W_\perp = 15$ MV/m (see Chapter 3).

[3] determined by wire-scan measurements in the CERN SPS

The measurements presented here show that the strongly defocused protons exit the plasma after $\sim$4 m ($<$ 10 m) and with a radial momentum of approximately 390 MeV/c. This corresponds to an average transverse wakefield amplitude of $>$70 MV/m, much larger than the maximum seed value of (15 MV/m). If the wakefields had not grown along the plasma, I would expect a maximum transverse momentum less than 120 MeV/c.

These results show that the transverse wakefield amplitude has reached a much larger amplitude than its seed value. It is clear evidence of the growth of the wakefields over the first few meters of plasma.

6.4.1 Growth Rate and Wakefield Amplitude

For a plasma density of 7.7×10^{14} electrons/cm^3, a radial proton bunch size of σ_r =0.15 mm and a bunch length of $\sigma_z \approx 8$ cm I measure a radial proton momentum of $\approx$ 390 MeV/c at 4 m, where the protons exit the wakefield. I attempt to evaluate the growth rate of the instability. The total radial momentum gain p_{max} can be described by:

$$p_{max} = p_0 + \frac{q}{c}\int_0^O W_{0,r} e^{\Gamma z} dz = 370\,\text{MeV/c} \tag{6.7}$$

where $p_0 = 17 \simeq 20$ MeV/c is the initial transverse momentum, O the point along the plasma where the protons exit the wakefields and $W_{0,r}$ the initial transverse wakefield amplitude a proton experiences in plasma.

As a proton starts experiencing the wakefields, it travels towards (focused) or away (defocused) from the axis and experiences varying wakefields along its trajectory, before leaving the wakefields. Here, I use a very simplified model for the wakefields that the proton experiences. I assume that the initial wakefield is the peak seed wakefield (at $r = \sigma_r$) and that the wakefields experienced until it leaves the wakefield is simply that initial amplitude but growing exponentially along the plasma. I use the point of exit of the wakefields determined experimentally ($O = 4$ m) and I assume that the proton velocity is approximately c ($\int_0^t dt = \frac{1}{c}\int_0^{ct} dz$) for Equation 6.7.

The initial seed wakefields calculated for these proton and plasma parameters are $W_{0,r} = 10$ MV/m at σ_z. Assuming that the initial transverse momentum p_0 is 20 MeV/c (as given by the bunch emittance) I calculate the growth rate Γ to be $\approx 0.88\,\text{m}^{-1}$ (from Equation 6.7). From linear theory I can

calculate the average growth rate over 4 m to be $\Gamma = 3.46\,\mathrm{m}^{-1}$.

In addition to the assumptions decribed here above, I expect the measured growth rate to be smaller than the theoretical value because linear theory assumes that the proton bunch and the plasma density are matched meaning that they are self-consistent solution of each other. In the experiment, the proton bunch is not matched to the plasma density at the plasma entrance and it takes some time for them to evolve self-consistently. During this time the wakefields only grow little because the change of radius is small and the change of the wakefield amplitude is also small when compared to the seed wakefields. Apart from that, simulations show that the growth rate from linear theory is only valid in the very beginning of the growth [49].

I can use the growth rate, I just calculated, to estimate the maximum radial wakefield amplitude $W_{r,max}$ by:

$$W_{r,max} = W_{0,r} \cdot e^{\Gamma O} \approx 340\,\mathrm{MV/m}, \tag{6.8}$$

where $W_{0,r} = 10\,\mathrm{MV/m}$ (the amplitude of the transverse seed wakefield at σ_z and σ_r). The corresponding maximum longitudinal wakefield amplitude is $W_{z,max} = W_{0,z} \cdot e^{\Gamma O} = 515\,\mathrm{MV/m}$, where $W_{0,z} = 15\,\mathrm{MV/m}$ is the amplitude of the longitudinal seed wakefield on-axis. These results indicate that the wakefields grew by a factor of ~ 34 or $\sim$3.5 exponentiations over the first 4 m of plasma, as a result of the strong transverse evolution of the proton bunch over that distance.

6.5 Defocused Proton Charge

To estimate how much charge is outside the proton bunch core (and was defocused by the transverse plasma wakefields), I performed the following measurement series in the June measurement campaign:

- ten measurements of proton bunches without laser (the proton bunch traverses rubidium vapour)
- ten measurements of protons and laser pulse (the proton bunch traverses plasma and self-modulates)
- ten background measurements with no protons and no laser pulse.

The vapour density for these measurements was 3.5×10^{14} atoms/cm^3. The laser pulse was placed in the center of the proton bunch with a pulse energy of approximately 200 mJ, the bunch population was 3×10^{11} protons and its length approximately 200 ps.

Figure 6.8 shows the horizontal projections of ten events after background subtraction and normalization to the maximum amplitude of the first measurement of the proton bunch populations (each color represents one measurement). The top panels show the profiles for the case without plasma (laser off), and the lower panels for the case with plasma and self-modulation (laser on). Note that this Figure shows the experimental parameter variations (proton bunch population, bunch jitter) of the measurement.

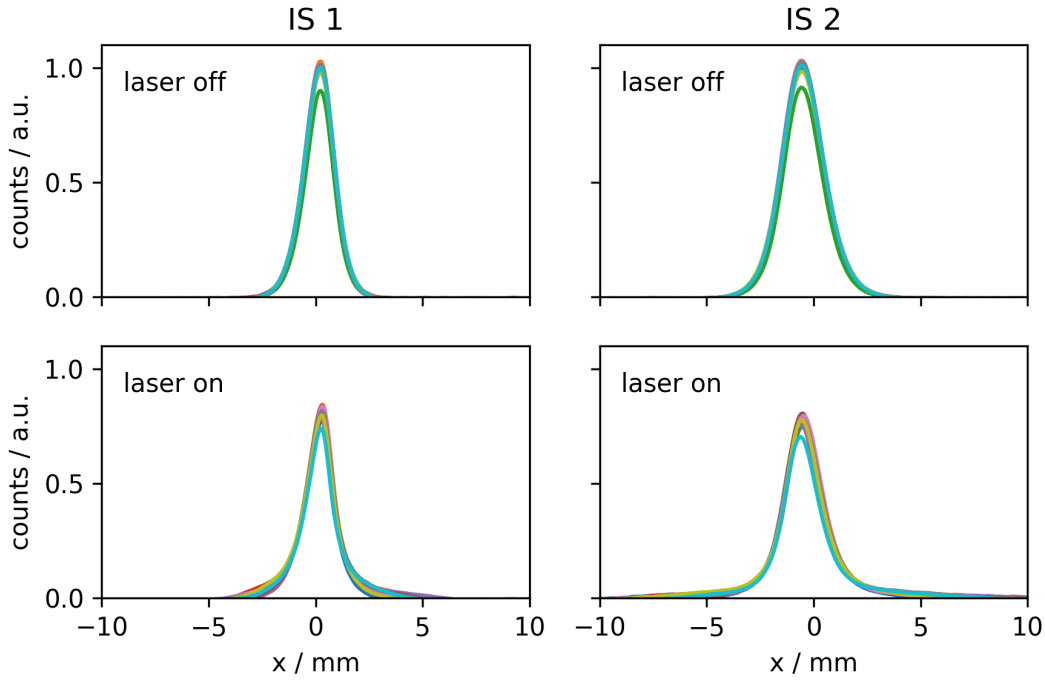

Figure 6.8: Unmodulated (top profiles) and the self-modulated (bottom profiles) proton bunch horizontal profiles on the two imaging station. Each chart shows the profile of ten events after background subtraction.

We note that the the amplitude of the profile decreases by roughly 20 % from the profile without plasma to the one with plasma. Furthermore, when the proton bunch self-modulates, wings appear next to the bunch core (as already determined before, see Section 6.1).

Figure 6.9 compares the average of the ten measurements obtained with

plasma to the average of the measurements without plasma (shown in Figure 6.8). Each measurement was normalized to the number of protons per bunch that were present. The difference in charge in the bunch core is marked by the yellow area, which corresponds to roughly 30 % of the total area of the profile without plasma (area under the red dotted curve). Since in these measurements, the laser pulse was in the center of the proton bunch (in time), I can estimate that due to the self-modulation process 60 % of the protons from after the laser radially exited the bunch core (and count as defocused protons).

In linear wakefield theory 50 % of the wakefield period has a defocusing field, so one could expect that 50 % of the protons are defocused. However, since during the development of the SSM the wakefield phase changes and wakefield amplitudes can reach non-linear values, overall more protons can experience a defocusing field and be defocused.

6.5.1 Self-Modulated Proton Bunch Core

To determine the transverse size of the proton distribution in case there is no plasma, I fit the bunch cores in Figure 6.9 (red dotted lines) with a Gaussian distribution. The observed radial bunch sizes are $\sigma_{r,u} = (0.731 \pm 0.001)\,\mathrm{mm}$ at IS 1 and $\sigma_{r,u} = (1.004 \pm 0.002)\,\mathrm{mm}$ at IS 2.

With self-modulation, the bunch core consists of two populations: the protons ahead of the laser pulse and the ones that are focused by the plasma wakefields. There is no reason to believe that both distributions have the same rms size. This assumption is confirmed by the fact that the radial bunch size (σ_r) obtained from a Gaussian fit depends on the radial extend of the fitting range. For example, the radial bunch size decreases from approximately 0.6 mm to 0.4 mm on IS 1 and 0.8 mm to 0.7 mm on IS 2 in case the fit range is decreased from $\pm 3\sigma_{r,u}$ to $\pm 1\sigma_{r,u}$, where $\sigma_{r,u}$ is the rms radial bunch size of transverse distribution without plasma. Note that after self-modulation the radial rms bunch size of the core decreases independently of the fit range compared to the size of the unmodulated bunch core. This indicates that the transverse size of the focused protons (after the laser pulse) is smaller than that of the incoming bunch.

In principle, the front of the proton bunch does not interact with the

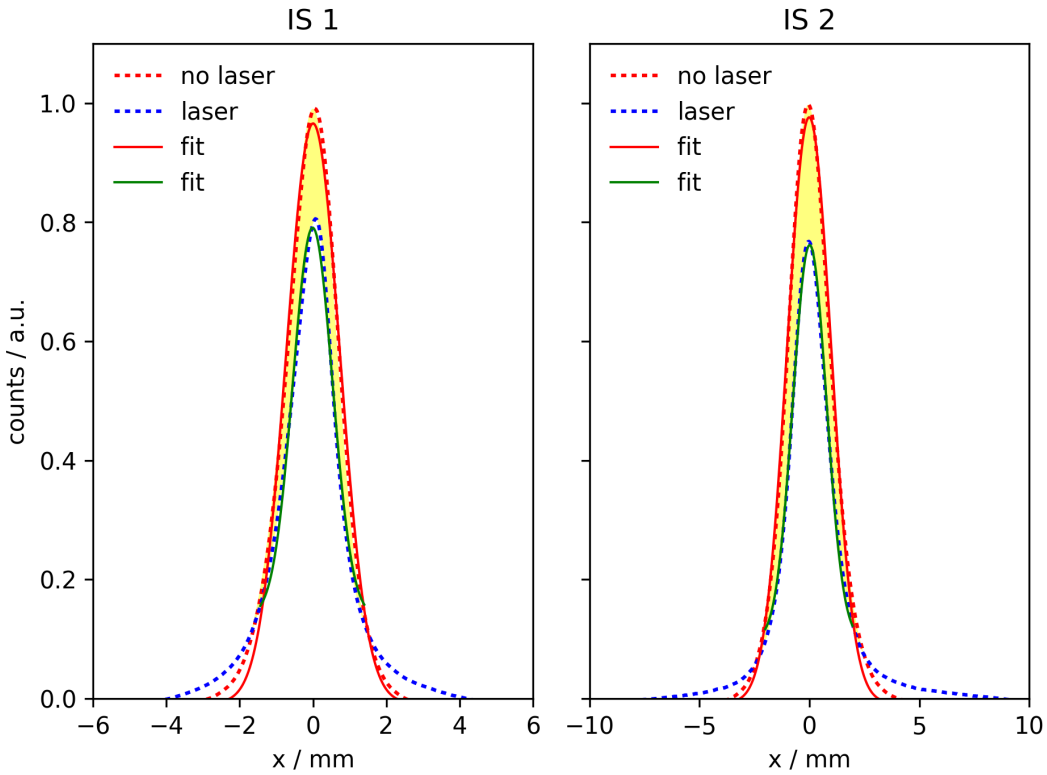

Figure 6.9: Comparison of the measurement of the transverse proton bunch profile in case there is plasma or no plasma (red and blue dotted curves). Each curve represents the average of ten measurements shown in Figure 6.8. The yellow area marks the difference between the two curves in the core region. Red solid lines show Gaussian fits of the bunch core for when there is no laser and green solid lines for when the proton bunch self-modulated in plasma (fit range: $\pm 2\sigma_{r,u}$ of the unmodulated proton bunch core, see Section 6.5.1).

rubidium vapour. However, in the experiment we have found evidence that before the main laser pulse, the one that creates the plasma with an electron density equal to the rubidium vapour density and seeds the SSM, a lower energy pre-pulse (approximately $\sim$10 ns ahead of the main pulse) creates a pre-plasma. The energy of the pre-pulse is estimated to be much lower ($< 1\,\%$) than the energy of the main pulse. We assume that also the plasma density is also much lower than the nominal density. The laser pre-pulse was removed with the help of pockel-cells for the August and September measurements, unfortunately this exact measurement has not been repeated.

As the front of the proton bunch enters the pre-plasma, plasma electrons start moving towards the bunch, and cancel part of the defocusing space

charge force of the bunch. As a result one expects that this part of the bunch reaches the screen with a smaller transverse size than they would have without pre-plasma. This is confirmed by measurements made with the streak camera. Simulation results also indicate that the focused protons form a distribution at the two screens that have a smaller transverse size that the incoming ones.

The measurement in Figure 6.9 shows that the time-integrated transverse size of the proton core (including the protons before and after the main laser pulse) decreases when the bunch traverses plasma and the second half of the bunch self-modulates. Even though from this measurement I cannot distinguish how much of this decrease in radial bunch size comes from the cancellation of space charge for the front of the bunch, or whether there is a decrease due to the focusing wakefields on the micro-bunches, the trend is as expected. However, time resolved images of the proton bunch can be used to answer this question.

6.6 Conclusions

Using the two-screen measurement setup, I detected protons with large radial positions at the two imaging stations. The observation of defocused protons together with the images of the micro-bunches measured by the streak camera are direct evidence of the development of the seeded-self modulation.

We measure maximum defocusing angles on the order of 1 mrad, as expected from simulations and theory. Simulations confirm our experimental results in details.

The fact that measurements show that the transverse momentum of the protons is larger than that of the initial seed wakefields applied over 10 m and that additionally the protons radially exit the wakefields earlier along the plasma proves that the SSM was growing within the 10 m of plasma.

Using a very simple model, I obtain estimates for the growth rate of the SSM as well as for the wakefield amplitudes that may have been driven by the proton bunch in the plasma. These numbers are of the same order of magnitude as those obtained from linear theory. Ultimate wakefield amplitudes will be obtained from electron acceleration experiments.

I also show that more than 60 % of the protons propagating in the plasma are defocused by the wakefields, meaning that 40 % of the protons drive

wakefields after the saturation of the SSM.

7 Conclusions and Outlook

7.1 Conclusions of the Work Presented in this Thesis

In this thesis I study physics properties of the seeded self-modulation in the AWAKE experiment, because AWAKE uses a relativistic self-modulated proton bunch to drive plasma wakefields. The following points were adressed:

- In order to experimentally observe and measure basic parameters of the seeded self-modulation we designed and built the two-screen measurement setup. With this setup I measure ≈ 2 and 10 m downstream the plasma the maximum radius of protons that are defocused by the transverse plasma wakefields. From the two maximum proton transverse distribution radii and the assumption that proton trajectories do not cross downstream the plasma, I calculate the maximum defocusing angle. From the maximum defocusing angle I estimate the total transverse proton momentum acquired in the wakefields.
- Based on the assumption that the maximum defocused protons experience a wakefield strength of $0.5\,E_{WB}$, where E_{WB} is the cold plasma wavebreaking field, and that the defocused protons interact with the plasma wakefields for a radial distance of $2\,c/\omega_{pe}$, I estimated that the maximum defocusing angle should be ≈ 1 mrad. This value is confirmed by simulations.
- For a plasma density of 7.7×10^{14} electrons/cm^3 I measured maximum defocusing angles around (0.98 ± 0.06) mrad, corresponding to a transverse momentum of (390 ± 25) MeV/c. We confirm by simulations that the calculation of the maximum defocusing angle is justified.
- From the maximum defocusing angle and the maximum proton radius at the IS, I can deduce the origin of the defocused protons along the plasma,

if the outermost protons on IS 1 are the same as on IS 2. I experimentally find that for a plasma density of 7.7×10^{14} electrons/cm^3 the protons leave the wakefields around 4 m, which is confirmed by simulations.

- When the protons do not interact with the plasma their rms transverse momentum from the bunch emittance is around 20 MeV/c, corresponding to an angle of 0.05 mrad. The total transverse momentum of the defocused protons is larger than the transverse momentum from the emittance plus the seed wakefields they could experience over 10 m (even though the protons exit earlier). Therefore I can show that the wakefields grow due to the SSM.
- I also show that the growth rate (estimated from the total transverse momentum and the point where the protons exit the wakefields and assuming a simple exponential growth of the seed wakefields) is a factor of four lower than the theoretical growth rate. I explain the difference in growth rate due to the fact that the theoretical prediction assumes matched beam and plasma parameters, whereas it is not the case in the experiment. Hence it is natural that the estimated growth is lower than the actual one. From the calculated growth rate I estimate the maximum transverse wakefield amplitude to be around 340 MV/m and the maximum longitudinal wakefield amplitude to be 515 MV/m.

The results presented in this thesis show that in the experiment: the self-modulation is seeded, the bunch modulates and the wakefields grow significantly along the plasma. To our knowledge it is the first time the growth of the self-modulation of a relativistic particle bunch is observed. These results combined with the direct observation of the proton micro-bunches in time (Doctoral Thesis of K. Rieger, MPP) unambiguously show that the SSM was observed in AWAKE.

During the experiment, the two-screen measurement worked very well and reliably and I was able to resolve the maximum defocused protons at all densities. In general the diagnostics is quite robust and straightforward and can be used to qualify and quantify many other effects: i.e. the difference between SSM and the hosing instability, hosing instability characteristics and filamentation of the proton bunch.

Since the time between the data taking (June 2017) and the handing in of

this thesis was short, this thesis only shows the very first and most important analysis results. Further analysis can be done (i.e. from the measurements with different plasma density gradients or proton bunch lengths...).

The main results of this thesis will be submitted for publication in the near future and expanded on a future publication.

The two-screen measurement setup could be improved by a third imaging stations in between the two existing ones: At the moment, I assumed that the outermost proton trajectories do not cross after the plasma exit because of the simulation results. I could add a third imaging station in between the existing two IS (i.e. 6 m after the plasma exit) to prove that this assumption is indeed justified.

7.2 Long Term Outlook for the AWAKE Experiment

AWAKE is a R&D proof-of-principle experiment and the final goal is to design and build a high-energy accelerator (0.1-1 TeV) based on the acquired knowledge.

So far, the experiment was able to demonstrate the development and growth of the seeded self-modulation in the 10 m of plasma. The physics of the SSM has been proven to exist and is understood. Its parameters scale as expected with experimental parameters, such as for example plasma density or proton bunch population.

In a next step, the AWAKE experiment will use the wakefields driven by the self-modulated proton bunch to accelerate externally injected low-energy electrons ($\sim$ 15 MeV) to energies of $\sim$ 1 GeV. This first demonstration of electron acceleration is planned for 2018.

The next big step for AWAKE is to control the proton bunch, plasma and laser parameters to the level where it can be used as an accelerator for physics experiments and to create an electron bunch with tens of GeV. The accelerated electron bunch must further have: a micron-level normalized emittance, a percent level relative energy spread and an electron bunch charge of 0.2-1 nC. This is the goal of AWAKE Run 2 which is scheduled from 2021 onwards.

If Run 2 were successful a proposal for a proton-driven plasma wakefield

accelerator producing electrons with 50-100 GeV for fixed target physics would be prepared as an intermediate step before proposing a plasma-based high-energy electron-proton physics collider [6].

Bibliography

[1] C. Grupen, Handbook of Particle Detection and Imaging. Chapter: Synchrotron Radiation.

[2] CLIC Conceptual Design Report, A Multi-TeV Collider based on CLIC Technology, Geneva (2012).

[3] V. Shiltsev, Crystal Ball: On the Future High Energy Colliders. PoS EPS-HEP2015 (2015) 515.

[4] E. Adli et al., A Beam Driven Plasma-Wakefield Linear Collider: From Higgs Factory to Multi-TeV, Proceedings of IPAC (2014).

[5] W. Leemans and E. Esarey, Laser-Driven Plasma-Wave Electron Accelerators, Physics Today (2009).

[6] A. Caldwell et al., Proton-Driven Plasma-Wakefield Acceleration, Nature Physics (2009), DOI:101038/NPHYS1248.

[7] T. Tajima et al., Laser Electron Accelerator, PRL 43 (1979).

[8] C. E. Clayton et al., Ultrahigh-Gradient Acceleration of Injected Electrons by Laser-Excited Relativistic Electron Plasma Waves, PRL 70 (1993).

[9] D. Strickland and G. Mourou, Compression of Amplified Chirped Optical Pulses, Optics Communications (1985).

[10] S. P. D. Mangles, et al., Monoenergetic Beams of Relativistic Electrons from Intense Laser-Plasma Interactions, Nature 431, 535–538 (2004); doi:10.1038/nature02939.

[11] C. G. R. Geddes et al., High-quality Electron Beams from a Laser Wakefield Accelerator using Plasma-Channel Guiding, Nature 431, 538–541 (2004); doi:10.1038/nature02900.

[12] J. Faure et al., A Laser-Plasma Accelerator Producing Monoenergetic Electron Beams, Nature 431, 541–544 (2004); doi:10.1038/nature02963.

[13] W. P. Leemans et al., Multi-GeV Electron Beams from Capillary-Discharge-Guided Subpetawatt Laser Pulses in the Self-Trapping Regime, PRL 113 (2004).

[14] P. Chen et al., Acceleration of Electrons by the Interaction of a Bunched Electron Beam with a Plasma, Phys. Rev. Lett. 54 (1985).

[15] J. B. Rosenzweig, Experimental Observation of Plasma Wake-Field Acceleration, PRL 61 (1988).

[16] I. Blumenfeld et al., Energy Doubling of 42 GeV Electrons in a Metre-Scale Plasma Wakefield Accelerator, Nature 445, 741-744 (2007).

[17] E. Kallos et al., High-Gradient Plasma-Wakefield Acceleration with Two Subpicosecond Electron Bunches, PRL 100 (2008).

[18] N. Kumar, et al., Self-Modulation Instability of a Long Proton Bunch in Plasmas, Phys. Rev. Lett. 104, 255003 (2010).

[19] Y. Fang et al., Seeding of Self-Modulation Instability of a Long Electron Bunch in a Plasma, PRL 112 (2014).

[20] P. Muggli et al., Electron Bunch Self-Modulation in a Long Plasma at SLAC FACET, Proceedings of IPAC (2014).

[21] AWAKE Collaboration, Proton-driven Plasma Wakefield Acceleration: a Path to the Future of High-Energy Particle Physics, Plasma Phys. Control. Fusion 56, 084013 (2014).

[22] A. Caldwell et al., Path to AWAKE: Evolution of the Concept, Nucl. Instr. Meth. A 829, 3 (2016), NIM doi:10.1016/j.nima.2015.12.050.

[23] E. Oz et al., An Accurate Rb Density Measurement Method for a Plasma wakefield Accelerator Experiment using a Novel Rb Reservoir, NIM A (2016).

[24] S. Mazzoni et al., Beam Instrumentation Developmentes for the Advanced Proton Driven Plasma Wakefield Acceleration Experiment at CERN, Proceedings of IPAC (2017).

[25] K. Rieger et al., GHz Modulation Detection using a Streak Camera: Suitability of Streak Cameras in the AWAKE Experiment, Review of Scientific Instruments 88, 025110 (2017).

[26] P. Muggli et al., AWAKE Readiness for the Study of the Seeded Self-Modulation of a 400 GeV Proton Bunch, arXiv:1708.01087, 2017, to be published in: Plasma Physics and Controlled Fusion.

[27] R. Keinings and M. E. Jones, Two-Dimensional Dynamics of the Plasma Wakefield Accelerator, The Physics of Fluids 30, 252 (1987).

[28] J. Dawson, Nonlinear Electron Oscillations in a Cold Plasma, PRL 113 (1959).

[29] D. H. Whittum et al., Electron-Hose Instability in the Ion-Focused Regime, PRL 67 (1991).

[30] K. Lotov et al., Natural Noise and External Wakefield Seeding in a Proton-Driven Plasma Accelerator, PRSTAB 16, 041301 (2013).

[31] A. Pukhov et al., Phase Velocity and Particle Injection in a Self-Modulated Proton-Driven Plasma Wakefield Accelerator, PRL 107 (2011), DOI: 10.1103/PhysRevLett.107.145003.

[32] K.V. Lotov, Phys. Plasmas, (1998), v.5, N 3, p.785-791.

[33] K.V. Lotov, Phys. Rev. ST Accel. Beams 6, 061301 (2003).

[34] `www.inp.nsk.su/~lotov/lcode/`.

[35] M. Turner et al., Proton Beam Defocusing as a Result of Self-Modulation in Plasma, Proceedings of NAPAC (2016).

[36] M. Turner et al., The Two-Screen Measurement Setup to Indirectly Measure Proton Beam Self-Modulation in AWAKE, NIM A (2017).

[37] M. Turner et al., Upgrade of the Two-Screen Measurement Setup in the AWAKE Experiment, IOP, Proceedings of IPAC (2017).

[38] E. Bravin et al., A New TV Beam Observation System for CERN, CERN-AB-2005-076. Proceedings of DIPAC (2005).

[39] S. Burger et al., Scintillation and OTR Screen Characterization with a 440 GeV/c Proton Beam in Air at the CERN HiRadMat Facility. Proceedings of IBIC (2016).

[40] I. Efthymiopoulos et al., A new Irradiation Facility for Material Testing at CERN. Proceedings of IPAC (2011).

[41] Jackson J. D., Classical Electrodynamics, Wiley (1999).

[42] T. Lefevre et al., A Large Scintillating Screen for the LHC Dump Line, Proceedings of DIPAC (2007).

[43] R. E. Shafer, A Tutorial on Beam Loss Monitoring, TechSource, Inc. Santa Fe, NM.

[44] A. Ferrari et al., FLUKA: A Multi-Particle Transport Code, CERN-2005-10 (2005), INFN/TC_05/11, SLAC-R-773.

[45] `http://www.efg2.com/Lab/ImageProcessing/TestTargets/#USAF1951` (02.10.2017)

[46] `https://docs.scipy.org/doc/scipy-0.16.1/reference/generated/scipy.ndimage.filters.median_filter.html` (02.10.2017)

[47] G. Fivres, Master Thesis, MPP (2017).

[48] M. Turner et al., A Method to Determine the Maximum Defocused Proton Radius of a Self-Modulated Proton Bunch, to be submitted to NIM A as part of the EAAC 2017 proceedings.

[49] K. Lotov, Physics of Beam Self-Modulation in Plasma Wakefield Accelerators, Physics of Plasmas (2015).

Appendix

Nuclear Instruments and Methods in Physics Research A 854 (2017) 100–106

Contents lists available at ScienceDirect

Nuclear Instruments and Methods in Physics Research A

journal homepage: www.elsevier.com/locate/nima

The two-screen measurement setup to indirectly measure proton beam self-modulation in AWAKE

M. Turner[a,b,*], B. Biskup[a,c], S. Burger[a], E. Gschwendtner[a], S. Mazzoni[a], A. Petrenko[a]

[a] CERN, Geneva, Switzerland
[b] Graz University of Technology, Graz, Austria
[c] Czech Technical University, Prague, Czech Republic

ARTICLE INFO

Keywords:
AWAKE
Beam instrumentation
Self-modulation instability
Beam driven plasma wakefield acceleration

ABSTRACT

The goal of the first phase of the AWAKE [1,2] experiment at CERN is to measure the self-modulation [3] of the $\sigma_z = 12$ cm long SPS proton bunch into microbunches after traversing 10 m of plasma with a plasma density of $n_{pe} = 7 \times 10^{14}$ electrons/cm^3. The two screen measurement setup [4] is a proton beam diagnostic that can indirectly prove the successful development of the self-modulation of the proton beam by imaging protons that got defocused by the transverse plasma wakefields after passing through the plasma, at two locations downstream the end of the plasma. This article describes the design and realization of the two screen measurement setup integrated in the AWAKE experiment. We discuss the performance and background response of the system based on measurements performed with an unmodulated Gaussian SPS proton bunch during the AWAKE beam commissioning in September and October 2016. We show that the system is fully commissioned and adapted to eventually image the full profile of a self-modulated SPS proton bunch in a single shot measurement during the first phase of the AWAKE experiment.

1. Introduction

1.1. The AWAKE experiment

The Advanced Proton-Driven Plasma Wakefield Acceleration Experiment (AWAKE) [1,2] is a proof-of-principle R & D experiment at CERN that uses a 400 GeV/c proton bunch, with 3×10^{11} protons/bunch, from the CERN SPS to create GV/m plasma wakefields over meter scale distances. To excite strong plasma wakefields efficiently, the proton beam bunch length has to be in the order of the plasma wavelength λ_{pe}. In the AWAKE experiment we use a 10 m long rubidium vapor source with a density of $n_{pe} = 7 \times 10^{14}$ electrons/cm^3 (which corresponds to a plasma wavelength of $\lambda_{pe} = 1.2$ mm) and the SPS proton bunch has a length of $\sigma_z = 12$ cm. Hence, the experiment relies on the development of the self-modulation instability [3] (SMI) to modulate the long proton bunch into micro-bunches spaced at the plasma wavelength. The SMI is seeded by the sharp proton beam edge (or sudden turn-on of the plasma) created by overlapping the proton bunch with a short (100 fs) laser pulse ionizing the rubidium. As the SMI develops, transverse plasma wakefields periodically focus and defocus the proton beam creating a micro-bunch structure. The goal of the first phase of the AWAKE experiment (starting in December 2016) is to prove that the SMI developed successfully and that GV/m plasma wakefields were created.

In the second phase of the experiment (starting in late 2017), 10–20 MeV electrons will be injected into the wakefield, and accelerated to an energy of several GeV. A schematic layout of the AWAKE experiment is shown in Fig. 1.

In this paper we describe in detail the design choices of the measurement setup designed to indirectly prove proton beam self-modulation in the AWAKE experiment at CERN. We discuss the performance and background response of the system based on measurements taken during the AWAKE proton beam commissioning in 2016 with an unmodulated Gaussian proton beam and no plasma.

1.2. Challenges and requirements of the two-screen measurement system

The idea of the two screen measurement [4] is to image the strongest defocused protons (defocused by the plasma wakefield) approximately 2 m and 10 m downstream the end of the plasma (see Fig. 2a) using two imaging stations (IS). From this measurement, we can calculate the maximum proton defocusing angle. Measuring maximum defocusing angles in the order of 1 mrad (instead of 0.05 mrad without plasma) indirectly proves that strong plasma wakefields were present in plasma. Additionally, by using the position and

* Corresponding author at: CERN, Geneva, Switzerland.

http://dx.doi.org/10.1016/j.nima.2017.02.064
Received 2 December 2016; Received in revised form 14 February 2017; Accepted 20 February 2017
Available online 21 February 2017

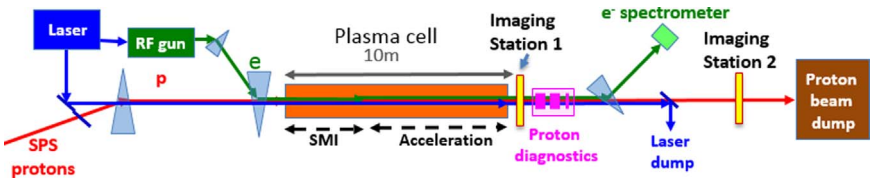

Fig. 1. Schematic layout of the AWAKE experiment.

angle of the maximum defocused protons, we determine at which position along the plasma these protons got their radial kick.

From plasma simulations, performed with 2D3v quasistatic LCODE [5,6], and using the AWAKE baseline parameters [1] we expect a self-modulated transverse proton beam distribution like the one shown with red dots in Fig. 3. The blue line in Fig. 3 shows the unmodulated Gaussian proton beam distribution that we expect to measure on the screens if there is no plasma present. Since we want to determine the maximum defocusing angle of the self-modulated proton bunch, it is crucial that the system can measure the outermost – or strongest defocused – protons [7], because the outermost protons experienced the highest product of wakefield strength times interaction distance.

The challenges of measuring a proton beam distribution like the one shown with red dots in Fig. 3 are:

- We want to image the outermost edge of the defocused beam but the beam core is 4 orders of magnitude more intense.
- We must be able to measure the self-modulated proton beam edge as well as the unmodulated proton beam (in case of no plasma) with the same system.
- The setup works in a radiation environment ($\approx 10^{12}$ high energy hadrons per cm^2 per year).

Based on this requirement we developed two specialized beam imaging stations (IS), based on available systems at CERN. Both IS include a choice of screens (including screens consisting of more than one material and screens with a hole) that emit optical light either via Optical Transition Radiation (OTR) or Scintillation and the setup uses a radiation-resistant analog camera to capture the emitted light. Fig. 2b shows the AWAKE experimental area, including the two imaging stations (IS) for the two screen measurement.

Further requirements on these detector stations are as follows:

- The screens withstand the impact of the 400 GeV/c proton beam with 3×10^{11} protons every 30 s.
- The optical light emitted by the proton beam edge (expected from plasma simulations: $\approx 10^6$ protons/mm^2) gives a clear signal on the camera.
- We require a measurement resolution of 0.4 mm to measure the maximum defocusing angle within an uncertainty of 10% and the origin of the defocused particles with a precision of ± 1.3 m.

2. The beam imaging station in AWAKE

Two imaging stations (IS1 and IS2) measure the transverse proton beam distribution 2 m and 10 m downstream the end of the plasma. The imaging stations, as shown in Fig. 4, consist of the support, vacuum vessel, screen insertion device, light emitting screens, illumination system, filter wheel, lens and camera. The light emitted by the imaging screens goes through a filter and a focusing lens (IS1: focal length=50 mm; IS2: focal length=35 mm) before it reaches the CCD image sensor. The analog interlaced video feed (camera: WATEC 902-H3 ULTIMATE (CCIR)) is then digitized to 400 × 300 pixels [8]. The field of view is 26.98×34.9 mm on IS1 and 57.51×71.42 mm on IS2. The camera is not synchronized to the proton bunch extraction from the CERN SPS. Independent of the proton bunch, the camera triggers every 20 ms. This does not affect the amount of light captured from Optical Transition Radiation (OTR) since OTR is emitted instantaneous. But it affects the amount of light captured from a scintillating screen because the light is emitted over tens of milliseconds. Previous measurements [9], performed with an unsynchronized camera, showed that the camera captured significantly less light (up to −50%) in approximately 30% of the images captured with a 1 mm thick Chromox screen. Consequently, we expect to reject approximately 30% of the performed measurements.

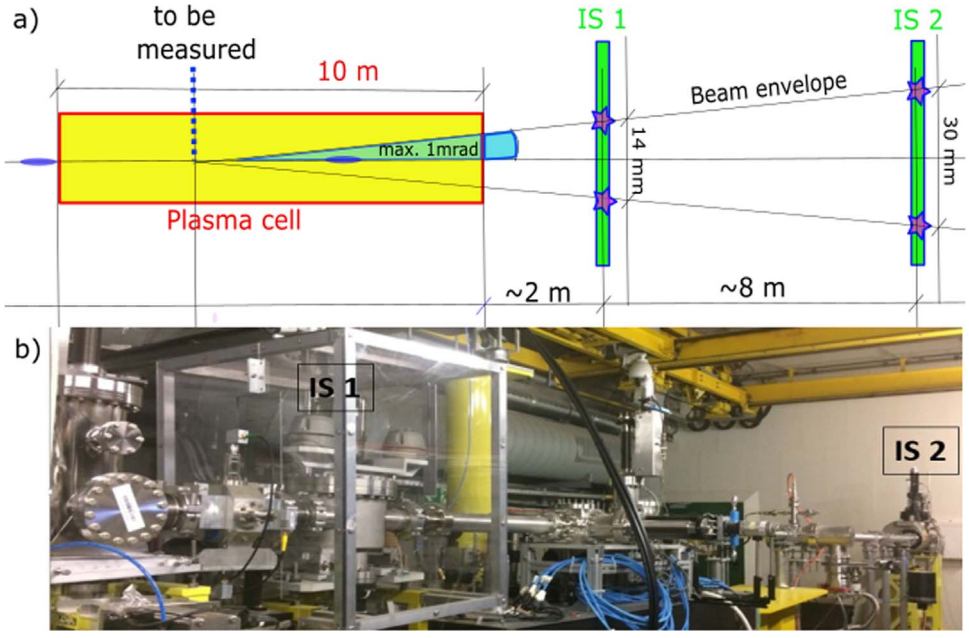

Fig. 2. (a) Schematic drawing of the two-screen setup. (b) An image of the AWAKE experimental area, showing the two installed imaging stations.

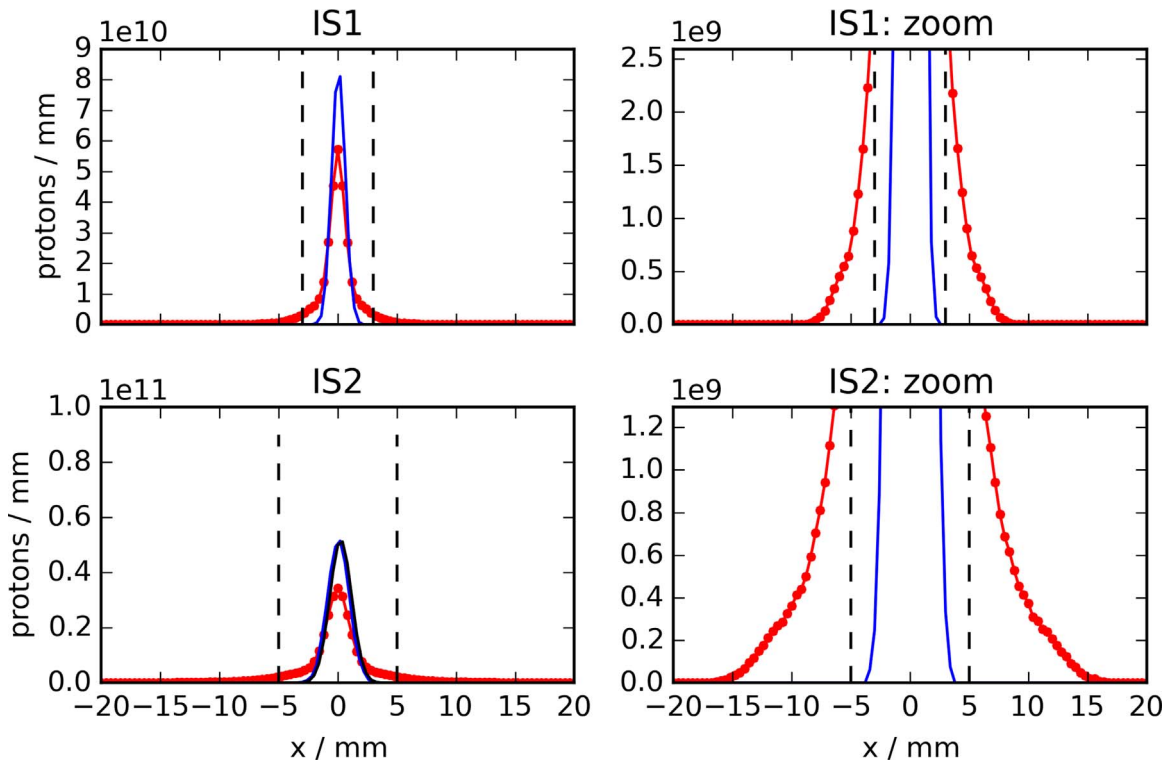

Fig. 3. Expected proton beam distribution with (red lines with dots) and without plasma (blue lines) on the first and second imaging station. The 2D image is integrated over the vertical plane. Vertical dashed lines show the size of the holes that were cut into the imaging screens. (For interpretation of the references to color in this figure caption, the reader is referred to the web version of this paper.)

1. The first imaging station holds two different screens (screen size=6 × 6 cm):
   1. SiAg: 0.3 mm thick silicon coated with silver (OTR).
   2. Chromox: 1 mm thick Al_2O_3: CrO_2 with a hole $r = 3$ mm (scintillator).
2. The second imaging station holds three different screens (screen size=10 × 10 cm):
   1. Chromox: 1 mm thick (scintillator).
   2. Chromox: 1 mm thick with a hole $r = 5$ mm (scintillator).
   3. Combined screen: 1 mm thick Chromox with an $r = 5$ mm, 1 mm thick Aluminum insertion at the center (scintillator + OTR).

The size of the holes was chosen based on Fig. 3 to cut off most of the beam core. Screens and filters can be changed remotely. The filters have an opening of 1 in and are limiting the aperture in the optical line from the screens to the camera for the first imaging station. In the second imaging station the acceptance is limited by the 1 in lens. Filters in the filter wheels were chosen to be transmitting 1% and 0.1% of the captured light for the first and 1%, 0.1% and 0.01% for the second imaging station.

2.1. Selected screen material properties

As discussed in Section 1.2, the imaging screens must fulfill the following requirements:

- All screens withstand the impact of the proton beam.

We tested 15 different screen materials in the HiRadMat [10] facility at CERN [9]. All screens withstood the proton beam impact (2×10^{11} protons/bunch at 440 GeV/c), but a change of color was noticed on two undoped Alumina samples. Based on the results of these measurements we choose to measure the defocused proton beam edge with a 1 mm thick Chromox screen (Al_2O_3: CrO_2) because it created the second strongest signal on the camera and did not blur the signal as much as the tested 3 mm Chromox screen.

As the self-modulated proton beam will pass through the imaging screens, it will deposit energy in the screen material. We calculated the temperature rise in the imaging screens, based on the energy deposit of the proton beam simulated with FLUKA [12]. In the case of Chromox we used the density ρ and heat capacity c of Aluminum ($\rho_{Alu} = 2.7$ g/cm^3, $c_{Alu} = 0.897$ J/(kg K)). We can neglect the Silver coating of the Silver coated Silicon screen, because the coating layer is only a few nm thick. ($\rho_{Si} = 2.3$ g/cm^3, $c_{Si} = 0.703$ J/(kg K)).

Fig. 5 shows that the maximum temperature rise in the screens ranges from 0.07 to 1.8 K per self-modulated proton beam pulse. The AWAKE experiment will get beam every 30 s and the screens will handle this small, locally limited temperature increase, as the melting point of the screens ranges from 660 to 2000 °C.

- The light emitted by the proton beam edge (expected from plasma simulations: ≈10^6protons/mm^2) gives a clear signal on the camera.

FLUKA calculations show that a 400 GeV/c proton loses about 1 MeV when traversing 1 mm of Chromox. From simulations we expect ~10^6 protons/mm^2 in the defocused proton beam edge and that 1 MeV of deposited energy emits ~10^4 photons [11] over 4π. The acceptance of our imaging system is limited by the 1 in opening of the lens and the distance between the screen and the lens (≈50 cm). We estimate that using the lowest demagnification approximately 3000 photons arrive on one pixel imaging ≈90 × 90 μm^2 (we know from experience with similar setups that there should be a minimum of 1000–2000 photons/pixel to get a clear signal).

- Screen resolution better than 0.4 mm.

The screen resolution is estimated by twice of the size that one pixel images and ranges from 180 μm on IS1 to 400 μm on IS2.

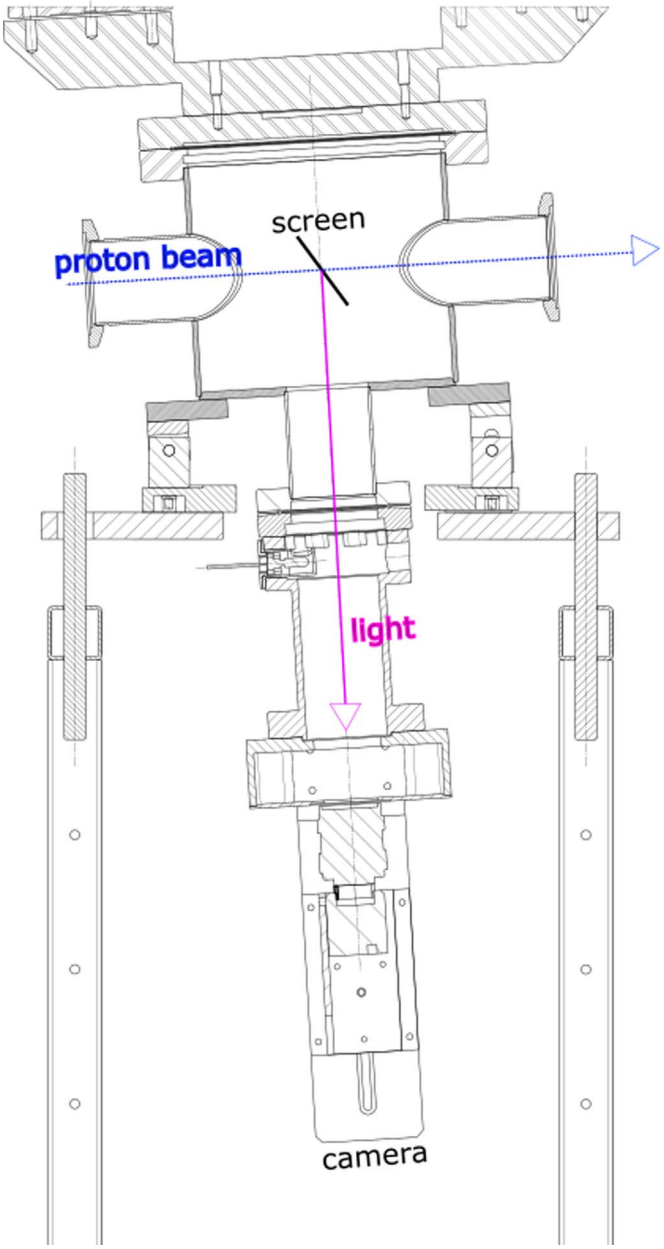

Fig. 4. Technical drawing of the first proton beam imaging station.

3. Optimized imaging screens

The self-modulated proton beam density projected onto a 2D screen extends over 4 orders of magnitude (see Fig. 3). The limited dynamic range (2–3 orders of magnitude) of the CCD camera makes the detection of the defocused proton beam edge challenging. One solution to measure the defocused edge is to cut a hole into the imaging screen (see vertical dashed lines in Fig. 3), so that the dense beam core can pass without interacting with the screen. Following this idea two 1 mm Chromox screens with a hole radius of 3 mm and 5 mm were installed in two imaging stations in the AWAKE tunnel.

3.1. Combined screen

Another possibility of handling the intense beam core is a combined screen (see Fig. 6). In the combined screen, the hole at the center of the scintillating Chromox screen was filled with the OTR emitting material Aluminum. A combined screen was installed in the third slot of the IS2. The left side of Fig. 7 shows a measurement of the combined screen during AWAKE proton beam commissioning in October 2016. There was no plasma, so we imaged an unmodulated Gaussian proton beam from the CERN SPS with a momentum of 400 GeV/c and 1×10^{11} protons per bunch.

During the beam commissioning, we captured light emitted by the Aluminum and Chromox screens on our cameras. After normalizing to the extracted proton beam intensity and the used optical filter we calculated that with our setup the Chromox screen emits 2700 ± 400 times more photons than the Aluminum screen.

The expected transverse proton beam sigma σ_r at the second imaging station (see blue line in Fig. 3) is $\sigma_r = 0.92$ mm. We measure the radial beam sigma in Fig. 7 by fitting a Gaussian distribution to the beam core and obtain from the fit $\sigma_r = 0.7 \pm 0.02$ mm which agrees within the resolution of the measurement. For large radial positions ($r > 5\sigma_r$) proton bunches are not perfectly Gaussian so we did not perform a fit on the data of the surrounding Chromox.

On the right side of Fig. 7 we boost the light emitted by the Aluminum at the center of the screen by 2700 (ratio between the light emission of Aluminum and Chromox) to reconstruct the full beam profile. Fig. 7 shows that the combined screen can measure beam intensities of almost five orders of magnitude in a singe-shot measurement using a standard CCD camera.

The defocusing angle of the defocused protons and the saturation point of the self-modulation instability can only be analyzed after we performed measurements with plasma.

3.2. Beam and screen alignment

As illustrated in Fig. 3, the proton beam should be aligned to the center of the hole in the screen within 0.5 mm (expected proton beam jitter: $\sigma_r = 100$ μm). We aligned the imaging screens by mechanically moving the IS tanks, after the final proton beam trajectory was set.

4. Signal to background measurements

The light emission of scintillators is proportional to the energy deposited in the material. Using FLUKA, we simulated the energy deposition of the self-modulated proton beam in the 1 mm thick Chromox screen of the second imaging station. To understand if inserting an imaging screen on IS1 influences the energy deposit on a screen inserted in IS2 (i.e. because of secondary particles production by the first screen), we studied the energy deposit in the Chromox screen of IS2 for three different scenarios:

1. IS1: Screen out.
2. IS1: SiAg in.
3. IS1: Chromox in.

Simulations did not show any measurable increase of energy deposit for scenarios (2) and (3).

During proton beam commissioning of the AWAKE experiment in September 2016, we benchmarked those simulation results. We imaged a unmodulated Gaussian proton beam with 1×10^{11} protons, using the combined screen of the second imaging station (IS2). The results are presented in Fig. 8. The red diamonds in the left part of the figure present the measurement for when no screen was inserted at IS1 (scenario 1), and the green ‘o’ when the SiAg screen was used in IS1 (scenario 2). In contrast of the simulations, we notice that the background increased by ≈1800 counts/bin.

As a consequence we studied the origin of the background by capturing empty images on IS2 (no screen inserted), while the SiAg screen was inserted in IS1 (black ‘+’) and we measured the same level of background as in scenario (2). Additionally the measured background level was independent of the filter used, so we concluded that secondary particles produced by the first imaging screens directly impact on the CCD chip of the camera.

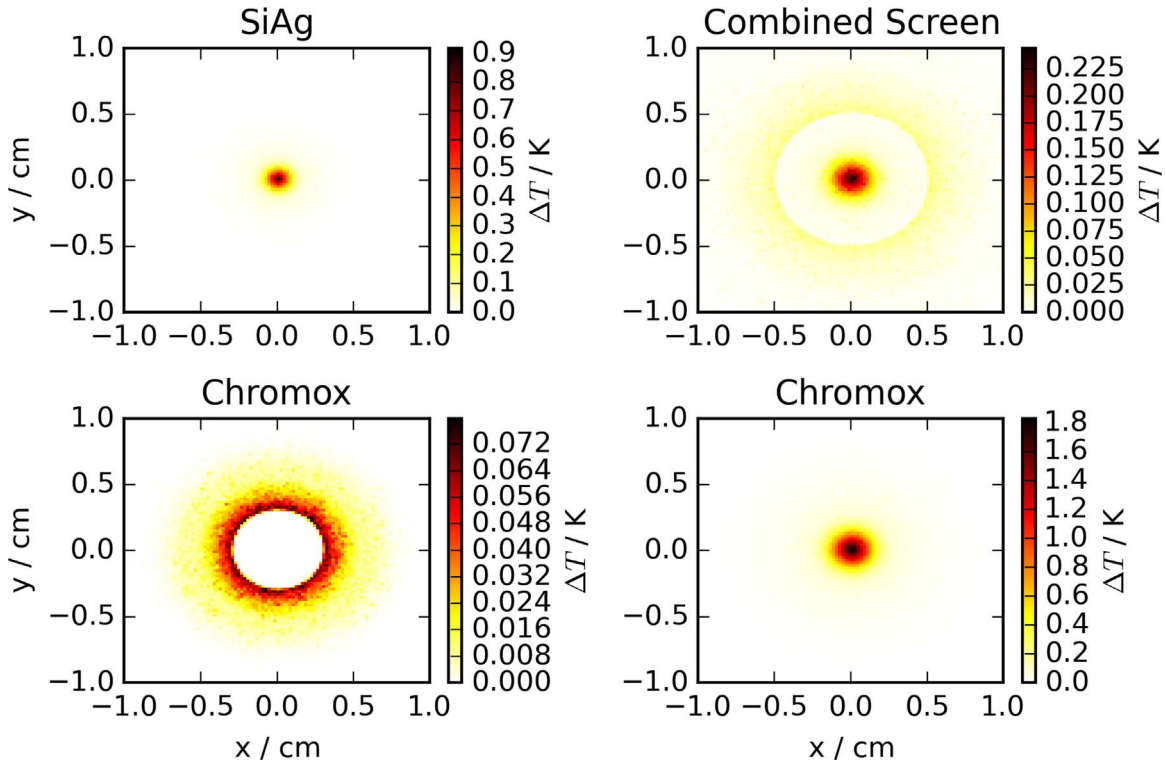

Fig. 5. Temperature rise in the imaging screens. The images on the left show the screens of the first imaging station and on the right of the second.

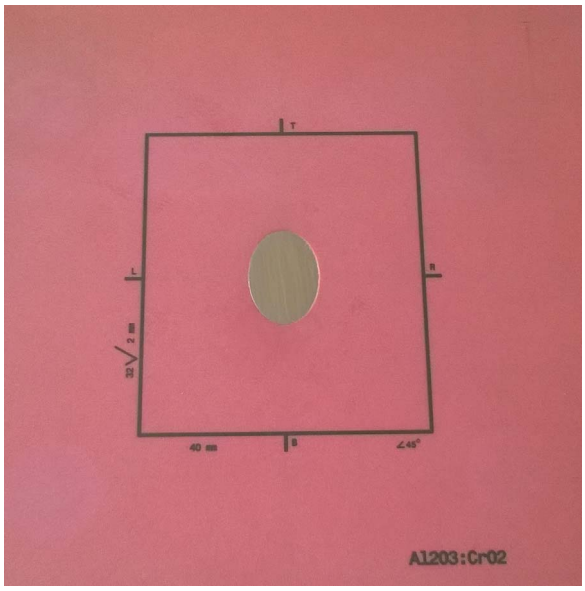

Fig. 6. Beam imaging screen combining the high-light-yield scintillating material Chromox for measuring the defocused proton beam edge together with the low-light-yield OTR emitting material Aluminum for the measurement of the intense beam core.

The nuclear interaction length of Silicon is 46.52 cm [13]. The thickness of the first imaging screen that we inserted was 0.3 mm which means that 1 out of 2500 protons has a nuclear interaction with the screen material and can create secondary particles. Combining this estimate with a previous one on Coulomb scattering of the protons [4], we do not expect any measurable change of the proton beam profile and we also confirmed this with measurement shown in the right side image of Fig. 8.

Fig. 8 shows the overlap of the measurement for when no screen was inserted at IS1 (scenario 1, red diamonds) and when the SiAg screen was used in IS1 (scenario 2, green 'o'). We subtracted the pedestal of 1800 counts from this measurement and achieved an overlap in the height of the signal. In the right image of Fig. 8 we observe neither a blurring nor a measurable distortion of the proton beam profile.

It was not possible to study the effect of the Chromox screen in IS1 on the measurement with IS2, because the unmodulated proton beam that we used during commissioning entirely passes through the $r = 3$ mm hole of the Chromox screen in IS1.

5. Conclusions

We have validated the design of two beam imaging stations installed downstream the plasma in the AWAKE experiment. These stations are designed to measure the defocused proton beam edge of the self-modulated proton beam by using a 1 mm thick Chromox screen. We chose the scintillator Chromox because it withstands the impact of the 400 GeV/c SPS proton bunch and emits enough light to detect a proton beam density of 10^6 protons/mm^2. To measure the self-modulated proton beam edge next to the four orders of magnitudes more intense beam core, we developed a combined screen which consists of an Aluminum screen surrounded by Chromox. Imaging an unmodulated Gaussian proton beam on the combined screen showed that the imaging system can measure proton beam intensities of almost five orders of magnitudes with a standard CCD camera.

The background signals of the imaging stations are understood and were measured in the AWAKE experiment environment: secondary particles produced by the first screen can impact on the camera of the second imaging station and increase the background level by ≈1800 counts/bin (in a vertically integrated beam image). Inserting a screen in the first imaging station does not worsen the measured proton beam profile on the second station.

The measurement setup is fully commissioned and ready for the measurement of the self-modulation instability of the proton beam in the AWAKE experiment.

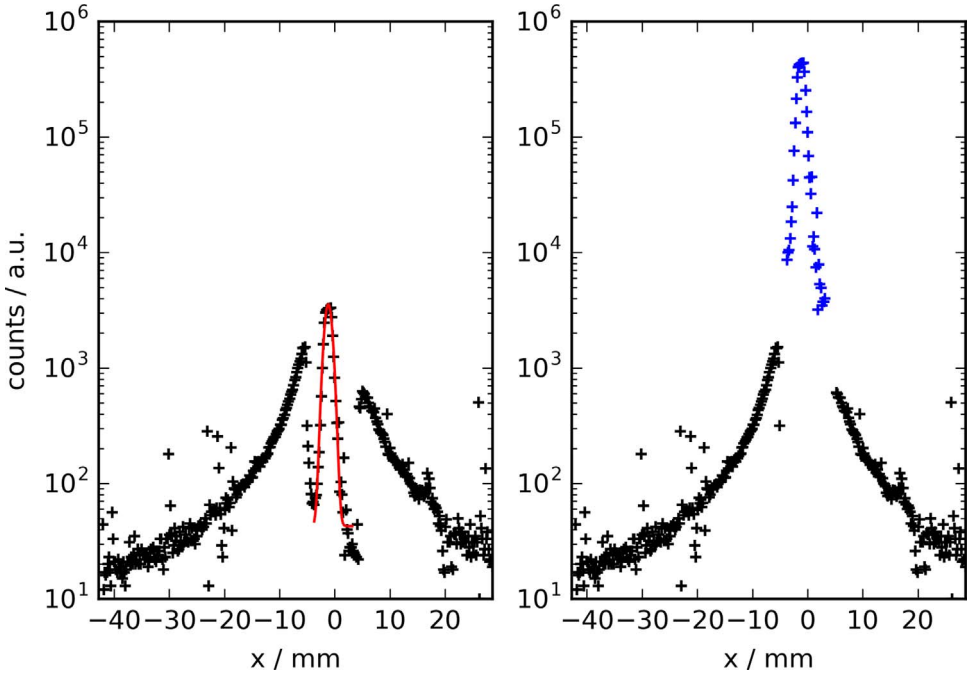

Fig. 7. The left image shows the central pixelline of a measurement with the combined screen of IS2. The right image shows the same data, but the beam core is boosted by the light emission ratio of Chromox over Aluminum. The red line of the left image shows a Gaussian fit of the measured beam core. (For interpretation of the references to color in this figure caption, the reader is referred to the web version of this paper.).

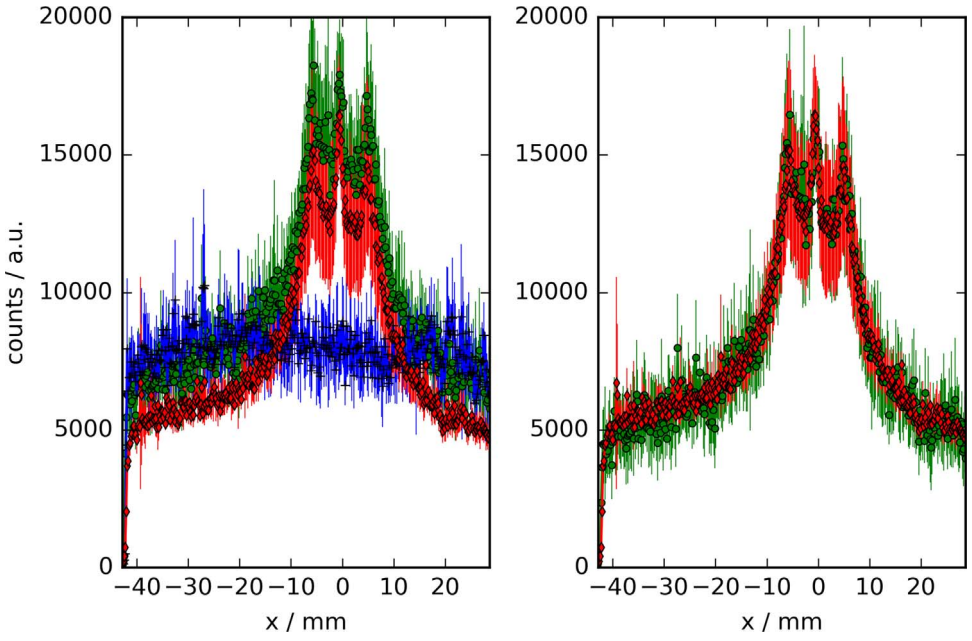

Fig. 8. Proton beam measurements of the combined screen performed during AWAKE beam commissioning. The dots of every curve represent the average of 8 measurements and the errorbars show the standard deviation. The data is integrated in the vertical plane. Red diamonds show measurement on the combined screen on IS2 for when no screen was inserted at IS1, the green 'o' when the SiAg screen was used in IS1 and the black '+' show the measurement on IS2 (no screen inserted) while the SiAg screen was used in IS1. (For interpretation of the references to color in this figure caption, the reader is referred to the web version of this paper.)

References

[1] E. Gschwendtner, et al., AWAKE, The Advanced Proton Driven Plasma Wakefield Acceleration Experiment at CERN, Nucl. Instrum. Methods A 829 (2016) 76–82. http://dx.doi.org/10.1016/j.nima.2016.02.026.
[2] A. Caldwell, et al., Path to AWAKE: evolution of the concept, Nucl. Instrum. Methods A 829 (2016) 3–16. http://dx.doi.org/10.1016/j.nima.2015.12.050.
[3] N. Kumar, et al., Self-modulation instability of a long proton bunch in plasmas, Phys. Rev. Lett. 104 (2010) 255003.
[4] M. Turner, et al., Indirect self-modulation instability measurement concept for the AWAKE proton beam, Nucl. Instrum. Methods A 829 (2016) 314–317. http://dx.doi.org/10.1016/j.nima.2016.01.060.
[5] ⟨www.inp.nsk.su/~lotov/lcode/⟩.
[6] K.V. Lotov, Fine wakefield structure in the blowout regime of plasma wakefield accelerators, Phys. Rev. ST Accel. Beams 6 (2003) 061301.

[7] M. Turner, et al., Proton beam defocusing as a result of self-modulation in plasma. Proceedings of NAPAC 2016, 2016.
[8] E. Bravin, et al., A new TV beam observation system for CERN, in: CERN-AB-2005-076. Proceedings of DIPAC 2005, 2005.
[9] S. Burger, et al., Scintillation and OTR screen characterization with a 440 GeV/c proton beam in air at the CERN HiRadMat Facility, in: Proceedings of IBIC 2016, 2016.
[10] I. Efthymiopoulos, et al., A new irradiation facility for material testing at CERN, in: Proceedings of IPAC 2011, 2011.
[11] T. Lefevre, et al., A large scintillating screen for the LHC dump line ⟨http://epaper.kek.jp/d07/papers/tupb28.pdf⟩.
[12] A. Ferrari, et al., FLUKA: a multi-particle transport code, CERN-2005-10, 2005, INFN/TC_05/11, SLAC-R-773.
[13] C. Patrignani, et al., Particle Data Group, Chin. Phys. C 40 (2016) 100001.

IOP Conf. Series: Journal of Physics: Conf. Series **874** (2017) 012031 doi:10.1088/1742-6596/874/1/012031

Upgrade of the two-screen measurement setup in the AWAKE experiment

Marlene Turner[1], Vincent Clerc, Ishkhan Gorgisyan, Edda Gschwendtner, Stefano Mazzoni and Alexey Petrenko

CERN, Geneva, Switzerland
[1] also at Technical University of Graz, Graz, Austria

E-mail: marlene.turner@cern.ch

Abstract. The AWAKE project at CERN uses a self-modulated 400 GeV/c proton bunch to drive GV/m wakefields in a 10 m long plasma with an electron density of $n_{pe} = 7 \times 10^{14}$ electrons/cm^3. We present the upgrade of a proton beam diagnostic to indirectly prove that the bunch self-modulated by imaging defocused protons with two screens downstream the end of the plasma. The two-screen diagnostic has been installed, commissioned and tested in autumn 2016 and limitations were identified. We plan to install an upgraded diagnostics to overcome these limitations.

1. Introduction

The Advanced Proton Driven Plasma Wakefield Acceleration Experiment (AWAKE)[1] is a proof-of-principle R&D project at CERN. The goal of AWAKE is to accelerate electrons using plasma wakefields with GV/m amplitude created by a self-modulated proton bunch. The proton bunch provided by the CERN SPS has a momentum of 400 GeV/c, a longitudinal size σ_z of 12 cm and a radial beam rms radius of $\sigma_r = 0.2$ mm. A 100 fs long, 450 mJ laser pulse ionizes 10 m of rubidium vapour and creates a plasma channel with a radius of 1 mm and a plasma density ranging from $10^{14} - 10^{15}$ electrons/cm^3.

The optimum proton bunch length for a given plasma density is given by $k_{pe}\sigma_z \cong \sqrt{2}$, where $k_{pe} = \omega_{pe}/c$ is the plasma wavenumber, ω_{pe} the angular plasma frequency and c the speed of light. For a plasma density of 7×10^{14} electrons/cm^3 (AWAKE baseline) the optimum bunch length is in the mm-range, much shorther than the $\sigma_z = 12$ cm of the proton bunch. Hence AWAKE relies on the development of the self-modulation-instability (SMI) [2] to modulate the long proton bunch into micro-bunches spaced at the plasma wavelength $\lambda_{pe} = 2\pi/k_{pe}$. The self-modulation instability is seeded by a sharp turn-on of the plasma, realized by placing the ionizing laser pulse in the center (temporally) of the proton bunch.

Seed wakefields periodically focus and defocus protons. As the instability develops, micro-bunches are formed due to the proton density modulation near the axis. These micro-bunches can then resonantly drive the plasma wave. AWAKE studies of the SMI are scheduled for 2016 and 2017, and electron acceleration of externally injected electrons is planned for 2018.

In this article we discuss the upgrade of a proton beam diagnostics to indirectly demonstrate that the self-modulation instability develops within the 10 m of plasma. The basic version of this setup is described in [3] and was successfully operated during a first AWAKE run in December

2016. We explain the limitations we observed with this setup and discuss a major upgrade on the system, to be operational before the next beam time in June 2017.

2. The goal of the indirect SMI two-screen measurement system

The basic idea of the two-screen diagnostic is to image the protons that are defocused by the transverse plasma wakefields and to measure their maximum defocusing angle. As indicated in Figure 1, we want to measure maximum radial displacement of the protons by inserting scintillating screens 2 and 10 m downstream the plasma. As the protons traverse the screen, the screen emits scintillation light. The radial, time-integrated proton beam profile is reconstructed by imaging the light onto a camera.

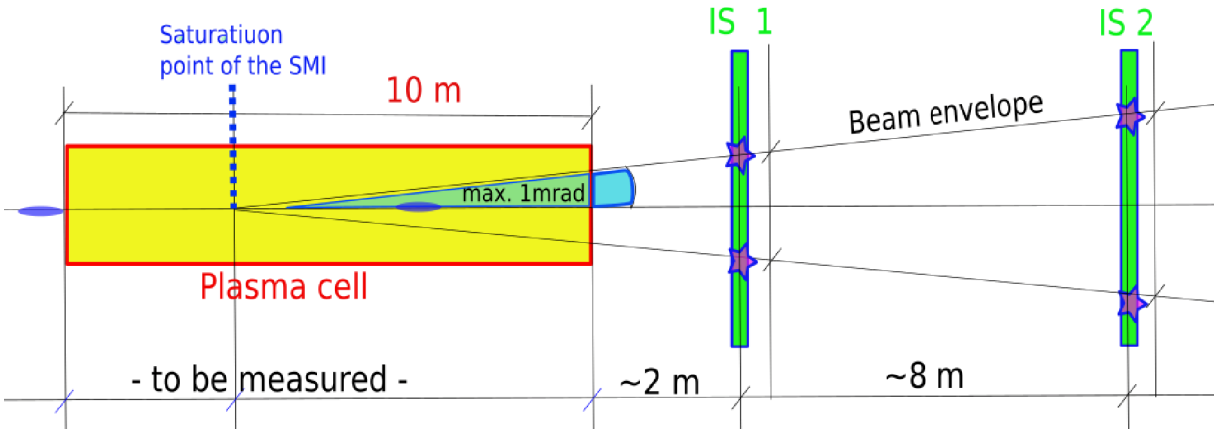

Figure 1. Schematic drawing of the principle behind the two screen measurement setup.

Figure 1 also suggests that we can calculate the maximum proton defocusing angle from the two beam images by connecting the measured maximum radial displacements. If SMI develops successfully we expect to measure a maximum defocusing angle around 1 mrad instead of the ≈ 0.05 mrad without plasma and SMI. Defocusing the proton beam from its natural divergence up to $\approx$1 mrad over a distance of ≈ 0.5 m (as expected from LCODE [4, 5] simulations) requires GV/m defocusing plasma wakefields.

Figure 2 shows the expected radial proton beam profiles at the two screen locations in case of no plasma and no SMI (blue line) and with SMI in plasma with a density of 7×10^{14} electrons/cm^3 (red line).

We want to detect the outermost proton beam edges and one major challenge for measuring these edges is that the beam density on the screen ranges over 4-5 orders of magnitude, while the dynamic range of the cameras is limited to 2-3 orders of magnitudes. We previously found that the Chromox screen light yield is directly (linearly) proportional to the proton beam density traversing the screen [6]. We do not expect any light yield degradation over time because of the low number of protons per bunch N_p ($N_p = 3\times10^{11}$) and the low repetition rate (1 bunch every 30 s).

3. The two screen measurement setup

Previously, we installed two imaging stations (IS1, IS2) 2 and 10 m downstream the end of the plasma (see Figure 1). Each imaging station consisted of a vacuum tank, a scintillating screen (Chromox:Al_2O_3:CrO_2), a filter wheel, a camera lens, a camera and an image readout system.

Since the dynamic range of the camera is limited to 2-3 orders of magnitude, we cut a hole with a radius of 3 and 5 mm into the first and the second screen, respectively (see vertical

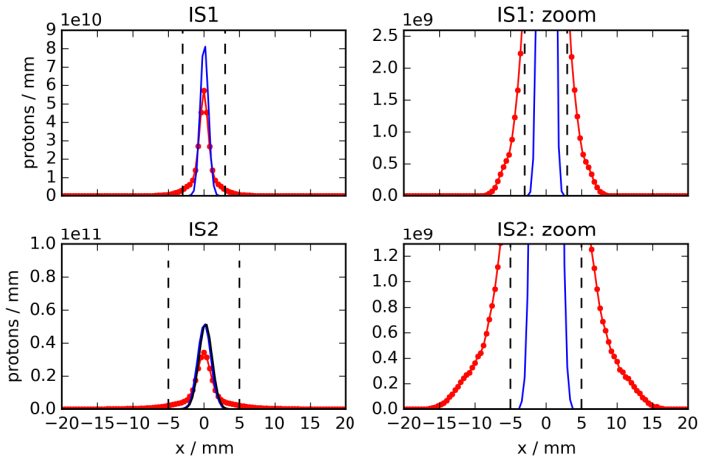

Figure 2. From LCODE [4, 5] simlations expected transverse profile of the self-modulated proton bunch for the AWAKE baseline parameters [3] (red) and no plasma (blue). Dashed lines indicate the size of the holes that were cut into the imaging screens (see the following section).

dashed lines in Figure 2). For one screen installed in IS2 we filled the hole with a low light yield material (aluminum) to create a combined screen. The two imaging stations were commissioned and successfully operated in December 2016, but we identified several limitations of the system:

- If the experimental observations differ from the expected simulation results shown in Figure 2 or we change for example the plasma density, we need to change the size of the hole in the screens. Changing screens is a major intervention that takes several days because it involves breaking the beam-line vacuum.
- The proton beam has to pass through the center of the hole in the screen with an accuracy of 0.1 mm. If the experiment decides to change the proton beam trajectory, the screens have to be realigned. Realignment can be done by precisely moving the vacuum tank, but due to safety reasons can imply breaking the vacuum.
- The imaging stations use analogue video cameras (standard system at CERN working well in radiation environment). The cameras are triggered every 20 ms and integrate over 20 ms, independently of the arrival time of the proton bunch. Hence we are unable to compare measurements in terms of signal intensity.
- Information regarding the beam core is either lost (if the screen has a hole) or limited (combined screen), due to the fixed light yield ratio between the screen materials in the combined screen.

We propose an upgrade to overcome the observed limitations and to make the system more flexible for the experiment.

4. The upgraded two screen measurement system

A schematic of the upgraded optics system for IS1 is shown in Figure 3.

We replaced the scintillating Chromox screen with a hole by a full Chromox screen. Instead of imaging the light emitted by the scintillator screen directly onto a camera, we split the light using a 3 inch pellicle beam splitter that reflects 8% and transmits 92% of the emitted light.

The reflected light is directly imaged onto the camera C1 by the lens L1. The image of camera C1 will provide information about the size and position of the beam core. The transmitted light is imaged by lens L2 (3 inch, f=200 mm) onto the plane M, where the mask is placed. The mask blocks the intense beam core by an opaque region in mask. A technical drawing of the mask setup is shown in Figure 4. The mask is reimaged by lens L3 onto camera C2.

The mask system consists of a 1 mm thick fused silica window with different sized opaque coatings, a glass holder, two stepper motors for horizontal and vertical alignment and a manual

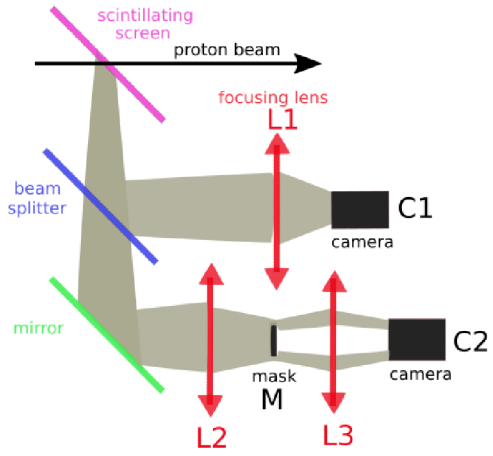

Figure 3. Schematic drawing of the optics setup of the upgraded imaging system of IS1.

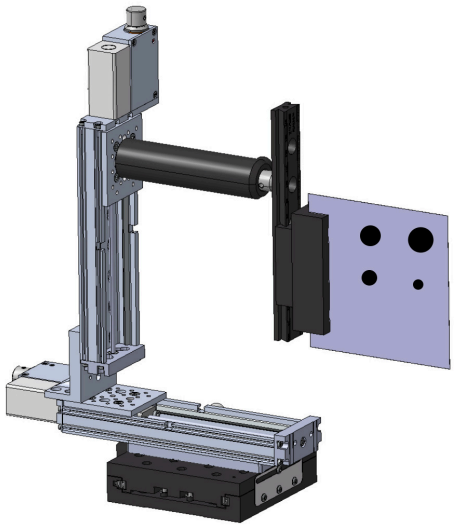

Figure 4. Schematic drawing of the light-core blocking mask system.

translation stage to faciliate imaging by longitudinal positioning on the table. The distances are chosen to have an image magnification of 0.5 in the mask plane. The light passing around the mask is then reimaged onto an externally triggered 12 bit camera (Basler ac1600-60gm).

The optics for IS2 are very similar to the one from IS1 (see Figure 3), but due to space restrictions the beam splitter comes after the mirror.

We have several different mask sizes available and we can remotely adjust and align the mask for various cases (i.e. plasma densities, changing proton beam trajectory, etc.) by varying the radius to which we want to block the beam core. We use a camera, that is synchronized to the proton beam -to capture all the emitted light- so that we can directly compare different events and explore the radial proton beam profile in details. We can now optimally observe the beam core and the defocused protons in terms of light intensity and mask size.

The procedure will be as follows: We locate the beam without mask, align the mask onto the beam and then adjust filters in the optical line to get the right exposure of the camera.

We previously found [3] that the main background contribution comes from secondary particles directly impacting onto the camera. The laser dump ≈ 30 cm upstream IS1 shields the imaging screen from low-energy electrons from the plasma. Since the plasma wakefield amplitude is low in this experiment, trapping and accelerating electrons is unlikely.

5. Summary

We discussed an upgrade of the indirect SMI two-screen measurement system to be installed in the AWAKE experiment and ready for operation in June 2017. The idea of the two screen measurement setup is to image protons that got defocused by the transverse plasma wakefields to indirectly show that the proton bunch self-modulated and wakefields were created in the 10 m of plasma. The upgraded system offers different mask sizes to block the light from the beam core, facilitates alignment of the masks with respect to the proton beam, enables comparability between measurements and images also the proton beam core.

In the upgraded system we split the light emitted by the scintillator screen and image one part directly onto a camera to obtain information about the beam core. The other part blocks the beam core with a mask with several mask sizes available, to detect the maximum defocused protons.

References

[1] Caldwell A *et al.* 2016 *Nucl. Instrum. Meth.* A **829** 3-16
[2] Kumar N *et al.* 2010 *Phys. Rev. Lett.* **104** 255003
[3] Turner M *et al.* 2017 *Nucl. Instrum. Meth.* A **854** 100-106
[4] `www.inp.nsk.su/~lotov/lcode/`
[5] Lotov K V 2003 *Phys. Rev. ST Accel. Beams* **6** 061301
[6] Burger S *et al.* 2016 *Proc. Int. Beam Instrumentation Conference* (Barcelona) 268

PROTON BEAM DEFOCUSING AS A RESULT OF SELF-MODULATION IN PLASMA

Marlene Turner,[1*] CERN, Geneva, Switzerland
Alexey Petrenko, Edda Gschwendtner, CERN, Geneva, Switzerland
Konstantin Lotov,[2] Alexander Sosedkin,[2] Novosibirsk State University, 630090, Novosibirsk, Russia
[1]also at Technical University of Graz, Graz, Austria
[2]also at Budker Institute of Nuclear Physics SB RAS, 630090, Novosibirsk, Russia

Abstract

The AWAKE experiment will use a 400 GeV/c proton beam with a longitudinal bunch length of $\sigma_z = 12$ cm to create and sustain GV/m plasma wakefields over 10 meters [1]. A 12 cm long bunch can only drive strong wakefields in a plasma with $n_{pe} = 7 \times 10^{14}$ electrons/cm^3 after the self-modulation instability (SMI) developed and microbunches formed, spaced at the plasma wavelength. The fields present during SMI focus and defocus the protons in the transverse plane [2]. We show that by inserting two imaging screens downstream the plasma, we can measure the maximum defocusing angle of the defocused protons for plasma densities above $n_{pe} = 5 \times 10^{14}$ electrons/cm^{-3}. Measuring maximum defocusing angles around 1 mrad indirectly proves that SMI developed successfully and that GV/m plasma wakefields were created [3]. In this paper we present numerical studies on how and when the wakefields defocus protons in plasma, the expected measurement results of the two screen diagnostics and the physics we can deduce from it.

INTRODUCTION

The Advanced Proton-Driven Plasma Wakefield Acceleration Experiment (AWAKE) is currently under construction at CERN. AWAKE will use a 400 GeV/c proton beam from the CERN SPS to excite GV/m plasma wakefields. The goal of AWAKE is to accelerate electrons to GeV energies in 10 m of plasma [1].

AWAKE uses a 10 m-long rubidium vapour source with a density of 7×10^{14} electrons/cm^3 [4]. A 450 mJ laser (4 TW, 100 fs) [5] ionizes the outermost electron of the rubidium atom and creates a plasma with a radius of 1 mm. The 400 GeV/c proton drive bunch has a longitudinal bunch length of $\sigma_z = 12$ cm, a radial bunch size $\sigma_r = 0.2$ mm, 3×10^{11} protons per bunch and an emittance of 3.6 mm mrad.

Using the linear plasma wakefield theory and the condition of most efficient wakefield excitation: $\sigma_z = \sqrt{2}c/\omega_{pe}$, where c is the speed of light, $\omega_{pe} = \sqrt{4\pi n_{pe} e^2/m_e}$ the plasma electron frequency, n_{pe} the plasma electron density, e the electron charge and m_e the electron mass, we can estimate that the optimum plasma density for $\sigma_z = 12$ cm is $n_{pe} = 4 \times 10^9$ electrons/cm^3, which corresponds to a maximum accelerating field of ≈ 6 MV/m. To create GV/m plasma wakefields AWAKE will use a plasma density of $n_{pe} = 7 \times 10^{14}$ electrons/cm^3 which corresponds to an optimum drive bunch length of $\sigma_z \approx 0.3$ mm.

The energy of the proton bunches available at CERN is enough to accelerate electrons up to the TeV range [6]. To reach GV/m wakefields, the experiment must rely on the self-modulation instability (SMI) to modulate the long proton bunch into micro-bunches spaced at the plasma wavelength λ_{pe} ($\lambda_{pe} = 1.2$ mm for $n_{pe} = 7 \times 10^{14}$ electrons/cm^3). These micro-bunches can then resonantly drive plasma wakefields.

The SMI is seeded by the ionization front created by a short laser pulse overlapping with the proton bunch [6]. The transverse wakefields periodically focus and defocus protons, depending on their position ξ along the bunch; the proton bunch, while being modulated, contributes to the wakefield growth.

Inserting two imaging screens downstream of the plasma, gives the possibility to detect the protons that are focused and defocused by the SMI.

Phase 1 of the AWAKE experiment will start in late 2016. The goal is to measure and understand the development of the SMI. In AWAKE phase 2 (2017-2018) externally injected electrons with the energy ≈ 15 MeV will be accelerated to GeV energies.

In this paper, we study the wakefields that act on the defocused protons and we look at the proton trajectories. We describe the measurable quantities of the two-screen images and show how we plan to determine the saturation point of the SMI from these images.

NUMERICAL SIMULATIONS

Wakefields Acting on the Proton Drive Bunch

Plasma simulations were performed with the quasi-static 2D3v code LCODE [7,8]. All following simulations use the AWAKE baseline parameters described in the Introduction section except that we used a more realistic proton beam emittance of 2.2 mm mrad instead of 3.6 mm mrad [9].

To understand the SMI and proton defocusing, we look at the wakefields that a proton experiences when traversing the plasma. Figure 1a shows the force - the contributions from the radial electric field E_r and the azimuthal magnetic field B_ϕ- that affects the proton with the highest radial momentum p_r. The resulting force in CGS units is:

$$F_r = E_r - B_\phi \quad (1)$$

* marlene.turner@cern.ch

In Figure 1b we show the radial proton position r as a function of the longitudinal coordinate z along the plasma.

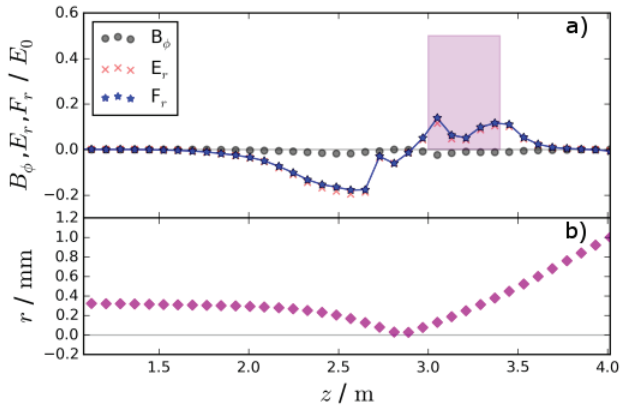

Figure 1: (a) Fields and the transverse force acting on the maximum defocused proton as a function of the longitudinal position z along the plasma. (b) The radial proton r position as a function of z.

Figure 1a shows that the proton deflection results mainly from the radial electric field E_r while the azimuthal magnetic field B_ϕ contributes around ten-times less. The transverse force acts on the protons from approximately 2 to 3.6 m propagation distance in plasma ($\approx$ 1.6 m).

We observe that the proton passes through a field that reaches up to 20% of the maximum wave-breaking field $E_0 = m_e c\omega_p/e$, which corresponds to $\sim$ 0.5 GV/m ($E_0 \sim$ 2.5 GV/m for the $n_{pe} = 7 \times 10^{14}$ electrons/cm^3). The average experienced wakefield is around $0.15\, E_0 \sim 0.375$ GV/m. Plasma wakefields in the simulation reach up to $0.4\, E_0 \sim$ 1 GV/m, but the proton experiences only a fraction of this field.

Simulations show that the maximum defocusing angle θ is on the order of 1 mrad.

In a previous article [3], we estimated this angle as:

$$\theta \sim \sqrt{\frac{m_e}{\gamma m_p}} \qquad (2)$$

where γ is the relativistic Lorentz factor of the proton and m_p is the proton mass. This estimate assumes that the proton experiences a wakefield of $0.5\, E_0$ over a distance of 40 cm (see the pink box in Fig. 1a). The resulting radial kick is approximately 1 mrad. Now we see that while the average force was overestimated by a factor of four, the interaction distance was underestimated by the same factor, so Eq. 2 is still valid and the maximum defocusing angle estimate stays at $\approx$ 1 mrad.

The proton shown in Figure 1 first experiences a focusing force towards the beam axis. There are no transverse wakefields on the axis, the proton crosses the axis. Then the proton enters a defocusing wakefield and experiences a defocusing force away from the beam axis. Our simulations confirmed that this kind of trajectory is typical for strongly defocused protons.

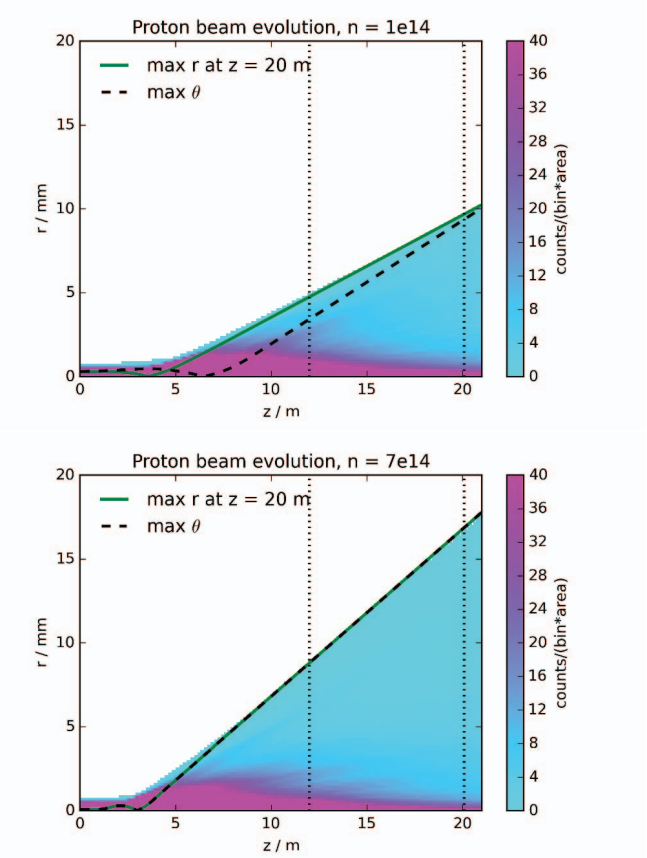

Figure 2: Proton beam density evolution for a plasma density of $n_{pe} = 1 \times 10^{14}$ electrons/cm^{-3} (top) and $n_{pe} = 7 \times 10^{14}$ electrons/cm^{-3} (bottom). The plasma starts at $z = 0$ and ends at $z = 10$ m.

The wakefields that the proton experiences in Figure 1 shift from the focusing to the defocusing phase of the wake, while the proton's longitudinal position ξ remains the same (15 cm after the seeding laser pulse). The wakefield at this ξ-position is determined by the proton distribution at the preceding part of the beam. Since the shape of the proton bunch evolves during SMI, the phase of the wakefield changes as well. The phase shift is an accumulated effect that increases along the proton bunch. We observed that protons at the rear part of the bunch generally defocus: if they start in the focusing region they appear in the defocusing field as the wakefields shifts. If they start in the defocusing field, they move radially too far out to experience a significant focusing field after the phase shift. As a consequence, the number of protons in the decelerating focusing phase decreases towards the end of the proton bunch and the wakefield amplitude saturates.

Maximum Defocusing Angle θ

We aim to experimentally measure the maximum angle of the defocused protons to indirectly prove that strong plasma wakefields were created. The proton beam size is measured 2 m and 10 m downstream from the plasma exit by inserting two imaging screens. If protons with the largest radial posi-

tion at the first screen also have the maximum defocusing angle, we can obtain this angle θ from the two beam images.

In Figure 2 we show a density plot of the proton beam evolution in and outside of the plasma (where $z = 0$ corresponds to the entrance of the plasma). In the top plot of Figure 2 the plasma density is $n_{pe} = 1 \times 10^{14}$ electrons/cm^{-3} and we see that at $z = 12$ m the outermost particle (green line) does not correspond to the one with the maximum defocusing angle θ (black line). In the bottom plot of Figure 2 though, where the plasma density is $n_{pe} = 7 \times 10^{14}$ electrons/cm^{-3}, we see that the outermost particle is the one with the maximum defocusing angle at both screens.

We analysed the trajectories for plasma densities ranging from $n_{pe} = 1 \times 10^{12}$ to 1.4×10^{15} electrons/cm^{-3} and concluded that we are able to measure the maximum defocusing angle θ for plasma densities above $n_{pe} = 5 \times 10^{14}$ electrons/cm^{-3}. The maximum defocused protons get their radial kick in proximity of the maximum wakefield amplitude along the plasma. The maximum wakefield amplitude is present at the saturation point of the SMI along the plasma. Consequently, for plasma densities above $n_{pe} = 5 \times 10^{14}$ electrons/cm^{-3} the origin location of the maximum defocused protons and SMI saturation point can be reconstructed by measuring the maximum proton beam size and calculating the maximum defocusing angle θ.

CONCLUSIONS

In AWAKE the main defocusing force that acts on the protons during the development of the SMI results from the radial electric field E_r. In the experiment, we expect that plasma wakefields on the order of 0.4 GV/m defocus protons over a distance of $\Delta z \approx 1.6$ m. The resulting maximum proton defocusing angle is ≈ 1 mrad. Consequently, measuring defocusing angles around 1 mrad proves that strong plasma wakefields were created and indirectly confirms the development of SMI.

We showed that the two-screen diagnostics can measure the maximum defocusing angle θ for plasma densities higher than $n_{pe} = 5 \times 10^{14}$ electrons/cm^{-3}. Having the maximum defocusing angle θ and the radial proton beam size, we can determine the saturation point of the SMI along the plasma.

REFERENCES

[1] AWAKE Collaboration, *"Proton-driven plasma wakefield acceleration: a path to the future of high-energy particle physics,"* *Plasma Phys. Control. Fusion,* vol. *56*, p. 084013, 2014.

[2] N. Kumar *et al., "* Self-Modulation Instability of a Long Proton Bunch in Plasmas,*"* *Phys. Rev. Lett*. vol. 104, p. 255003, 2010.

[3] M. Turner *et al.*, *"*Indirect Self-Modulation Instability Measurement Concept for the AWAKE Proton Beam,*"* *Nucl. Instr. Meth. A,* vol. 829, p. 314, 2016, NIM doi: 10.1016/j.nima.2016.01.060.

[4] E. Oz *et al.*, *"*A novel Rb vapor plasma source for plasma wakefield accelerators,*"* *Nucl. Instr. Meth. A,* vol. 740, p. 197, 2014, NIM doi:10.1016/j.nima.2013.10.093.

[5] J. Moody *et al., "*Laser propagation effects during photoionization of meter scale rubidium vapor source,*"* in *Proc. IPAC2015*, p.2499.

[6] A. Caldwell *et al., "*Path to AWAKE: Evolution of the concept,*"* *Nucl. Instr. Meth. A,* vol. 829, p. 3, 2016, NIM doi:10.1016/j.nima.2015.12.050.

[7] `www.inp.nsk.su/~lotov/lcode/`

[8] K.V.Lotov, *"*Fine wakefield structure in the blowout regime of plasma wakefield accelerators,*"* *Phys. Rev. ST Accel. Beams,* vol. 6, p. 061301, 2003.

[9] C. Bracco *et al.,* "Beam studies and experimental facility for the AWAKE experiment at CERN," *Nucl. Instr. Meth. A,* vol. 740, p. 48, 2014, NIM doi: 10.1016/j.nima.2013.10.060.

A Method to Determine the Maximum Defocused Proton Radius of a Self-Modulated Proton Bunch

M. Turner[a], E. Gschwendtner[a], P. Muggli[a,b]

[a]*CERN, Geneva, Switzerland*
[b]*Max-Planck Institute for Physics, Munich, Germany*

Abstract

The AWAKE experiment at CERN aims to drive strong plasma wakefields with a self-modulated proton drive bunch. During the self-modulation process, protons are defocused by the transverse plasma wakefields and form a halo around the focused bunch core. The two-screen setup integrated in AWAKE measures the transverse, time-integrated proton bunch distribution downstream the 10 m long plasma to detect defocused protons. By measuring the maximum radii of the defocused protons we attempt calculate properties of the self-modulation. In this article, we develop a routine to identify the maximum radius of the defocused protons, based on a standard contour method. We compare the maximum radius to the logarithmic lineouts of the image to show that the radius identifies the edge of the signal above background level.

Keywords: AWAKE, Seeded Self-Modulation, Plasma Wakefield Acceleration, Two-Screen Setup

1. Introduction

In the AWAKE [1] experiment at CERN, we use the two-screen measurement setup [2, 3] to detect protons that are defocused by the transverse plasma wakefields during the self-modulation process. By identifying the maximum radius of the defocused proton distribution we can learn about the properties and development of the self-modulation. The two-screen setup consists of two imaging stations that measure the transverse, time integrated proton bunch distribution downstream the end of the plasma.

Each imaging station uses a scintillating Chromox (Al_2O_3:CrO_2) screen and two cameras, that are synchronized to the bunch arrival. When the bunch traverses the scintillating screen, it deposits energy in the material and the material emits photons in the visible range. The number of photons is proportional to the energy deposit in the material, which is proportional to the number of protons. We then image the emitted light onto cameras.

From simulations we expect that for each strongly defocused proton, we get $10^4 - 10^5$ protons that were not defocused and stay in the bunch core. To detect both: the maximum defocused protons and the ones in the core, we use two cameras.

We split the light emitted by the scintillating screen with a beam-splitter. One part is directly imaged by a lens onto the first camera, which we call the core camera (Basler ac1300-30gm). The second part is imaged onto a 1 mm thick glass window with round opaque coatings that have an optical density larger than 5 and block the light emitted by the bunch core. The light passing around the coatings is then imaged by another lens onto the chip of the second camera, which we call the halo camera (Basler ac1600-60gm).

In this article we describe a routine that enables us to determine the maximum radius of the proton distribution on the halo camera images. This maximum radius is the basis for all further calculations. A typical measurement of the defocused proton distribution taken by one of the halo cameras is shown in Figure 1. Note that the core of the bunch is blocked by the mask, and that the distribution has a distinct edge.

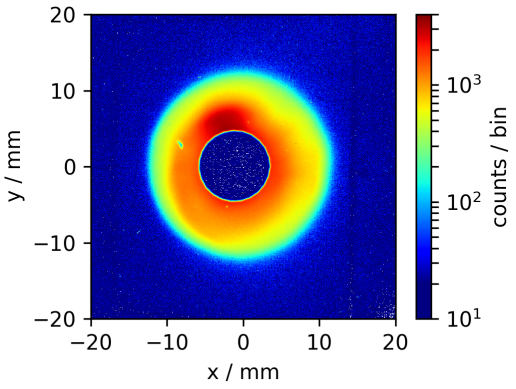

Figure 1: Typical image of a defocused proton distribution measurement by one of the halo cameras of the imaging stations. Note the logarithmic scale. The core of the bunch core is blocked by a mask.

2. Method

In order to determine the maximum defocused proton radius, we put together a procedure that (semi-) automatically determines the largest radius at which light and thus protons are detected from the halo camera images. This procedure assumes

-as observed in simulations- that the defocused proton halo has a distinct maximum radius. The method uses a standard contour subroutine for 2D images [1]. We perform the following steps on the images:

1) We apply a median filter [4] to remove pixels with high counts due to secondary particles impacting on the camera chip and pixel upset. We verify that the median filter does not change the transverse profile especially close to the edge of the distributions.

Previously, we recorded the centroid (Gaussian fit) of the proton distribution on both core and halo cameras without plasma or mask to obtain relative coordinates and scales. This info is now used to determine the proton bunch core centroid on the halo camera image, with mask, from its location on the core cameras.

2) Calculation of contours of the counts distribution of the halo cameras.

3) Selection of the longest closed outer contour above background level around the signal as the edge of the halo: when the selected level of the contour is chosen too low, the contour is not closed around the center of the bunch and is very short. When the contour level is set too high, the contour does not represent the maximum defocusing radius and is shorter. The height of this level is selected and tested on one image of each imaging station and of each series, then tested and cross-checked with several images of the measurement series (i.e. measurement performed with the same camera settings), and then applied to each measurement of the series. Afterwards, every contour of every image is verified by eye and the maximum radius that was selected is compared to the images lineouts and projections.

4) Calculation of the maximum proton radius from the distance of each point of the contour to the bunch center position: the maximum proton radius for each image is calculated as the mean of the radii of each contour point. We use the standard deviation of the measured radii to characterize the variation in determining the maximum defocused proton radius.

Note that the uncertainty of the maximum is determined by the resolution of the setup as well as the asymmetry of the measured signal [2].

3. Results

We calculate the maximum proton radius of Figure 1 based on the procedure described in Section 2. The contour that was determined as being the edge of the distribution (red) is shown at the same time as the proton bunch center (white cross) in Figure 2. In this case, the average radius is 13.1 mm and the standard deviation of the radii along the contour is 0.4 mm.

To verify that the maximum radius of the proton distribution makes sense, we compare the radius we obtain for the maximum defocusing edge to the horizontal and vertical projection of the measurement, on a logarithmic scale. Figure 3 shows the

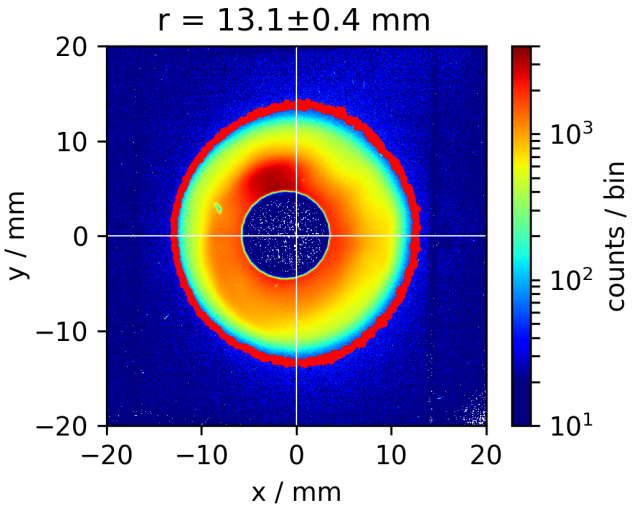

Figure 2: Same measurement image as Figure 1, where the calculated contour is shown in red. The center of the proton bunch core is marked by a white cross. Note the logarithmic scale.

maximum proton bunch radius (vertical bars where the green area marks the uncertainties) as well as the horizontal and vertical projections of the measurement shown in Figure 3. We see that the maximum defocusing edge determined by the contour method indeed identifies the outermost edge of the profiles.

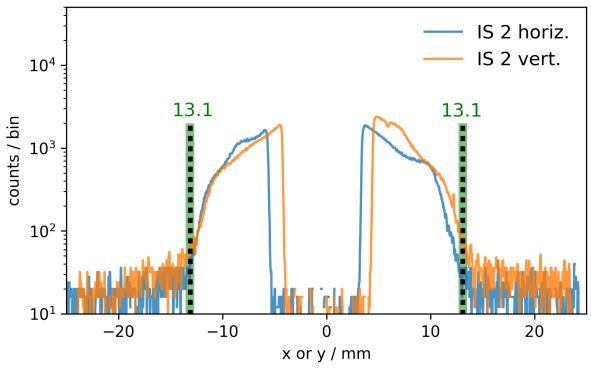

Figure 3: Horizontal (blue) and vertical(orange) lineouts of Figure 2. The maximum radius determined with the contour procedure is shown as the black vertical dashed lines and the uncertainty as the green thick line.

Most importantly, the lineouts clearly show that the recorded distributions have a clear edge and not a vanishing one. Therefore, the edge we determine is the true edge of the distribution and is not dominated by the arbitrary crossing between the signal and the camera background level.

4. Conclusions

In the AWAKE experiment at CERN we are interested in the protons that are defocused by the transverse plasma wakefields, and in their maximum radial position on the two imaging stations. Thus, in this article we present a method to determine

[1] Python: contour-function from the matplotlib package

[2] because of cylindrial symmetry in the measurement, the signal is expected to be symmetric

the maximum radius of a measured proton distribution with a distinct maximum radius. The method uses a standard Python contour routine and selects the longest closed contour above background level, closed around the core of the distribution. From this contour, we can calculate the mean radius from the bunch center and the standard deviation of the mean radius. The bunch center is determined by Gaussian fits from the images of the cameras recording the bunch core. By comparing the maximum radius to the lineouts and profiles of the measurements, we show that the calculated radius identifies the edge of the proton distribution.

Appendix A. References

[1] P. Muggli et al., AWAKE readiness for the study of the seeded self-modulation of a 400 GeV proton bunch, arXiv:1708.01087, 2017, to be published in: Plasma Physics and Controlled Fusion.

[2] M. Turner et al., The two-screen measurement setup to indirectly measure proton beam self-modulation in AWAKE, NIM A (2017).

[3] M. Turner et. al., Upgrade of the Two-Screen Measurement Setup in the AWAKE Experiment, Proceedings of IPAC (2017).

[4] `https://docs.scipy.org/doc/scipy-0.16.1/reference/generated/scipy.ndimage.filters.median_filter.html` (02.10.2017)